

A FAILURE PREDICTION MODEL
FOR WINDOW GLASS

by

William Lynn Beason

Institute for Disaster Research
Texas Tech University
Lubbock, Texas 79409

May, 1980

REPORT DOCUMENTATION PAGE	1. REPORT NO. NSF/RA-800231	2.	3. Recipient's Accession No. PDOI 148421
4. Title and Subtitle A Failure Prediction Model for Window Glass		5. Report Date May 1980	
7. Author(s) W. L. Beason		6.	
9. Performing Organization Name and Address Texas Tech University College of Engineering Institute for Disaster Research Lubbock, TX 79409		8. Performing Organization Rept. No.	
12. Sponsoring Organization Name and Address Engineering and Applied Science (EAS) National Science Foundation 1800 G Street, N.W. Washington, D.C. 20550		10. Project/Task/Work Unit No.	
15. Supplementary Notes		11. Contract(C) or Grant(G) No. (C) (G) PFR7724063	
16. Abstract (Limit: 200 words) An analytical method is presented to predict the strength of window glass plates subjected to lateral loads. The failure prediction model will be used to assess glass plate strength to be used in designing window glass. The model relates the probability of glass plate failure to fundamental glass plate surface properties. It incorporates the following: (1) an analytical representation of the variation of glass strength with different environmental factors; (2) a geometrically non-linear plate analysis; and (3) a statistical representation of glass plate surface flow properties. The model is formulated so that surface flow properties are dependent only upon the type and treatment of the glass, and are independent of factors such as plate aspect ratio, plate glass surface area, and load duration. Validity of the nonlinear plate analysis, incorporated in the model, was demonstrated by comparison of actual and theoretically derived glass plate stresses and deflections. It also was shown that surface flow parameters employed in the production model are independent of plate response. Hence, the failure prediction model was verified.		13. Type of Report & Period Covered	
17. Document Analysis a. Descriptors Window glass Sheet glass Plate glass Damage b. Identifiers/Open-Ended Terms Glass plate failure c. COSATI Field/Group		14.	
18. Availability Statement NTIS		19. Security Class (This Report)	21. No. of Pages
		20. Security Class (This Page)	22. Price

FOREWORD

The work reported herein was conducted as a part of a continuing program of research at Texas Tech University involving engineered window glass. The program is administered through the Institute for Disaster Research in the College of Engineering.

The director and principal investigator of the project for failure prediction of window glass was Dr. W. Lynn Beason. The project was supported by the National Science Foundation under Award No. PFR 77-24063, the Institute for Disaster Research, and the Department of Civil Engineering at Texas Tech University. This report was adapted for publication from Dr. Beason's dissertation of the same title. Any opinions, findings, conclusions, or recommendations expressed or implied in this publication are those of the author and do not necessarily reflect the views of the research sponsors.



ACKNOWLEDGEMENTS

The author wishes to acknowledge the guidance and counsel given in the conduct of this research by members of his graduate committee. The author is particularly indebted to Drs. J. R. McDonald and J. E. Minor, who provided invaluable assistance and constructive criticism. The author wishes to thank Mr. W. A. Dalgliesh of the National Research Council of Canada, who provided excellent advice at critical points in the development of the research reported herein. In addition, the contributions of Mr. P. L. Harris in performing laboratory testing reported herein are recognized.

ABSTRACT

An analytical method is advanced to predict the strength of window glass plates subjected to lateral loads. The failure prediction model relates the strength of glass plates to fundamental properties of the glass plate surface. The failure prediction model incorporates all factors which are known to significantly affect the strength of glass and all factors which influence plate behavior. The failure prediction model is offered as a realistic assessment of glass plate strength to be used in window glass design.

The failure theory employed in the glass plate failure prediction model states that glass plates fail as the result of large local tensile stresses. These large local stresses are induced by the interaction of surface tensile stresses with minute stress raising surface flaws. Because the strength of glass is controlled by the stress raising characteristics of the surface flaws, the strength of glass varies with all factors which alter these surface flaw characteristics. A literature search is conducted to identify factors which lend significant variability to the strength of glass. An available analytical representation of these glass strength variations is incorporated into the failure prediction model.

A geometrically nonlinear plate analysis is employed in the failure prediction model to calculate the surface tensile stresses in a rectangular glass plate. Selection of plate boundary conditions representative of window glass installations is based upon comparisons of experimental glass plate responses with available theoretically determined plate responses. Based upon these comparisons, it is determined that the best idealized boundary conditions to model window glass are:

- (1) the plate edges are free to rotate,
- (2) the plate edges are free to slip in the plane of the plate, and
- (3) the plate edges are restrained from lateral displacement.

A geometrically nonlinear plate analysis which employs these boundary conditions is advanced to model the response of a rectangular glass plate subjected to a uniform lateral load.

The failure prediction model relates the strength of glass plates to fundamental characteristics of the glass plate surface flaws. The probability that a glass plate exposed to a lateral load will fail is the probability that a surface flaw capable of initiating failure is located on the glass plate surface. Appropriate probability theory is reviewed and adapted to model the occurrence and severity of the surface flaws and is incorporated in the failure prediction model.

The surface flaw characteristics employed in the failure prediction model must be estimated from the results of carefully controlled glass plate tests to failure. This process is independently performed for two different sets of glass plate failure data. The two sets of glass plates tested were of similar surface condition, but significantly different geometry. The strength of one geometry of glass plate is then accurately predicted using the surface flaw characteristics estimated from the failure data from the other geometry of glass plate. It is thus shown that the strength of glass is related to fundamental properties of the glass plate surface.

TABLE OF CONTENTS

	<u>Page</u>
LIST OF TABLES.....	ix
LIST OF FIGURES.....	xiii
I. INTRODUCTION.....	1
II. THE RESEARCH PROBLEM.....	3
A. Review of Current Glass Design Procedures..	5
B. Research Approach.....	11
1. Glass Strength.....	13
2. Plate Stresses.....	13
3. Statistical Failure Theory.....	15
4. Verification.....	15
III. THE STRENGTH OF GLASS.....	16
A. The Failure Mechanism.....	17
B. Observed Variations of Glass Strength.....	21
1. Variations of Glass Strength With Exposure to Water.....	21
2. Variations of Glass Strength With Temperature.....	24
3. Variations of Glass Strength With Load Duration.....	27
C. Analytical Expressions of Glass Strength Variations.....	29
IV. NONLINEAR ANALYSIS OF GLASS PLATES.....	37
A. Review of Nonlinear Plate Solutions.....	38
1. Review of Nonlinear Plate Equations....	41

	<u>Page</u>
2. Nonlinear Plate Solutions for Simply Supported Rectangular Plates....	45
3. Comparison of Nonlinear Plate Solutions to Actual Glass Plate Behavior.....	50
B. Development of Nonlinear Plate Solution....	53
1. Formulation of Nonlinear Plate Solution.....	54
2. Validity of Nonlinear Plate Solution...	59
C. Comparison of Results of Nonlinear Plate Solution to Glass Test Results.....	65
V. GLASS PLATE FAILURE PREDICTION MODEL.....	78
A. Formulation of the Glass Plate Failure Prediction Model.....	79
1. Equivalent Stresses.....	80
2. Statistical Theory.....	81
3. Numerical Integration of Risk Function.	87
4. Summary of Failure Prediction Model....	91
B. Determination of the Glass Plate Surface Flaw Parameters.....	92
1. Glass Strength Data.....	93
2. Equivalent Strength Conversion.....	94
3. Equivalent Strength Statistics.....	96
4. Total Equivalent Plate Areas.....	101
5. Determination of the Best k Surface Flaw Parameter.....	101
6. Selection of the Best Surface Flaw Parameters.....	116
C. Validity of the Failure Prediction Model...	120

	<u>Page</u>
1. Differences in GPL Plates.....	120
2. Independence of the Glass Plate Surface Flaws.....	122
IV. CONCLUSION.....	127
A. Summary of Accomplishments.....	127
B. Directions of Future Research.....	129
LIST OF REFERENCES.....	130
APPENDICES.....	138
Appendix A. Analysis of Glass Plate Fracture Patterns.....	140
Appendix B. Algebraic Manipulations of Nonlinear Plate Analysis.....	150
Appendix C. Computer Program to Perform Nonlinear Plate Analysis.....	159
Appendix D. Glass Plate Tests.....	169
D.1 Glass Test Facility.....	169
D.2 Glass Test Results.....	173
Appendix E. Statistical Calculations.....	180
E.1 Fundamentals of Statistical Methods..	181
E.2 Calculations.....	185

LIST OF TABLES

<u>Table</u>		<u>Page</u>
I	Biaxial Stress Correction Factor, c	86
II	Example Equivalent Area Table.....	90
III	Equivalent Failure Loads for GPL Glass Plates..	97
IV	Grouped Frequency Table for Square GPL Glass Plate Equivalent Failure Loads.....	98
V	Grouped Frequency Table for Rectangular GPL Glass Plate Equivalent Failure Loads.....	99
VI	Total Equivalent Area Table for Square GPL Glass Plates.....	106
VII	Total Equivalent Area Table for Rectangular GPL Glass Plates.....	107
VIII	Total Equivalent Areas, S_m , for Square GPL Glass Plates.....	108
IX	Total Equivalent Areas, S_m , for Rectangular GPL Glass Plates.....	109
X	Mean Total Equivalent Area Table for Square GPL Glass Plates.....	112
XI	Mean Total Equivalent Area Table for Rectangular GPL Glass Plates.....	113
XII	Comparison of Calculated and Theoretical Square GPL Glass Plate Failure Load Statistics.....	114
XIII	Comparison of Calculated and Theoretical Rectangular GPL Glass Plate Failure Load Statistics.....	115
XIV	Comparison of Actual and Calculated Square GPL Theoretical Equivalent Failure Load Data.....	123
XV	Comparison of Actual and Calculated Rectangular GPL Theoretical Equivalent Failure Load Data...	125
D. I	Failure Data for Square GPL Glass - Exterior Surface in Tension.....	175

<u>Table</u>	<u>Page</u>
D.II Failure Data for Square GPL Glass - Interior Surface in Tension.....	176
D.III Failure Data for Rectangular GPL Glass - Exterior Surface in Tension.....	177
D.IV Failure Data for Rectangular GPL Glass - Interior Surface in Tension.....	178
E.I Mean Total Equivalent Area Table for Square GPL Glass Plates: $m = 4$	186
E.II Mean Total Equivalent Area Table for Square GPL Glass Plates: $m = 5$	187
E.III Mean Total Equivalent Area Table for Square GPL Glass Plates: $m = 6$	188
E.IV Mean Total Equivalent Area Table for Square GPL Glass Plates: $m = 7$	189
E.V Mean Total Equivalent Area Table for Rectangular GPL Glass Plates: $m = 4$	190
E.VI Mean Total Equivalent Area Table for Rectangular GPL Glass Plates: $m = 5$	191
E.VII Mean Total Equivalent Area Table for Rectangular GPL Glass Plates: $m = 6$	192
E.VIII Mean Total Equivalent Area Table for Rectangular GPL Glass Plates: $m = 7$	193
E.IX Calculation of Theoretical Square GPL Glass Plate Equivalent Failure Load Statistics: $m = 4$, $k = 9.94 \times 10^{-18}$	194
E.X Calculation of Theoretical Square GPL Glass Plate Equivalent Failure Load Statistics: $m = 5$, $k = 2.25 \times 10^{-21}$	195
E.XI Calculation of Theoretical Square GPL Glass Plate Equivalent Failure Load Statistics: $m = 6$, $k = 4.97 \times 10^{-25}$	196
E.XII Calculation of Theoretical Square GPL Glass Plate Equivalent Failure Load Statistics: $m = 7$, $k = 1.06 \times 10^{-28}$	197

<u>Table</u>	<u>Page</u>
E.XIII Calculation of Theoretical Rectangular GPL Glass Plate Equivalent Failure Load Statistics: m = 4, k = 7.30×10^{-18}	198
E.XIV Calculation of Theoretical Rectangular GPL Glass Plate Equivalent Failure Load Statistics: m = 5, k = 1.72×10^{-21}	199
E.XV Calculation of Theoretical Rectangular GPL Glass Plate Equivalent Failure Load Statistics: m = 6, k = 3.83×10^{-25}	200
E.XVI Calculation of Theoretical Rectangular GPL Glass Plate Equivalent Failure Load Statistics: m = 7, k = 7.89×10^{-27}	201
E.XVII Comparisons of Actual and Theoretical Mean Equivalent Failure Loads - Preferred Surface Flaw Parameters.....	202
E.XVIII Comparisons of Variances of Actual and Theoretical Equivalent Failure Loads - Preferred Surface Flaw Parameters.....	203
E.XIX Comparisons of Actual and Theoretical Square GPL Glass Plate Equivalent Failure Load Distributions - Preferred Surface Flaw Parameters.....	204
E.XX Comparisons of Actual and Theoretical Rectangular GPL Glass Plate Equivalent Failure Load Distributions - Preferred Surface Flaw Parameters.....	205
E.XXI Calculation of Theoretical Square GPL Glass Plate Equivalent Failure Load Statistics: m = 6, k = 3.83×10^{-25}	207
E.XXII Calculation of Theoretical Rectangular GPL Glass Plate Equivalent Failure Load Statistics: m = 6, k = 4.97×10^{-25}	208
E.XXIII Comparisons of Actual and Theoretical Mean Equivalent Failure Loads - Alternate Surface Flaw Parameters.....	209
E.XXIV Comparisons of Variances of Actual and Theoretical Equivalent Failure Loads - Alternate Surface Flaw Parameters.....	210

<u>Table</u>	<u>Page</u>
E.XXV Comparisons of Actual and Theoretical Square GPL Glass Plate Equivalent Failure Load Distributions - Alternate Surface Flaw Parameters.....	211
E.XXVI Comparisons of Actual and Theoretical Rectangular GPL Glass Plate Equivalent Failure Load Distributions - Alternate Surface Flaw Parameters.....	212

LIST OF FIGURES

<u>Figure</u>	<u>Page</u>
1 Typical Glass Design Chart.....	6
2 Procedural Components of Glass Plate Failure Prediction Model.....	12
3 Cross Section of Idealized Flaw.....	19
4 Variations of Glass Strength with Temperature...	26
5 Variations of Glass Strength with Load Duration (Minor 1974).....	30
6 Corrosion of Idealized Surface Flaw.....	32
7 Rectangular Plate Coordinate System.....	42
8 Idealized In-Plane Displacements of Plate Edges.	49
9 Comparisons of Central Deflections of Square Plates with Different Boundary Conditions.....	52
10 Logic Flow Chart for Nonlinear Plate Solution...	60
11 Central Deflections of Simply Supported Square Plate with Zero In-Plane Reactions.....	63
12 Central Stresses of Simply Supported Square Plate with Zero In-Plane Reactions.....	64
13 Constants Used in Ishizaki's Empirical Load Deflection Equation.....	68
14 Comparisons of Actual and Calculated Glass Plate Central Deflections: Aspect Ratio = 1:1.....	70
15 Comparisons of Actual and Calculated Glass Plate Central Deflections: Aspect Ratio = 1:1.25.....	71
16 Comparisons of Actual and Calculated Glass Plate Central Deflections: Aspect Ratio = 1:1.33.....	72
17 Comparisons of Actual and Calculated Glass Plate Central Deflections: Aspect Ratio = 1:1.67.....	73
18 Comparisons of Actual and Calculated Glass Plate Central Stresses: Aspect Ratio = 1:1.....	75

<u>Figure</u>	<u>Page</u>
19 Comparisons of Actual and Calculated Glass Plate Central Stresses: Aspect Ratio = 1:2.....	76
20 Comparisons of Actual and Calculated Glass Plate Central Stresses: Aspect Ratio = 1:4.....	77
21 Representative Relative Cumulative Frequency for Glass Plate Failure Load.....	82
22 Calculation of Equivalent Glass Plate Failure Loads.....	95
23 Equivalent Failure Load Histograms for GPL Glass Plates.....	100
24 MEPT Stress Contours for Square GPL Glass Plate for Mean Equivalent Failure Load.....	102
25 MEPT Stress Contours for Rectangular GPL Glass Plate for Mean Equivalent Failure Load.....	103
26 MCEPT Stress Contours for Square GPL Glass Plate for Mean Equivalent Failure Load.....	104
27 MCEPT Stress Contours for Rectangular GPL Glass Plate for Mean Equivalent Failure Load.....	105
28 Comparisons of Actual and Theoretical Square GPL Relative Cumulative Equivalent Failure Load Frequencies.....	118
29 Comparisons of Actual and Theoretical Rectangular GPL Relative Cumulative Equivalent Failure Load Frequencies.....	119
A.1 Location of Fracture Origin.....	142
A.2 Schematic of Glass Plate Fracture Surface.....	142
A.3 Schematic of Fracture Mirror.....	144
A.4 Typical Rectangular GPL Glass Plate Fracture Pattern: $\sigma_{max} > \sigma_{min}$	147
A.5 Typical Square GPL Glass Plate Fracture Pattern: $\sigma_{max} = \sigma_{min}$	147
C.1 Computer Program for Nonlinear Plate Analysis...	157

<u>Figure</u>	<u>Page</u>
C.2 Sample Output from Nonlinear Plate Analysis Computer Program.....	165
D.1 Schematic of Glass Plate Test Facility.....	170
D.2 Square GPL Glass Plate Test Chamber.....	172

CHAPTER I

INTRODUCTION

There is a need within engineering practice for an analytical method to predict the probability of failure of window glass plates subjected to lateral loads. The failure prediction technique should include provision for all significant factors which influence glass strength and all significant factors which influence plate behavior. The ultimate use of the glass plate failure prediction model will be to provide a realistic assessment of glass plate strength to be used in the design of window glass.

Current window glass design information is based upon empirical representations of glass plate strength. Discussions in pertinent literature call attention to potential problems with this approach and emphasize the need for a rational method to determine the strength of window glass.

Recent advances in stress analysis techniques have made it possible to characterize more accurately the distribution of stresses in thin rectangular glass plates. Proposed new methods to predict the strength of glass plates incorporate results of the newly developed stress analyses. However, these new methods which predict glass strength continue to rely substantially upon empirical formulations and simplifying assumptions.

The failure prediction model advanced herein considers both the strength of glass and glass plate behavior. The strength of glass is related to fundamental properties of the glass plate surface. Glass plate behavior is described using a nonlinear plate analysis. Thus, fundamental relationships between load and stress and between stress and surface condition are recognized.

Chapter II expands upon the need for a failure prediction model for window glass and sets forth the research approach. Chapter III contains an evaluation of the glass plate failure mechanism and provides a basis for incorporating the significant factors which influence glass strength into the failure prediction model. A geometrically nonlinear, large deflection plate analysis is presented in Chapter IV to calculate the stresses in glass plates subjected to lateral loads. Chapter V contains the formulation of the glass plate failure prediction model. Finally, Chapter VI presents a summary of accomplishments and provides direction for future research.

CHAPTER II

THE RESEARCH PROBLEM

The design of window glass to resist lateral loads consists of two steps:

- (1) description of the design lateral load, and
- (2) selection of the minimum glass plate thickness from window glass design charts.

Uniform lateral loads representative of wind loads are the major type of lateral load considered for window glass design. Wind load characteristics depend upon building geometry and the local wind environment. Improved understandings of wind effects on buildings have become available as the results of both wind tunnel and full-scale experiments (Davenport 1976, Peterka and Cermak 1975, Dalgliesh 1979). However, glass plate strength information for use in window glass design has remained essentially the same for more than twenty years. Recent interest has focused on the limitations of the currently available window glass design information (Saffir 1976, Ishizaki 1977, Beason and Minor 1978). In addition, recent highly publicized instances of window glass failures in relatively moderate windstorms have called attention to potential problems with current window glass design procedures (Engineering News Record 1974, 1977).

Product recommendations concerning the strength of window glass have been widely circulated by major United

States glass manufacturers (PPG Industries 1975, Libbey-Owens-Ford Company 1980). These product recommendations are based upon glass plate strength tests (Orr 1957, Hershey and Higgins 1973). Because these glass plate strength characterizations were available and in apparent accord, similar window glass design charts were adopted for use as minimum standards in major building codes (Uniform Building Code 1973, Standard Building Code 1979, BOCA Basic Building Code 1975).

Recently, product recommendations presented by one manufacturer have changed radically (PPG Industries 1979). This company has advanced new glass plate strength information based upon stress analysis and glass strength data (Tsai and Stewart 1976). Publication of this new information has raised serious questions regarding design information presented in current building codes.

The basis for the glass plate strength information referenced in major building codes is examined below. This discussion is followed by a presentation of the research approach used to develop an analytical glass plate failure prediction model. A window glass design procedure based on the failure prediction model presented herein will be accomplished in further research at Texas Tech University.

A. Review of Current Glass Design Procedures

A review of current glass design information suggests that basic glass plate strength information that is presented in manufacturers literature (Libbey-Owens-Ford Company 1980) and building codes (Uniform Building Code 1973, Standard Building Code 1979, BOCA Basic Building Code 1975) in the United States is essentially the same. Figure 1 presents a typical glass design chart for rectangular glass plates supported continuously on four sides. This widely circulated design chart presents the minimum thickness of rectangular annealed glass of a particular area that is required to resist a given design lateral load.

Historically, windspeed data used as a basis to specify wind loads are presented in terms of annual extreme fastest mile windspeeds (Thom 1954, 1960, 1968). A fastest mile windspeed is the average velocity of a one mile shaft of air as it passes a point. Therefore, a design load associated with a windspeed in excess of 60 mph has a duration of 60 seconds or less. Although it is not clearly stated by all presenters, durations of the design loads presented in Figure 1 have become associated with durations of the associated fastest mile windspeeds or about 60 seconds. However, rationale to associate the design loads presented in Figure 1 with a 60-second or any load duration is not clear. This is a

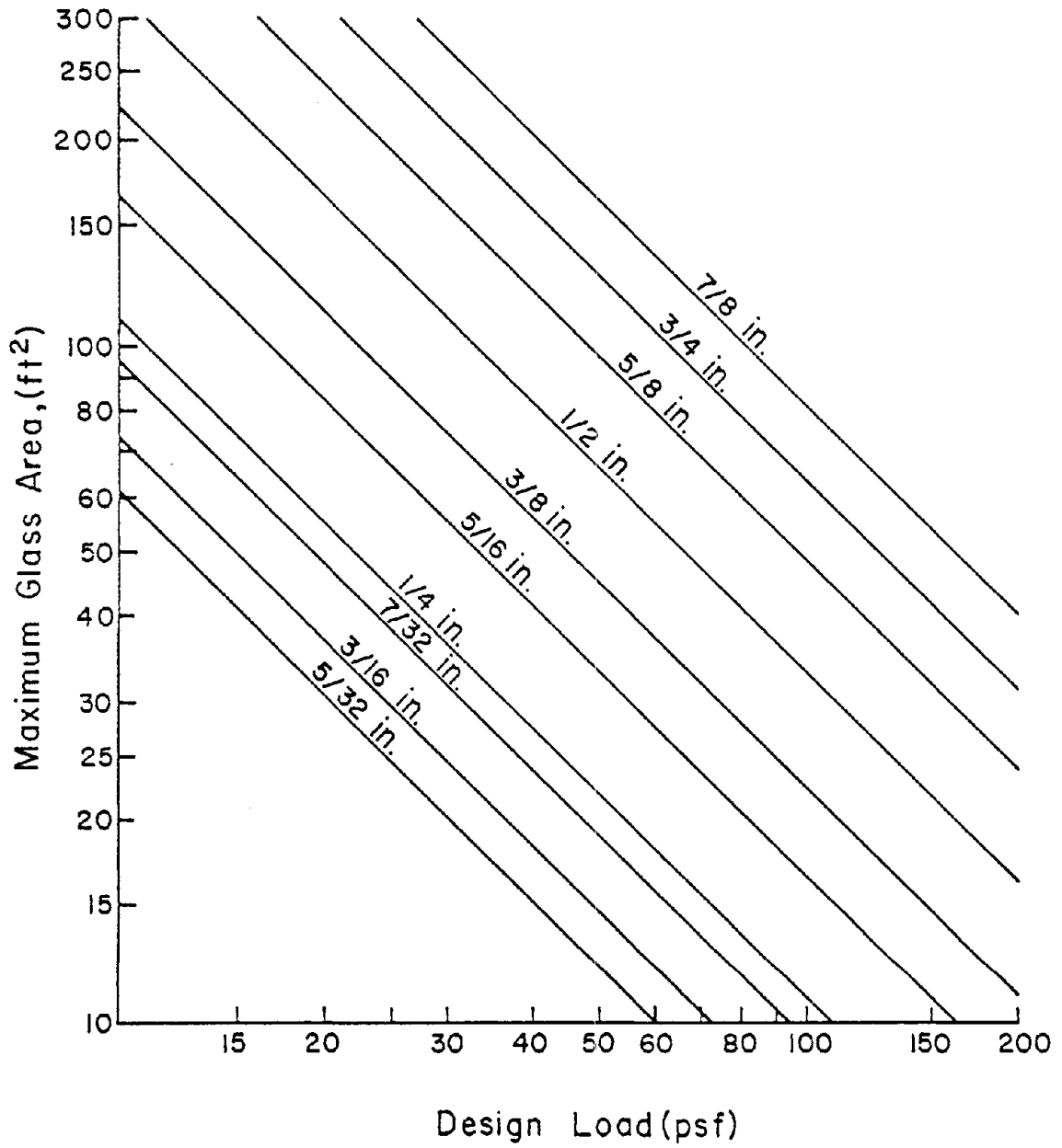


FIGURE 1. TYPICAL GLASS DESIGN CHART

very significant problem with current glass design methods because the strength of glass is highly dependent upon load duration (Ref. Chapter III).

Qualifications associated with the glass design chart presented in Figure 1 vary with the presenter. The chart is considered to be applicable for plate aspect ratios ranging from 1:1 to 1:3 or from 1:1 to 1:5, and for maximum lateral edge deflections up to 1/175 of the span. Further, the chart design load is considered to reflect either a design factor of 2.5 or a probability of a single plate failure of 8/1000.

Glass plate strength information available in the open literature which relates directly to window glass design charts contained in current building codes was first presented by Orr (1957). Orr reported results of 20 static tests to failure of new glass plates. The glass plates were exposed to increasing uniform lateral loads until failure. The uniform loads were increased in increments so that the central lateral deflection of a particular plate was increased in steps of 0.10 or 0.20 in. Pertinent data were recorded between load increments. The time required to fail a particular plate ranged from 5 to 25 minutes. The glass plates tested ranged in area from 47 to 80 sq ft, in thickness from 0.114 to .383 in., and in aspect ratio from 1:1 to 1:1.67. The test series contained, at most, two replications of any unique combination of area, thickness, aspect ratio, and glass type.

The following empirical equation was advanced by Orr (1957) to represent the measured variations of total glass plate failure load with glass plate thickness

$$P = 7600 (t + t^2) \quad (2.1)$$

where P is the total failure load (lbs) acting on the glass plate surface, and t is the nominal thickness (in.) of the glass plate. A more convenient expression is obtained if Equation (2.1) is divided by the area of the glass plate, yielding

$$p = [7600 (t + t^2)]/A \quad (2.2)$$

where p is the lateral load (psf), and A is the area of glass plate (sq ft).

The glass design chart presented in Figure 1 can be reproduced using Orr's (1957) results. To do this, it is assumed that the failure load for a given glass plate area is normally distributed with a mean value, p , given by Equation (2.2) and with a standard deviation calculated by assuming an appropriate coefficient of variation. Design loads presented in Figure 1 can then be determined by calculating the failure load associated with an 8/1000 probability of failure. If a coefficient of variation of 25 percent, as has been suggested by manufacturer's literature (PPG 1964), is used, the design load corresponding to an 8/1000 probability of failure is found by dividing

the mean failure load by 2.5. Therefore, presenters of Figure 1 associate the design loads with either an S/1000 probability of failure or a design factor of 2.5.

More elaborate test programs have since been conducted to determine the failure loads of new window glass plates subjected to uniform lateral loads (Bowles and Sugarman 1962, Hershey and Higgins 1973). It is not strictly proper to compare these different test results directly because of differences in loading rates and probable differences in glass plate surface conditions. Notwithstanding these differences, comparisons between mean glass failure loads predicted using Equation (2.2) and the independently determined glass strength data suggest that Equation (2.2) is a poor estimator of the variation of glass strength with variations of glass plate thickness, area, and aspect ratio. However, glass plate failure loads predicted with Equation (2.2) appear to be conservative for strengths of new glass plates from a design standpoint.

Major questions regarding the validity of current glass design information have been posed as the result of the release of the new set of product recommendations by PPG Industries (1979). These new product recommendations are the result of both experimental and analytical research

(Tsai and Stewart 1976). Information presented suggests that the strength of glass plates varies significantly with aspect ratio as well as with area and thickness. In some instances, the uniform lateral load corresponding to an 8/1000 probability of failure is less than half of the corresponding lateral load suggested in Figure 1. However, these new product recommendations have not, as yet, replaced the glass design chart presented in Figure 1 in building codes.

The above observations suggest that current representations of glass plate strength used for design purposes do not reflect, realistically, the strength of glass plates. Factors such as plate geometry and load duration are not properly treated in current glass design information. The major reason for the current situation is that until recently, major questions have existed regarding the nature of the stresses induced in a glass plate by a uniform lateral load. It is impossible to rigorously treat the problem of glass plate failure prediction without a knowledge of the induced stresses.

Recent studies address the strength of glass plates (Brown 1974, Tsai and Stewart 1976, PPG Industries 1979). Each of these studies recognize, to some extent, the importance of glass strength variations with factors such as plate geometry, load duration, and the need for an accurate assessment of the stresses induced in a glass plate by

lateral loads. However, none of these studies has gained widespread acceptance by glass designers.

B. Research Approach

A failure prediction model is presented herein to estimate the strength of window glass plates subjected to uniform lateral loads. The failure prediction model relates the probability of glass plate failure to fundamental glass plate surface properties. The glass plate failure prediction model incorporates: (1) an analytical representation of the variation of glass strength with different environmental factors (Ref. Chapter III), (2) a geometrically nonlinear plate analysis (Ref. Chapter IV), and (3) a statistical representation of the glass plate surface flaw properties (Ref. Chapter V). The failure prediction model is formulated so that the surface flaw properties are dependent only upon the type and treatment of the glass, and are independent of factors such as plate aspect ratio, glass plate surface area, and load duration.

Figure 2 presents major procedural components of the failure prediction model. Application of the failure prediction model is demonstrated in Chapter V using a set of glass plate strength data developed by testing a homogeneous sample of glass plates of different aspect ratios and areas.

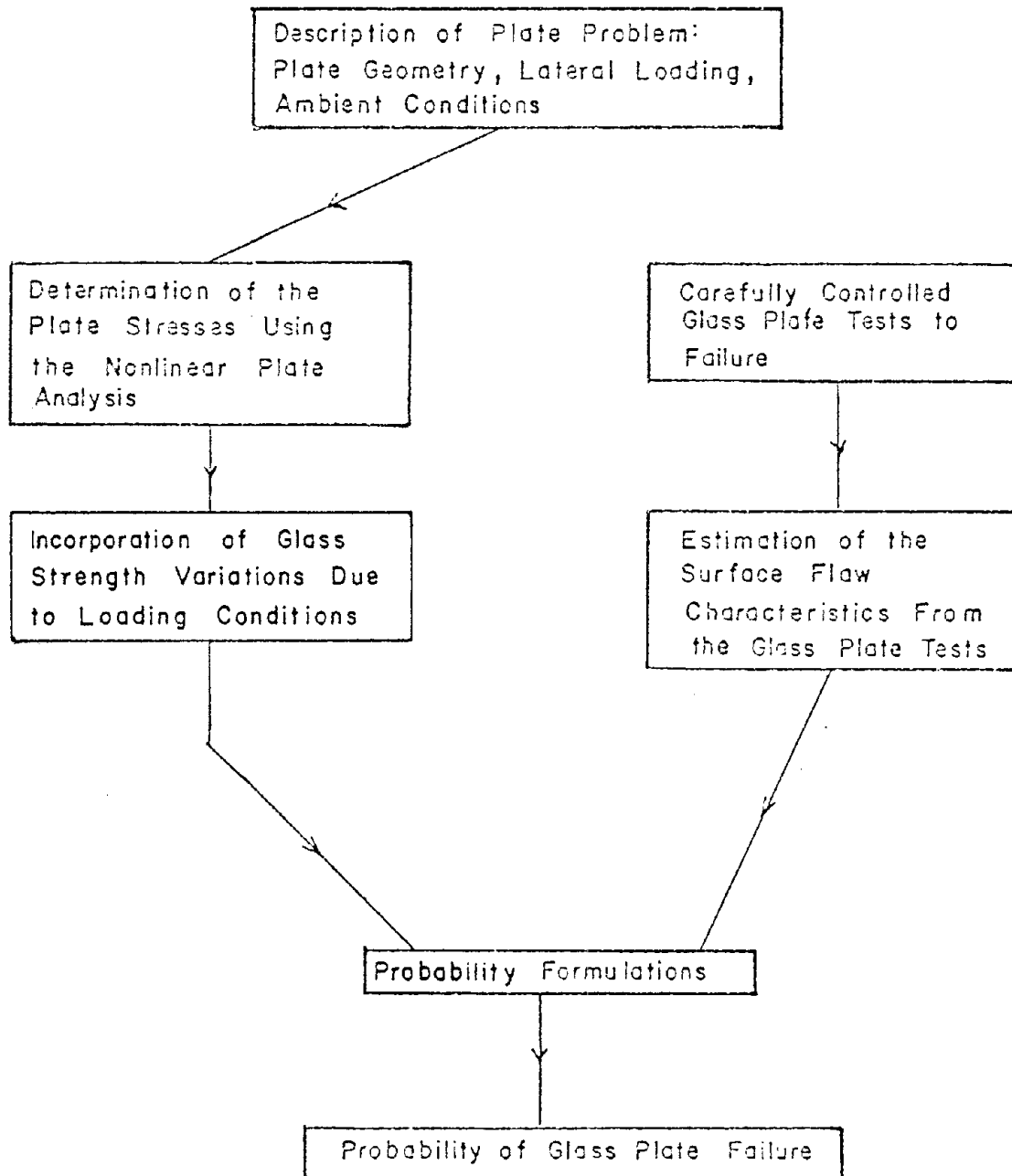


FIGURE 2. PROCEDURAL COMPONENTS OF GLASS PLATE FAILURE PREDICTION MODEL

1. Glass Strength

The most popular glass failure theory suggests that glass plates subjected to lateral loads fail as the result of the interaction of minute surface flaws with surface tensile stresses (Griffith 1920). By nature of their geometry and orientation with respect to the maximum normal tensile stress, the surface flaws cause large local stress concentrations in the glass plate. Failure initiates when the stress raising characteristics of a particular flaw and the attendant nominal tensile stress combine to cause a critical local stress in the glass plate. Geometries of the surface flaws can change to increase or decrease their stress-raising characteristics as a result of a phenomenon known as stress corrosion (Brown 1974). Stress corrosion is facilitated by the chemical action of water on the glass and by the presence of surface tensile stress. Because of stress corrosion, the strength of glass is dependent upon the duration of applied loading through a phenomenon known as static fatigue.

2. Plate Stresses

To predict the probability of failure of a glass plate, an accurate determination of the surface tensile stresses must be made. An annealed glass plate exposed to a uniform lateral pressure typically experiences central deflections in excess of the plate thickness prior to failure. Plates experiencing central deflections of

this magnitude sustain significant middle plane strains. Therefore, a nonlinear plate analysis which accounts for the actions of the resulting middle plate forces must be used (Timoshenko 1959).

The surface tensile stresses in a glass plate are highly dependent upon the nature of the boundary conditions to which the glass plate is exposed. The boundary of a typically installed glass plate is subjected to varying degrees of rotational, in-plane and lateral restraints. It is the opinion of some glass researchers that the boundary conditions of typically installed glass plates approach the idealized situation where the edges are simply supported and free to slip in-plane (Tsai and Stewart 1976). Until recent interest in the response of glass plates, this plate boundary situation has received little attention since it was first treated by Kaiser (1936).

The nonlinear plate analysis presented herein employs the von Karman differential equations (Timoshenko 1959). Solution of the two nonlinear plate equations is achieved using an iterative technique coupled with a Galerkin method. Results of the nonlinear plate solution are compared to other nonlinear plate solutions and to experimental glass plate test results.

3. Statistical Failure Theory

The probability that a glass plate exposed to lateral load fails is the probability that at least one glass plate surface flaw is capable of initiating failure, given the resulting distribution of surface tensile stresses. Both the occurrence and severity of the glass plate surface flaws must be modeled to predict the probability of failure of a particular glass plate. A statistical material strength theory introduced by Weibull(1939) is used as a basis to model the glass plate surface flaw characteristics. The statistical formulation employs two parameters to model the surface flaw characteristics. Values of the surface flaw parameters must be estimated from data generated from carefully controlled glass plate tests to failure.

4. Verification

To demonstrate use of the failure prediction model, two different geometries of glass plates with similar surface conditions were tested to failure with time controlled lateral loads. The best surface flaw parameters to represent the failure strengths of both geometries of glass plates tested were then determined independently. Validity of the failure prediction model is demonstrated by accurately predicting the strength of one glass plate geometry using the surface flaw parameters determined from the other geometry.

CHAPTER III
THE STRENGTH OF GLASS .

It is assumed in the development of the failure prediction model presented herein that the strength of glass plates is controlled by the characteristics of minute surface flaws. The surface flaws give rise to large local stress concentrations which initiate failure. The fundamentals of this failure theory were originally presented by Griffith (1920). The original Griffith theory along with interpretations presented by Shand (1965) are reviewed in this chapter.

The strength of glass has been observed to vary significantly with both environmental exposure and load duration. Several pertinent experiments found in the literature are examined to emphasize the reality of these glass strength variations. Experimental results reviewed indicate that any credible failure prediction model for glass plates must account for these observed variations of glass strength.

To incorporate observed glass strength variations into the failure prediction model, the strength variations are related to the surface flaw characteristics in a deterministic fashion. Development of a stress corrosion theory advanced by Brown (1974) is presented in this chapter. The stress corrosion theory explains glass strength variations with relative humidity, temperature, and load dura-

ation. The stress corrosion theory is incorporated into the failure prediction model presented in Chapter V.

A. The Failure Mechanism

A. A. Griffith (1920) observed that many brittle materials such as glass fail at stresses much less than their inherent material strength. To account for this behavior, Griffith suggested that the failure of brittle materials is the result of large local stress concentrations induced in the materials by minute flaws.

Griffith (1920) presented an analytical development for the special case of a flat homogeneous plate of uniform thickness containing a straight, narrow crack passing completely through its thickness. The analytical formulations were restricted to the case where the crack was oriented perpendicular to the direction of the maximum principal tensile stress. Validity of this analytical formulation was demonstrated experimentally by Griffith.

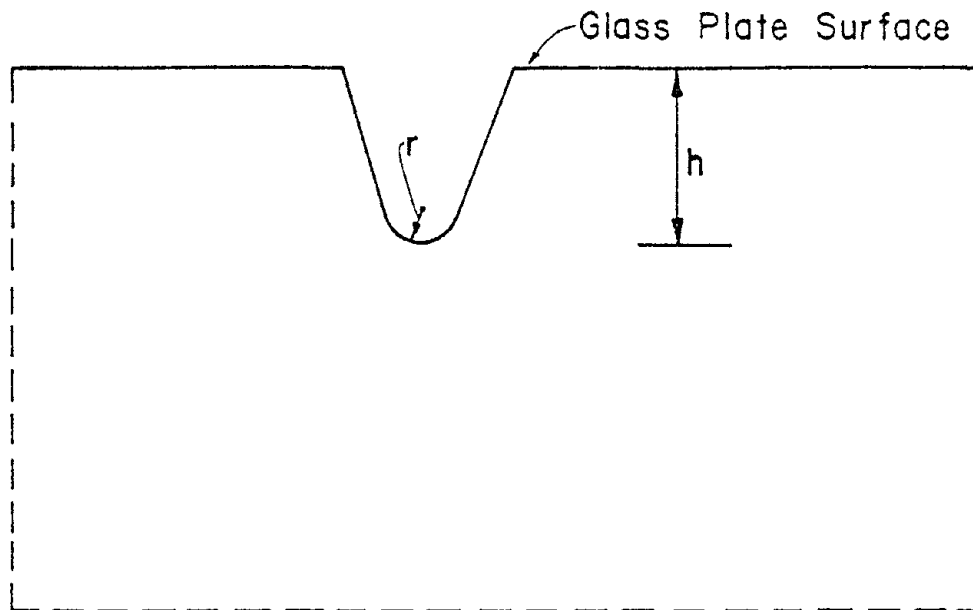
The original Griffith formulations were too restrictive to apply directly to the behavior of glass plates. However, many glass researchers believe that glass fracture is the result of tensile stresses interacting with minute flaws on the surface of the glass (Shand 1954, Weyl 1946, Jones 1949, Levengood 1957, Wiederhorn 1967, Rader 1967, Preston 1942, Stanworth 1950).

In a series of papers concerning the fracture of glass, E. B. Shand extended the fundamental concepts of the Griffith theory to develop a more applicable glass fracture theory (Shand 1954, Shand 1959, Shand 1961, Shand 1965, Shand 1969). Shand considered a straight surface flaw with a depth of penetration into the surface of the glass plate which is small with respect to the thickness of the glass plate. Figure 3 shows the cross section of such an idealized surface flaw. The maximum local stress, σ_m , associated with an idealized surface flaw occurs at the flaw tip and is given by

$$\sigma_m = \sigma_a K (h/r)^{1/2} \quad (3.1)$$

where σ_a is the maximum principal tensile stress to which the flaw is subjected, K is a stress concentration which depends upon the flaw geometry, h is the flaw depth, and r is the effective radius of the flaw tip (Shand 1965).

Shand (1965) reported that the nominal tensile stress present in a glass specimen at the time of failure can range from 1000 psi to values in excess of 300,000 psi. He attributed this wide range of variability to different factors which reduce the strength of glass including the treatment of the glass, its environmental exposure, the effects of load duration, and the stress concentration effects of the surface flaws. He further reported that the strength degrada-



$$\sigma_m = \sigma_a K \left(\frac{h}{r}\right)^{\frac{1}{2}}$$

Where

- σ_m — Maximum Stress at Flaw Tip
- σ_a — Nominal Stress in Flaw Area
- K — Flaw Geometry Factor
- h — Flaw Depth
- r — Effective Flaw Tip Radius

FIGURE 3. CROSS SECTION OF IDEALIZED FLAW

tion due to the stress concentration effects of the flaw geometry as represented by Equation (3.1) is perhaps fifty times as important as the strength degradation effects of all other factors combined.

The concept of stress raising flaws causing glass failure is substantiated by the fact that a glass plate failure can usually be traced back to a single point of origin (Ref. Appendix A). Further, the location of the failure origination point does not necessarily coincide with the point of the maximum nominal stress, indicating that there is a variability associated with the stress raising potential of different flaws. The one particular flaw which initiates glass plate failure is termed the critical flaw.

Analytical formulations by Griffith (1920) and by Shand (1965) do not treat the general situation where the flaw is oriented at some angle to the direction of the maximum principal stress such that the stress concentration is less than maximum. However, it is clear from an examination of stress concentration theory that the orientation of a flaw with respect to the orientation of the maximum principal tensile stress must play an important role in determining whether or not a particular flaw is capable of initiating failure (Seely and Smith 1952). Further, it is doubtful if the precise geometry of surface flaws or glass plates will ever be known. Therefore, it

is not likely that direct application of Equation (3.1) can be made. The concept of the surface flaw failure mechanism is useful only in interpreting the behavior of the glass plates.

B. Observed Variations of Glass Strength

The strength of glass varies significantly with environmental exposure and load duration. Because the strengths of most common engineering materials are not nearly as sensitive to normal variations of environment and load duration as is the strength of glass, realization of the dependence of glass strength on so many different factors is often difficult for an engineer not familiar with the behavior of glass. For this reason, a detailed examination of several different experiments reported in the literature is made in this section. The experimental results are divided into three groups which show the dependence of glass strength on the presence of water, temperature, and load duration.

1. Variations of Glass Strength with Exposure to Water

The strength of glass is significantly affected by exposure of the glass surface to water, either liquid or vapor. Results of three independent experiments are examined to demonstrate the dependence of glass strength on exposure to water.

Baker and Preston (1946) tested 7/32 in. diameter glass rods using a bending load. The rods were baked at temperatures up to 350°C and then stored in a desiccator for a period of two weeks prior to testing to assure that the specimen surfaces were completely dry. Some of the specimens were soaked in water prior to testing. The load duration was varied from 0.1 sec. to 100 sec. Relevant conclusions are:

- (1) in a near vacuum, thoroughly baked glass specimen surfaces not exposed to water have an ultimate tensile strength which is independent of load duration,
- (2) glass specimens whose surfaces are simultaneously exposed to moisture and tensile stress rapidly lose strength, and
- (3) glass specimens whose surfaces are exposed only to moisture may become stronger.

Stockdale, Tooley, and Ying (1951) tested a large number of freshly drawn, annealed glass rods with diameters of 0.11 to 0.12 in. The specimens were stored in a desiccator after fabrication to assure a thoroughly dry surface. Some of the specimens were subjected to water treatments consisting of total immersion in doubly distilled water at a temperature of 90°C. The duration of the water immersion treatment ranged from 5 minutes to 24 hours. The specimens were then tested to failure using uniaxial tension loads. Major conclusions are:

- (1) glass with thoroughly dry surfaces and which are not subjected to water treatment experience no significant strength variations with storage time,
- (2) untreated glass specimens broken while submerged in water are weaker than specimens broken in air, and
- (3) extended periods of water treatments prior to loading tends to increase the strength of the glass specimens.

Schoening (1960) performed a series of experiments on laminated glass beams fabricated by gluing microscope cover slides together. The resulting specimens had approximate dimensions of 38 x 6 x 0.16 mm. The laminated specimens were stored in a desiccator for two weeks prior to testing. The specimens were then placed in a test apparatus and the total system was baked in a vacuum at 350°C for one hour, and allowed to cool to room temperature. The glass specimens were then exposed to different relative water vapor pressures for two hours and tested with a bending load. Relevant conclusions are:

- (1) glass specimens exposed to no water vapor pressure maintain the highest strength,

- (2) the strength of the glass specimens reduces with increasing relative water vapor pressure up to a relative water vapor pressure of about 50 percent, and
- (3) the ratio of the strength of glass specimens tested in saturated water vapor to the strength of glass specimens tested in a vacuum is about 0.56.

Results of these three projects demonstrate the dependence of glass strength on exposure to water. The strengths of glass specimens tested in a vacuum are independent of load duration. The strengths of glass specimens exposed to water during the course of the test are dependent on the load duration and tend to be less than analagous dry strengths. In addition, exposure of glass specimens to water prior to loading can result in a significant increase in strength. Based upon these experimental results, it is clear that the glass failure prediction model must account for the variation of glass strength with exposure to water.

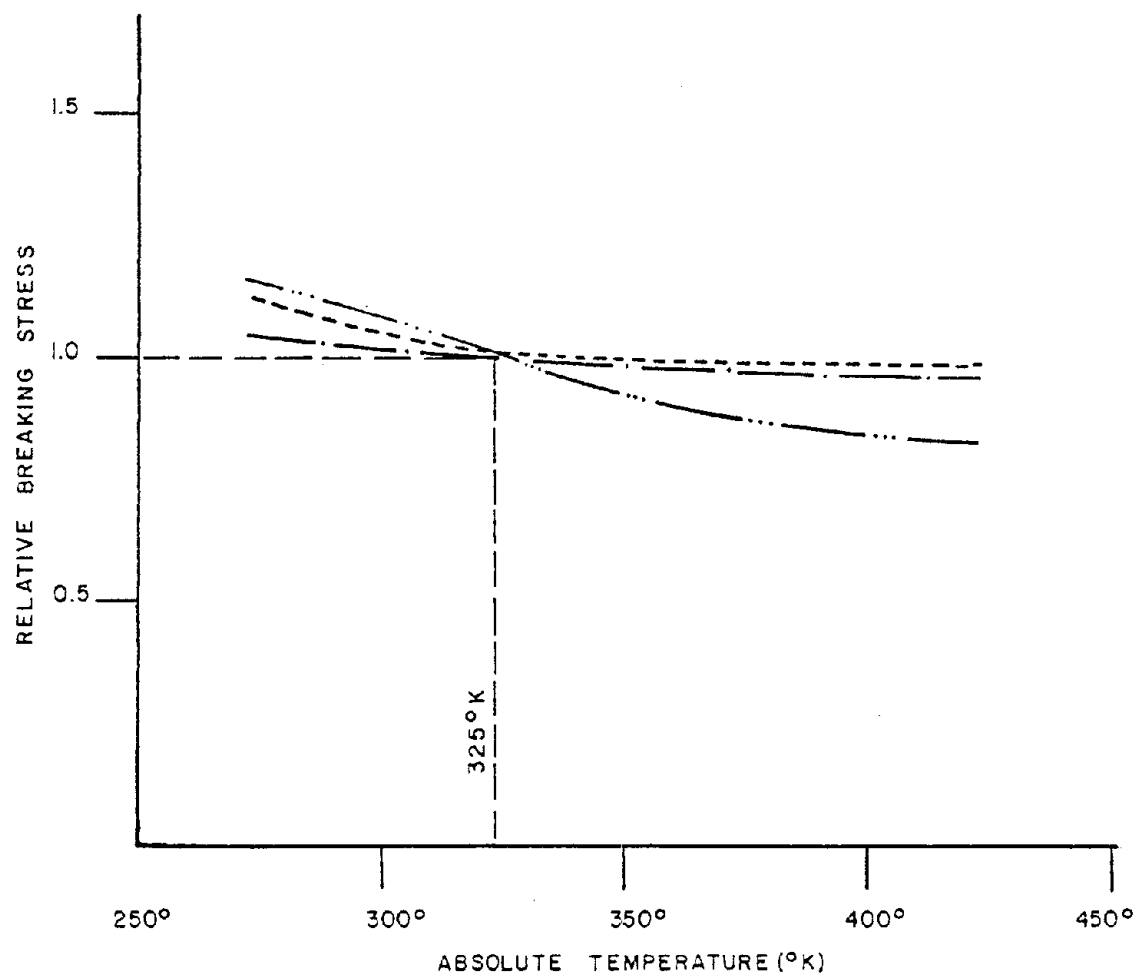
2. Variations of Glass Strength with Temperature

The strength of glass varies significantly with temperature (Vonnegut and Glathart 1946, Jones and Turner 1942,

Smekal 1936). Comparisons of experimental results presented by these researchers reveal that the nature of the variation of glass strength in a range of 73° to 773°K is uncertain (Stanworth 1950, Shand 1958). However, since ordinary window glass is not normally subjected to such severe temperature variations, variations of glass strength are examined in a range of temperatures from 250° to 450°K. A comparison of available glass strength data in this narrower range of temperatures is made in this section.

Glass strength data are available for specimens of different geometries, including fibers, bars, strips, and rods (Vonnegut and Glathart 1946, Jones and Turner 1942, Smekal 1936, Charles 1958). Because of the differences in the specimen geometries as well as differences in load durations and test conditions, the available data cannot be compared directly. To make a direct comparison of the various data, the reported failure stresses from each experiment were normalized by dividing the reported strengths by their respective strengths at 323°K. These normalized data are presented in Figure 4.

Based upon data presented in Figure 4, it can be concluded that the strength of glass decreases with increasing temperature in the temperature range of interest. This trend was present in each data set examined. The data suggest that glass can experience as much as a 40 percent reduction of strength as the temperature increases from 250°



- Glass Rods (Vonnegut and Glathart 1946)
- Glass Bars (Jones and Turner 1942)
- Glass Fibers (Smekal 1936)

FIGURE 4. VARIATIONS OF GLASS STRENGTH WITH TEMPERATURE

to 450°K. Therefore, the failure prediction model should account for the variation of glass strength with temperature.

3. Variations of Glass Strength with Load Duration

The strength of glass exposed to normal amounts of humidity is highly dependent upon the duration of the applied loading (Black 1935, Charles 1958, Mould and Southwick 1959, Shand 1961). This phenomenon is termed static fatigue by ceramic scientists. Results of three research projects conducted with glass specimens that were prepared from actual window glass are reviewed in this section. In addition, results from experiments employing specially fabricated specimens are examined to further emphasize the load duration dependence of glass strength.

Black (1935) performed a series of tests which clearly show that the strength of glass is dependent on load duration. Black tested eighty specimens of new plate glass beams, 2 x 10 x 7/64 in., exposed to eight different load durations. The glass beams were simply supported, and subjected to central loadings. In the first six test series, the specimens were exposed to linearly increasing loads which caused failure in a range of times from 7 to 960 seconds. The average maximum tensile stresses occurring in the beams ranged from 10765 psi for an average

load duration of 7 seconds to 6494 psi for an average load duration of 960 seconds. In the last two test series, the beams were exposed to a constant load inducing a maximum tensile stress in the beams of either 3080 psi or 4400 psi and the time to failure of the specimens was measured. In the 4400 psi test series, 9 out of 10 specimens were broken within 40 hours and 1 remained unbroken after 20 days. In the 3080 psi test, 1 specimen failed in seven days and the remaining 9 specimens remained unbroken at the end of 20 days.

Thompson and Cousins (1949) performed a series of tests on small glass plates, 14 x 19 in., of two different nominal thicknesses, 3/32 in. and 1/8 in. These glass plates were subjected to blast pressures that caused failure in a few hundredths of a second. The results of these tests were compared to strengths determined by failing similar glass plates with linearly increasing loads which caused failure in about 60 seconds. It was found that the strength of glass specimens which failed in about 0.01 seconds was about twice that of the specimens that failed in 60 seconds. Further, it was observed that variations of load durations in the hundredths of a second range caused significant variations in the strength of the glass specimens.

Shand (1961) tested small glass strips, 3/4 x 4-1/2 x 3/32 in. He introduced artificial flaws on the surfaces

of the specimens with a specially fabricated tool. These flaws were introduced to reduce the variability of the failure strengths associated with flaw occurrence and geometry so that load duration effects could be more easily measured. Tests were conducted with load durations ranging from 1 second to about 300 hours. The failure strengths of glass specimens ranged from about 11000 psi at a load duration of 1 second to about 6000 psi at a load duration of 300 hours.

Static fatigue has been observed in other experiments conducted on specially fabricated glass specimens. Figure 5 presents a summary of the static fatigue results presented by several different researchers (Minor 1974). In each experiment examined, the strength of glass specimens exposed to normal amounts of atmospheric humidity decreased significantly as the load duration increased. Therefore, the failure prediction model should account for the variation of glass strength with load duration.

C. Analytical Expressions of Glass Strength Variations

In the previous section it was shown that the strength of glass varies significantly with exposure to water, temperature, and load duration. In the failure prediction model presented in Chapter V, the strength of glass is related to the characteristics of the surface flaws. To incorporate the appropriate strength variations into the

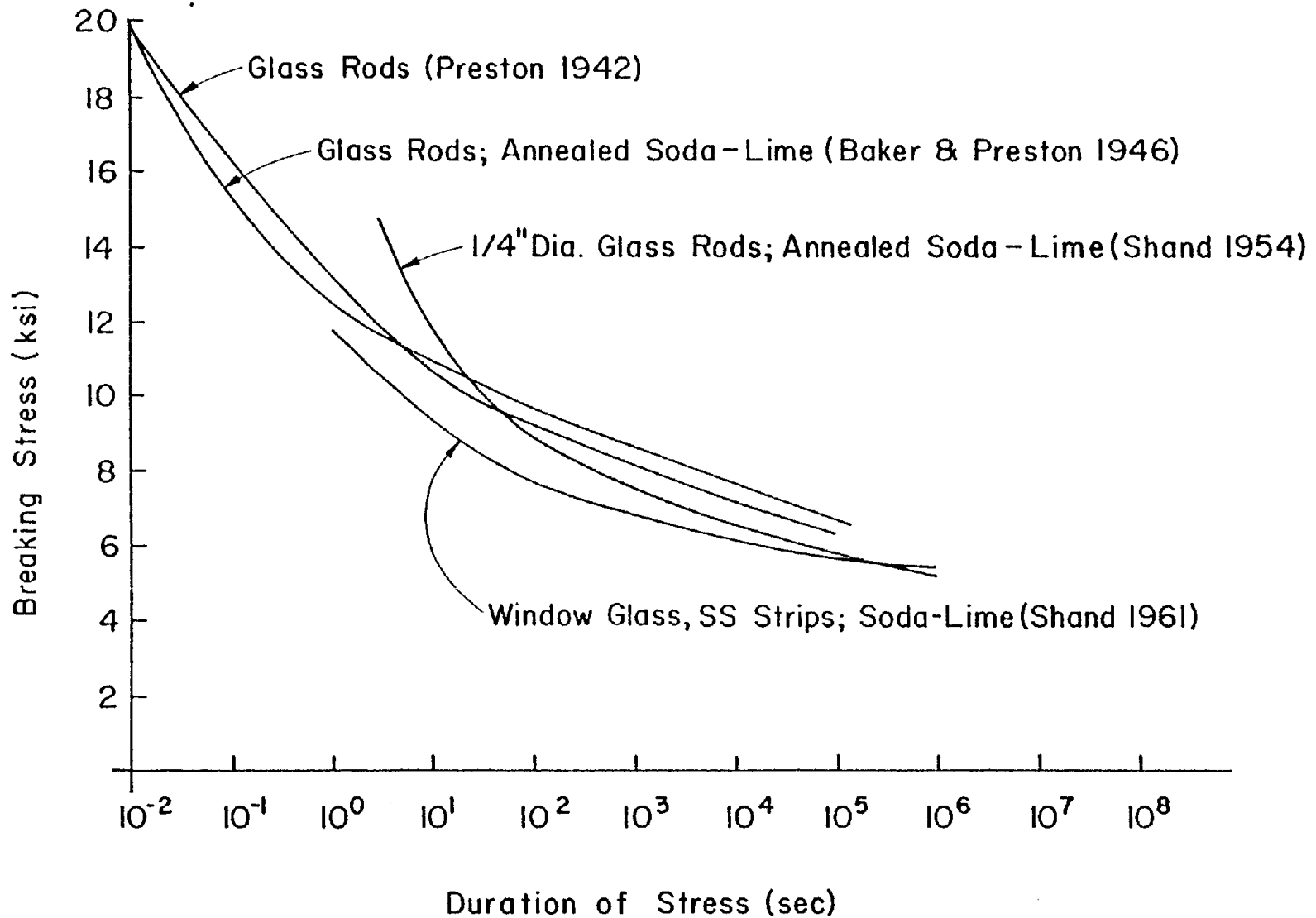
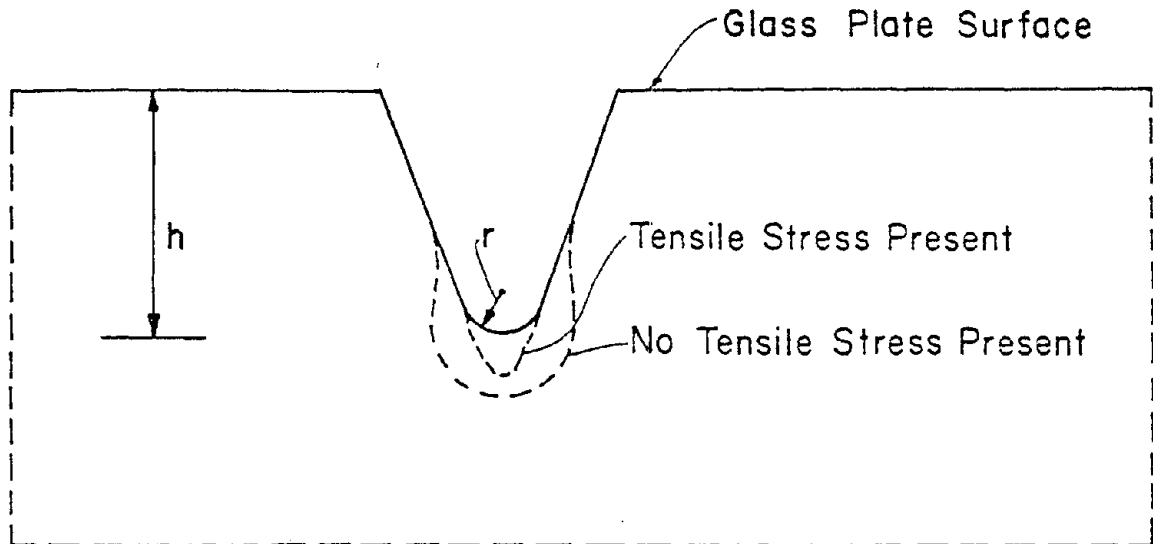


FIGURE 5. VARIATIONS OF GLASS STRENGTH WITH LOAD DURATION (Minor 1974)

failure prediction model, a relationship presented by Brown (1974) is used to relate strength variations to the surface flaw characteristics. The Brown formulation is an extension of previous research conducted by Charles (1958) and Wiederhorn (1967). Development of the Brown formulation is presented in this section.

The observed variations of glass strength are believed to be the result of the corrosion of the glass surface flaws (Charles 1958, Weiderhorn 1967, Brown 1974, Associate Committee of the National Building Code 1977). Flaw corrosion occurs as a result of the action of water on the glass surface. Corrosion of a flaw can change its depth, h , and flaw tip radius, r , as defined in Equation (3.1). If a flaw is exposed to water and tensile stress it is conjectured that the flaw radius, r , decreases and flaw depth, h , increases resulting in an increase in the stress raising potential of the flaw. If a flaw is exposed only to water then the flaw radius increases at a faster rate than the the flaw depth so that the net effect is a decrease in the stress raising potential of the flaw. These two flaw corrosion processes are illustrated in Figure 6.

Charles (1958) presented a theoretical development to model flaw corrosion which takes into account the rate of flaw corrosion as a function of the applied stress and the ambient temperature. Charles assumed that the rate of flaw depth corrosion, V_x , is related to the nominal tensile stress and temperature as follows



$$\sigma_m = \sigma_a K \left(\frac{h}{r} \right)^{\frac{1}{2}}$$

Both Tensile Stress and Water are Present

r Becomes Smaller

h Becomes Larger

Only Water is Present

r Becomes Larger

h Becomes Larger

FIGURE 6. CORROSION OF IDEALIZED SURFACE FLAW

$$V_x \propto \sigma^n \exp[-A/(RT)] \quad (3.2)$$

where σ is the tensile stress to which the flaw is exposed, A and n are constants, R is the universal gas constant, and T is the absolute temperature. If a flaw is subjected to a constant stress to failure, then the change of flaw depth, d , experienced by the flaw is related to the nominal tensile stress as follows

$$d \propto \sigma^n \exp[-A/(RT)] t_f \quad (3.3)$$

where t_f is the time to failure. If the change of flaw depth required to initiate failure is assumed to be independent of the stress level then the right-hand side of Equation (3.3) must be constant.

$$\text{constant} = \sigma^n \exp[-A/(RT)] t_f \quad (3.4)$$

Equation (3.5) can then be used to express the variation of failure stress as a function of load duration and temperature. Charles found experimentally that n is approximately equal to 16 and that A is approximately equal to 18.8 Kcal/Mole for window glass, when R is taken to be 1.986 Cal/Mole-°K and the absolute temperature, T , is given in °K.

Other researchers have developed empirical relationships to model the variation of the strength of glass with

load duration (Mould and Southwick 1959, Glathart and Preston 1946). The appearance of these empirical representations are substantially different than Equation (3.4). However, all of the available static fatigue relationships yield essentially the same results.

Wiederhorn (1967), investigating the effects of relative humidity on crack propagation velocity or flaw corrosion, concluded that the velocity of flaw depth corrosion is linearly related to the ambient relative humidity in a range of relative humidities from 10-100 percent. Therefore, Equation (3.4) can be rewritten to include the variation of glass strength with relative humidity as

$$\text{constant} = \text{RH } \sigma^n \exp[-A/(RT)] t_f \quad (3.5)$$

where RH is the relative humidity expressed as a decimal fraction and the other constants are as previously defined.

Recently Brown (1974) reexamined the work of Charles and others and concluded that a better representation of available strength data could be obtained if the expression for the rate of corrosion were modified. The resulting expression to model the variation of glass strength with load duration, temperature, and relative humidity is

$$\text{constant} = \int_0^{t_f} \text{RH}[\sigma(t)/T]^n \exp[-\gamma_0/(RT)] dt \quad (3.6)$$

where t_f is the time to failure, $\sigma(t)$ is the stress at the critical flaw as a function of time. Brown determined that the constant γ_0 is approximately equal to 25.0 Kcal/Mole using the data presented by Charles (1958), while the other constants maintained their original values. In addition to more closely representing available strength data, Equation (3.6) allows a time variant stress to be treated.

Equation (3.6) models the corrosion to failure of a surface flaw subjected to tensile stress. The constant value of Equation (3.6) represents a basic measure of the strength associated with a particular flaw. If the value of the constant is determined experimentally, the magnitude of stress required to fail the same flaw at a different temperature, relative humidity, and load duration can be calculated. The magnitude of the constant stress, $\tilde{\sigma}$, required to fail a particular flaw at a set of reference conditions is given by

$$\tilde{\sigma} = \left[\frac{\int_0^{t_f} RH [\sigma(t)/T]^n \exp[-\gamma_0/(RT)] dt}{t_r RH_r \exp[-\gamma_0/(RT_r)] T_r^{-n}} \right]^{\frac{1}{n}} \quad (3.7)$$

where the numerator is evaluated for the conditions at the time of the test and t_r , RH_r , and T_r are the reference load duration, relative humidity, and temperature.

The following steps can be used to calculate an equivalent constant failure load at reference conditions for a glass plate tested to failure under controlled conditions:

- (1) The failure initiation point on the glass plate is located using techniques explained in Appendix A.
- (2) The variation of stress with time at the failure initiation point is determined using experimental or theoretical techniques (Ref. Chapter IV).
- (3) The equivalent constant stress at the failure initiation point is then calculated using Equation (3.7).
- (4) Finally, using an experimental or theoretical technique the equivalent constant failure stress is related to the equivalent constant failure load.

Using this procedure the variations of strength due to humidity, temperature, and load duration can be removed from a data set. The strength characteristics of the modified data set are then applicable for the reference conditions.

CHAPTER IV
NONLINEAR ANALYSIS OF GLASS PLATES

The probability of failure of a glass plate subjected to a particular loading is dependent upon the glass plate surface flaw characteristics and the distribution of surface tensile stresses. A complete characterization of the surface tensile stresses is necessary to rigorously predict the probability of glass plate failure. An analysis technique is presented in this chapter to model the distribution of surface tensile stresses acting in a rectangular glass plate.

Glass plates commonly experience maximum deflections which are well in excess of their thickness prior to failure. When the deflections of a plate are of this magnitude, a geometrically nonlinear plate analysis must be used to model the plate response (Timoshenko 1959). When a plate experiences geometric nonlinearity the boundary restraints have a particularly significant effect upon the plate response. Because of the complexities involved with geometrically nonlinear plate analysis, coupled with the often unique nature of the boundary conditions associated with window glass installations, the problem of glass plate analysis has not been well addressed.

Plate solutions employing different boundary conditions are reviewed to determine the proper set of idealized boundary conditions to be used to model glass plates.

Boundary displacements of importance in relation to the glass plate problem are: lateral edge displacement, edge rotation, and in-plane edge displacement. These boundary displacements can be subject to varying degrees of restraint depending upon the nature of the window glass installation. It is shown through comparisons of experimental and analytical data that the case where the edges of the plate are simply supported and free to slip in-plane provides a reasonable approximation to actual window glass boundary conditions.

There are a limited number of plate solutions available which employ the proper boundary conditions. With the exception of recently reported finite element results (Moore 1979, Tsai and Stewart 1976), this problem has been treated only once, by Kaiser (1936). There are insufficient theoretical results available for use with the failure prediction model. Therefore, a geometrically nonlinear plate analysis for use with the failure prediction model is developed.

The geometrically nonlinear plate analysis presented in this section is developed using the von Karman nonlinear plate equations (Levy 1942). The von Karman equations are expressed in terms of lateral plate deflections and an Airy stress function. Use of the Airy stress function enables middle plane or membrane forces to be conveniently treated. Simultaneous solution of the two nonlinear plate

equations is obtained through use of an iterative technique coupled with a Galerkin method. This method of solution was chosen because reasonable estimates of plate deflections and stresses could be obtained using relatively small amounts of computation time.

Results of the nonlinear plate analysis are compared to available theoretical results that are presented in the literature. It is thus shown that results of the nonlinear plate solution are in agreement with available theoretical results. Further, it is shown that results of the nonlinear plate analysis agree reasonably well with available experimental glass plate data.

A. Review of Nonlinear Plate Solutions

When the maximum lateral deflection of a plate exceeds half of its thickness it experiences significant stretching of its middle surface. As a result, membrane forces are introduced into the plate. Classical linear plate theory ignores the presence of the membrane forces and therefore cannot be used to analyze glass plates. A geometrically nonlinear plate analysis which takes into account the action of membrane forces must be used to analyze glass plates.

The von Karman nonlinear plate equations were developed to model thin plates experiencing large deflections (Timoshenko 1959). However, the lateral plate deflections

should remain small with respect to the rectangular dimensions of the plate or assumptions employed in development of the von Karman equations will be violated (Szilard 1974). Window glass plates usually fail before their lateral deflections exceed the limitations of the von Karman equations. The von Karman equations along with other fundamental plate formulations are reviewed in this section.

Most glass installations are designed so that the lateral deflection of the plate edge is limited and usually there is little or no rotational restraint at the plate edge. Therefore, a simply supported edge condition is assumed to be reasonably typical of window glass plates. Development of membrane action in a simply supported plate is highly sensitive to the degree of in-plane edge restraint provided. Therefore, plate solutions employing different degrees of idealized in-plane edge restraint are reviewed. Central deflections determined for simply supported plates with different degrees of in-plane restraint are compared to central deflections measured in a well-documented set of glass plate tests (Bowles and Sugarman 1962). It is shown that the case of a simply supported plate with edges free to slip in-plane closely approximates glass plate response.

1. Review of Nonlinear Plate Equations

The von Karman nonlinear plate equations as presented by Levy (1942) using rectangular coordinates are

$$\frac{\partial^4 F}{\partial x^4} + 2 \frac{\partial^4 F}{\partial x^2 \partial y^2} + \frac{\partial^4 F}{\partial y^4} = E \left[\left(\frac{\partial^2 w}{\partial x \partial y} \right)^2 - \frac{\partial^2 w}{\partial x^2} \frac{\partial^2 w}{\partial y^2} \right] \quad (4.1)$$

$$D \left(\frac{\partial^4 w}{\partial x^4} + 2 \frac{\partial^4 w}{\partial x^2 \partial y^2} + \frac{\partial^4 w}{\partial y^4} \right) = P_z + h \left(\frac{\partial^2 F}{\partial y^2} \frac{\partial^2 w}{\partial x^2} + \frac{\partial^2 F}{\partial x^2} \frac{\partial^2 w}{\partial y^2} - 2 \frac{\partial^2 F}{\partial x \partial y} \frac{\partial^2 w}{\partial x \partial y} \right) \quad (4.2)$$

where w is the lateral plate deflection, F is an Airy stress function, D is the flexural rigidity of the plate, h is the plate thickness, P_z is the lateral load acting on the plate and E is the modulus of elasticity of the plate. An appropriate rectangular coordinate axis is presented in Figure 7. The flexural rigidity, D , of the plate is given by

$$D = \frac{Eh^3}{12(1-\nu^2)} \quad (4.3)$$

where ν is the Poisson's ratio of the plate.

The Airy stress function, F , is related to the membrane stresses, σ_x' , σ_y' , σ_{xy}' , by the following relationships

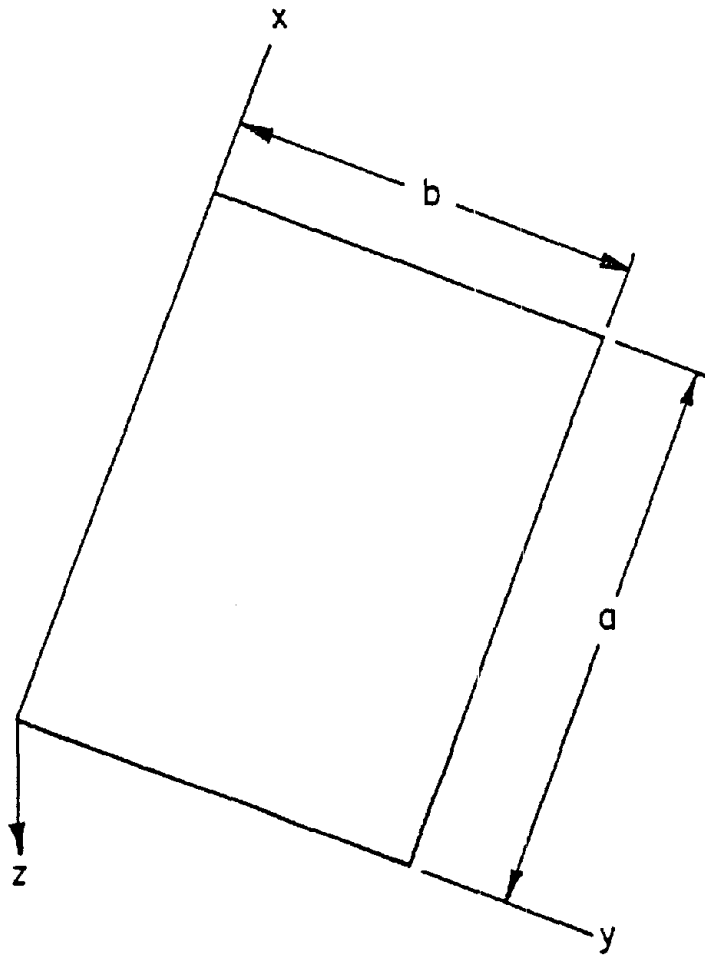


FIGURE 7. RECTANGULAR PLATE COORDINATE SYSTEM

$$\sigma_x' = \frac{\partial^2 F}{\partial y^2} \quad (4.4)$$

$$\sigma_y' = \frac{\partial^2 F}{\partial x^2} \quad (4.5)$$

$$\tau_{xy}' = - \frac{\partial^2 F}{\partial x \partial y} \quad (4.6)$$

The bending moments per unit length in the plate are given by

$$m_x = -D \left(\frac{\partial^2 w}{\partial x^2} + \mu \frac{\partial^2 w}{\partial y^2} \right) \quad (4.7)$$

$$m_y = -D \left(\frac{\partial^2 w}{\partial y^2} + \mu \frac{\partial^2 w}{\partial x^2} \right) \quad (4.8)$$

$$m_{xy} = D (1-\mu) \left(\frac{\partial^2 w}{\partial x \partial y} \right) \quad (4.9)$$

where m_x is the moment per unit length in the x direction, m_y is the moment per unit length in the y direction, and m_{xy} is the twist per unit length in the x-y plane. The extreme fiber bending and shearing stresses acting in the plate are given by

$$\sigma_x'' = -\frac{6D}{h^2} \left(\frac{\partial^2 w}{\partial x^2} + \mu \frac{\partial^2 w}{\partial y^2} \right) \quad (4.10)$$

$$\sigma_y'' = -\frac{6D}{h^2} \left(\frac{\partial^2 w}{\partial y^2} + \mu \frac{\partial^2 w}{\partial x^2} \right) \quad (4.11)$$

$$\tau_{xy}'' = -\frac{6(1-\nu)D}{h^2} \left(\frac{\partial^2 w}{\partial x \partial y} \right) \quad (4.12)$$

The total extreme fiber stresses in the plate are found by adding the membrane and bending stresses as follows

$$\sigma_x = \sigma_x' + \sigma_x'' \quad (4.13)$$

$$\sigma_y = \sigma_y' + \sigma_y'' \quad (4.14)$$

$$\tau_{xy} = \tau_{xy}' + \tau_{xy}'' \quad (4.15)$$

In addition to lateral displacements a rectangular plate can experience in-plane edge displacements depending upon the plate boundary conditions. The in-plane edge displacements perpendicular to the plate edges in the x and y directions are given by u and v, respectively. To calculate an in-plane edge displacement, u, in the x direction at a point on the edge of the plate, components of in-plane edge displacements due to both middle plane strain and plate curvature across the width of the plate must be considered. The in-plane edge displacement in the x direction at a given point on the edge of a plate is given as follows

$$u = \int_0^a \left[\frac{1}{E} \left(\frac{\partial^2 F}{\partial y^2} - \nu \frac{\partial^2 F}{\partial x^2} \right) - \frac{1}{2} \left(\frac{\partial w}{\partial x} \right)^2 \right] dx \quad (4.16)$$

where a is the plate dimension in the x direction. Likewise, the in-plane edge displacement in the y direction at a given point on the edge of the plate is given by

$$v = \int_0^b \left[\frac{1}{E} \left(\frac{\partial^2 F}{\partial x^2} - \mu \frac{\partial^2 F}{\partial y^2} \right) - \frac{1}{2} \left(\frac{\partial w}{\partial y} \right)^2 \right] dy \quad (4.17)$$

where b is the plate dimension in the y direction.

2. Nonlinear Plate Solutions for Simply Supported Rectangular Plates

Nonlinear plate solutions with simply supported edges and different degrees of in-plane edge restraints are reviewed in this section. Solutions employing the following three different types of idealized boundary conditions are reviewed:

- (1) simply supported edges which are restrained from in-plane displacement,
- (2) simply supported edges which are free to slip in-plane, but constrained to remain straight, and
- (3) simply supported edges which are free to slip in-plane.

The first and third sets of idealized boundary conditions offer the most and least in-plane edge restraint, respectively. Therefore, the in-plane restraint of window glass boundaries should be between these two extremes.

Timoshenko (1959) presented an approximate solution to Equations (4.1) and (4.2), for the case of a simply supported plate with in-plane edge displacement prevented. Timoshenko assumed that the bending and membrane actions of the plate could be decoupled. This was achieved by combining independent solutions for plates experiencing only membrane action and for plates experiencing only bending. Development of the Timoshenko approximate solution for a square plate is outlined below.

The two differential equations representing only membrane action in a plate are found by setting the flexural rigidity term to zero in Equations (4.1) and (4.2), yielding

$$\frac{\partial^4 F}{\partial x^4} + 2 \frac{\partial^4 F}{\partial x^2 \partial y^2} + \frac{\partial^4 F}{\partial y^4} = E \left[\left(\frac{\partial^2 w}{\partial x \partial y} \right)^2 - \frac{\partial^2 w}{\partial x^2} \frac{\partial^2 w}{\partial y^2} \right] \quad (4.18)$$

$$h \left(\frac{\partial^2 F}{\partial y^2} \frac{\partial^2 w}{\partial x^2} + \frac{\partial^2 F}{\partial x^2} \frac{\partial^2 w}{\partial y^2} - 2 \frac{\partial^2 F}{\partial x \partial y} \frac{\partial^2 w}{\partial x \partial y} \right) = -P_z \quad (4.19)$$

Simultaneous solution of Equations (4.18) and (4.19) results in the following expression for the central deflection, w_0 , of a square membrane with a Poisson's ratio of 0.25 and with sides of length $2a$

$$w_0 = 0.802 a \sqrt[3]{\frac{q_m a}{Eh}} \quad (4.20)$$

where q_m is the uniform load to which the membrane is exposed.

The well-known differential equation for plate bending is found by setting the Airy stress function to zero in Equation (4.2) yielding

$$D \left(\frac{\partial^4 w}{\partial x^4} + 2 \frac{\partial^4 w}{\partial x^2 \partial y^2} + \frac{\partial^4 w}{\partial y^4} \right) = P_z \quad (4.21)$$

Solution of Equation (4.21) results in the following expression for the central deflection, w_o , of a square plate with sides of length $2a$ and with a Poisson's ratio of 0.25

$$w_o = 0.730 \frac{q_b a^4}{Eh^3} \quad (4.22)$$

where q_b is the uniform load to which the plate is subjected.

Equations (4.20) and (4.22) can be rewritten as

$$q_m = \frac{w_o^3 Eh}{0.516 a^4} \quad (4.23)$$

$$q_b = \frac{w_o Eh^3}{0.730 a^4} \quad (4.24)$$

Using the principle of superposition the total load, q , required to induce a maximum central deflection of w_o in a plate capable of both membrane and bending action is approximated as

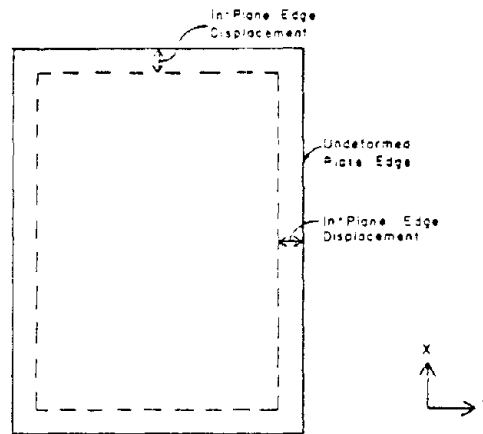
$$q = \frac{w_o Eh^3}{0.730a^4} + \frac{w_o^3 Eh}{0.516a^4} \quad (4.25)$$

Equation (4.25) is an approximate load deflection relationship for the case of a simply supported square plate with in-plane movement of the edges prevented.

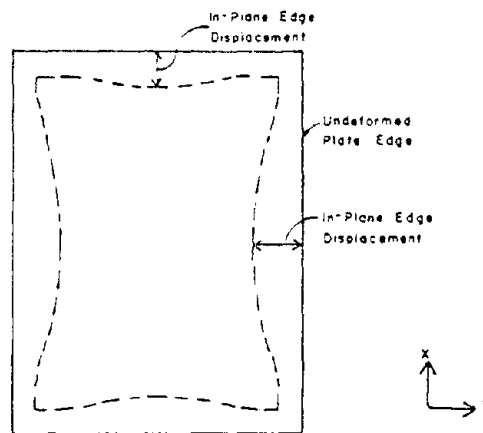
Levy (1942) presented two exact solutions for simply supported rectangular plates exposed to uniform lateral loads. In the first solution, in-plane edge displacements were prevented by applying an appropriate in-plane force normal to the plate boundary. These boundary conditions are equivalent to those assumed by Timoshenko (1959) in the previously discussed approximate solution.

In the second Levy (1942) solution, the in-plane force normal to the plate boundary was set to zero allowing some in-plane displacement of the plate edges. However, the edges of the plate in the second solution were constrained to remain straight. In-plane edge displacements of a rectangular plate subject to the second set of constraints are shown in Figure 8. This pattern of in-plane edge displacements can occur only if the plate edges are rigidly stiffened (Timoshenko 1959). The first set of Levy boundary conditions represents the most rigid condition for a simply supported plate while the second set of Levy boundary conditions represents a less rigid situation.

To achieve a situation where the edges of the plate are totally free to slip in-plane, the in-plane forces both



(a) In-Plane Edge Displacements Where Plate Edges Are Free to Slip In-Plane and Constrained to Remain Straight



(b) In-Plane Edge Displacements Where Plate Edges Are Totally Free to Slip

FIGURE 8. IDEALIZED IN-PLANE DISPLACEMENTS OF PLATE EDGES

normal and tangent to the plate boundary must be zero. Kaiser (1936) presented a finite difference solution to the von Karman equations for this situation. Kaiser assumed that both the normal and shear membrane stresses along the plate boundary were zero assuring that no in-plane boundary reactions could be transmitted to the plate. In this situation in-plane edge displacements along the plate boundary are not constant as they were in the second Levy solution (Kaiser 1936, Timoshenko 1959, Moore 1979). In-plane deflections along a plate edge vary from a minimum at the plate corners to a maximum at the midpoint between two plate corners as shown in Figure 8. This combination of boundary conditions represents the most flexible condition for a simply supported plate.

3. Comparison of Nonlinear Plate Solutions to Actual Glass Plate Behavior

Comparisons of calculated and actual glass plate lateral deflection data are made in this section. These comparisons are made so that the best set of idealized boundary conditions to model glass plates can be selected. A particularly well-documented set of glass plate data presented by Bowles and Sugarman (1962) is used to represent the behavior of glass plates.

Bowles and Sugarman (1962) presented the following empirical relationship between load and central deflection for square glass plates

$$\frac{P}{16E} \left(\frac{\lambda}{h}\right)^4 = 1.37 \left(\frac{\delta}{h}\right) + 0.17 \left(\frac{\delta}{h}\right)^3 \quad (4.26)$$

where P is the uniform load, λ is the length of a side, δ is the central plate deflection, h is the plate thickness, and E is the modulus of elasticity of the plate. Equation (4.26) is of the same form as the approximate relationship, Equation (4.25), presented by Timoshenko (1959). The first term on the right side of Equation (4.26) represents the bending action of a plate and follows directly from Equation (4.25). The second term on the right side of Equation (4.26) represents the membrane action of the plate. The constant associated with the second term was selected so that Equation (4.26) would closely represent the measured results of several hundred glass plate tests.

Figure 9 presents a comparison of the theoretical load-deflection curves for simply supported plates with varying degrees of in-plane restraint with the empirical load-deflection relationship presented by Bowles and Sugarman (1962). It is clear from an examination of Figure 9 that the degree of in-plane restraint provided at the boundary of a simply supported plate has a highly significant effect upon the plate rigidity. Comparison of the load-deflection curves presented in Figure 9 show that the Kaiser (1936) load deflection curve is very similar to the Bowles and Sugarman empirical load-deflection curve. Further, experimental measurements presented by Anians

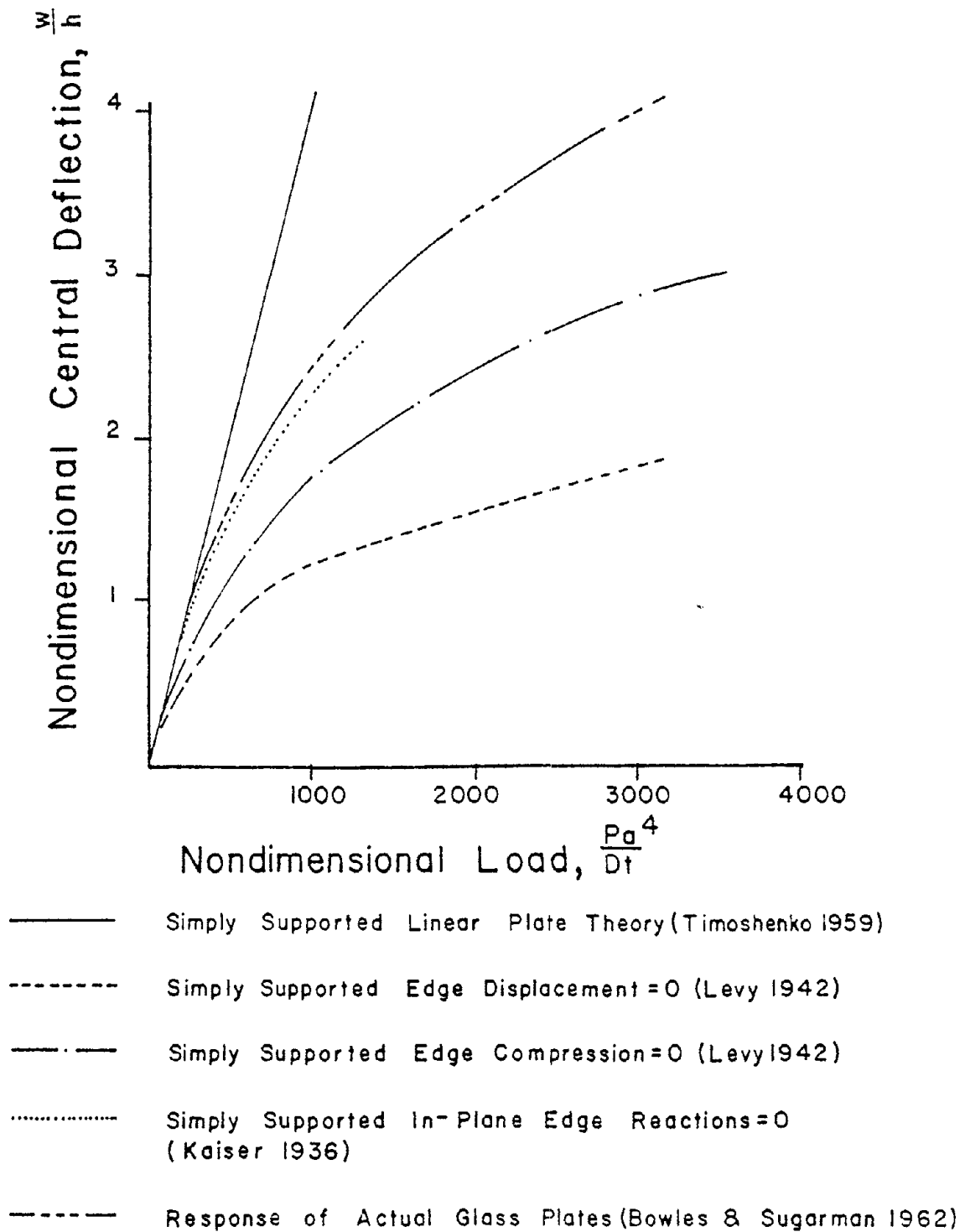


FIGURE 9. COMPARISONS OF CENTRAL DEFLECTIONS OF SQUARE PLATES WITH DIFFERENT BOUNDARY CONDITIONS

(1979) show that actual in-plane displacement of the edges of a glass plate are similar to those predicted by the Kaiser (1936) solution (Ref. Fig. 8). These facts combine to suggest that a glass plate is best modeled by assuming that the plate edges are simply supported and free to slip in-plane.

B. Development of Nonlinear Plate Solution

Results of nonlinear plate solutions which employed the boundary conditions selected to model glass plates were reviewed (Kaiser 1936, Tsai and Stewart 1976, Moore 1979, Al-Tayyib 1980). However, insufficient theoretical results are available for use with the failure prediction model. Therefore, a nonlinear plate analysis is developed.

Nonlinear plate solutions can be developed using several available methods (Szilard 1974). The finite element method is currently one of the most popular analysis techniques. The finite element method relies heavily on matrix manipulation and is usually formulated in general terms so that a variety of different problems can be solved. However, solutions of geometrically nonlinear problems using matrix formulations characteristically require large amounts of computation time. An alternative solution technique presented by Szilard was chosen for use in the nonlinear plate solution. The Szilard solution technique employs an iterative procedure to achieve a simultaneous

solution to the von Karman nonlinear plate equations. The nonlinear plate analysis thus developed requires significantly less computation time than a finite element analysis.

Formulation of the nonlinear plate solution is presented in this section. In addition, calculated stresses and deflections obtained from the nonlinear plate solution are compared to independent theoretical results to establish validity of the solution.

1. Formulation of Non-linear Plate Solution

Equations (4.1) and (4.2) are the governing differential equations for thin plates experiencing large lateral deflections. The nonlinear plate solution presented herein employs an iterative technique whereby Equations (4.1) and (4.2) are solved by alternately assuming the lateral deflection to be constant in Equation (4.1) and the membrane stress function to be constant in Equation (4.2). Individual solutions of the two nonlinear plate equations are accomplished using a Galerkin method and numerical integration. This solution technique is outlined by Szilard (1974).

Application of the Galerkin method to Equations (4.1) and (4.2) results in the following equations (Szilard 1974)

$$\iint_A \left[\frac{1}{h} \left(\frac{\partial^4 F}{\partial x^4} + 2 \frac{\partial^4 F}{\partial x^2 \partial y^2} + \frac{\partial^4 F}{\partial y^4} \right) - \left(\frac{\partial^2 w}{\partial x \partial y} \right)^2 + \frac{\partial^2 w}{\partial x^2} \frac{\partial^2 w}{\partial y^2} \right] \cdot$$

$$\delta F \, dx dy = 0 \quad (4.27)$$

$$\iint_A \left[\frac{D}{h} \left(\frac{\partial^4 w}{\partial x^4} + 2 \frac{\partial^4 w}{\partial x^2 \partial y^2} + \frac{\partial^4 w}{\partial y^4} \right) - \left(\frac{\partial^2 F}{\partial^2 y} \frac{\partial^2 w}{\partial x^2} + \frac{\partial^2 F}{\partial x^2} \frac{\partial^2 w}{\partial y^2} - \right. \right. \\ \left. \left. - 2 \frac{\partial^2 F}{\partial x \partial y} \frac{\partial^2 w}{\partial x \partial y} \right) - \frac{1}{h} P_z \right] \delta w \, dx dy = 0 \quad (4.28)$$

Infinite series are employed to represent the lateral plate deflection, w , the membrane stress function, F , and the lateral loading, P_z . Selections of the infinite series to represent the lateral deflections and the membrane stress function are made such that all the boundary conditions are satisfied. Consistent with the conclusion of section IV.A, the following three boundary conditions are assumed in the nonlinear plate solution:

- (1) the lateral deflections of the plate along the boundary are zero,
- (2) the bending moments normal to the plate edge are zero, and
- (3) the in-plane plate reactions at the boundary are zero.

The first two boundary conditions presented above can be stated as

$$\begin{aligned}
 w = 0 \quad m_x = 0 \quad & \text{for } x = 0 \text{ and } x = a \\
 w = 0 \quad m_y = 0 \quad & \text{for } y = 0 \text{ and } y = b \quad (4.29)
 \end{aligned}$$

Taking the coordinate axes as shown in Figure 7, the above boundary conditions are satisfied if the following expression for lateral deflection is used

$$w(x,y) = \sum_{m=1,3,\dots}^K \sum_{n=1,3,\dots}^L w_{mn} \sin \frac{m\pi x}{a} \sin \frac{n\pi y}{b} \quad (4.30)$$

where w_{mn} is a coefficient chosen to satisfy the nonlinear plate equations, a is the plate dimension in the x direction, and b is the plate dimension in the y direction, K and L are the maximum indices for the lateral deflection coefficients.

For the plate boundary to have zero in-plane reactions the boundary of the plate must be free of both normal and shear membrane stresses or

$$\begin{aligned}
 \sigma_x' = 0 \quad \tau_{xy}' = 0 \quad & \text{for } x = 0 \text{ and } x = a \\
 \sigma_y' = 0 \quad \tau_{xy}' = 0 \quad & \text{for } y = 0 \text{ and } y = b \quad (4.31)
 \end{aligned}$$

These boundary conditions are satisfied if the membrane stress function is represented by

$$F(x,y) = \sum_{m=2,4,\dots}^I \sum_{n=2,4,\dots}^J F_{mn} \left(1 - \cos \frac{m\pi x}{a}\right) \left(1 - \cos \frac{n\pi y}{b}\right) \quad (4.32)$$

where F_{mn} is a coefficient chosen to satisfy the nonlinear plate equations and I and J are the maximum indices for the membrane stress function coefficients. The functions in the expansion of Equation (4.32) are not orthogonal; hence, care must be taken to include all cross product terms in formulation of the solution that would otherwise vanish.

The following expression is used to represent the uniform lateral load

$$P_z(x, y) = \sum_{m=1,3 \dots}^K \sum_{n=1,3 \dots}^L \frac{16P}{\pi^2 mn} \sin \frac{m\pi x}{a} \sin \frac{n\pi y}{b} \quad (4.33)$$

where P is the magnitude of the uniform lateral load.

To formulate the nonlinear plate solution, the expressions for the lateral deflections, the lateral loads, and the membrane stress function must be substituted into Equation (4.27) and (4.28). This substitution results in two sets of nonlinear simultaneous equations both in terms of unknown lateral deflection coefficients, w_{ij} 's, and unknown membrane stress function coefficients, F_{ij} 's. Mechanics of this substitution are presented in Appendix B. The number of simultaneous equations generated from Equations (4.27) or (4.28) is the same as the number of series terms used in the lateral deflection expression or the membrane stress function expression, respectively. For simplicity, an equal number of series terms were used for each equation.

Szilard (1974) presented the following iterative procedure to estimate the unknown coefficients:

- (1) A set of lateral deflection coefficients are assumed.
- (2) Using the assumed lateral deflection coefficients a corresponding set of membrane stress function coefficients are determined using the nonlinear equations generated from expression (4.28).
- (3) Using the set of membrane stress function coefficients calculated in step (2), a new set of lateral deflection coefficients are determined using the nonlinear equations generated from expression (4.27).
- (4) Steps (2) and (3) are repeated until satisfactory convergence is achieved.

Convergence of the coefficients using this method can be slow or impossible depending upon the quality of the initial assumptions and upon the degree of nonlinearity experienced by the plate.

To improve convergence of the iteration described above, an under-relaxation of the lateral deflection coefficients was incorporated into the Szilard iteration scheme. In addition, checks were installed in the iteration procedure to detect divergence of the lateral deflection coefficients. If divergence is detected the original lateral deflection coefficients are suitably modified

and the iteration is reinitiated. A logic flowchart for the iteration procedure thus developed is presented in Figure 10. This modified iteration procedure converges much quicker than the iteration procedure outlined by Szilard (1974).

A computer program was developed to perform the nonlinear plate analysis as described in this section. The program is written in the standard ANSI Fortran computer language. Input to the computer program consists of the number of expansion terms to be employed in the various expressions, the elastic material properties, the plate geometry, the magnitude of the uniform lateral load, the convergence criteria, the number of numerical integration divisions, and the initial values of the lateral deflection coefficients. A copy of the computer program along with input/output instructions is provided in Appendix C.

2. Validity of Nonlinear Plate Solution

Results of four different nonlinear plate analyses which employed the proper boundary conditions were reviewed in the course of this research (Kaiser 1936, Tsai and Stewart 1976, Moore 1979, Al-Tayyib 1980). Results presented by these researchers include both stresses and lateral deflections. Each of these analyses including the one presented herein are based upon numerical techniques and are

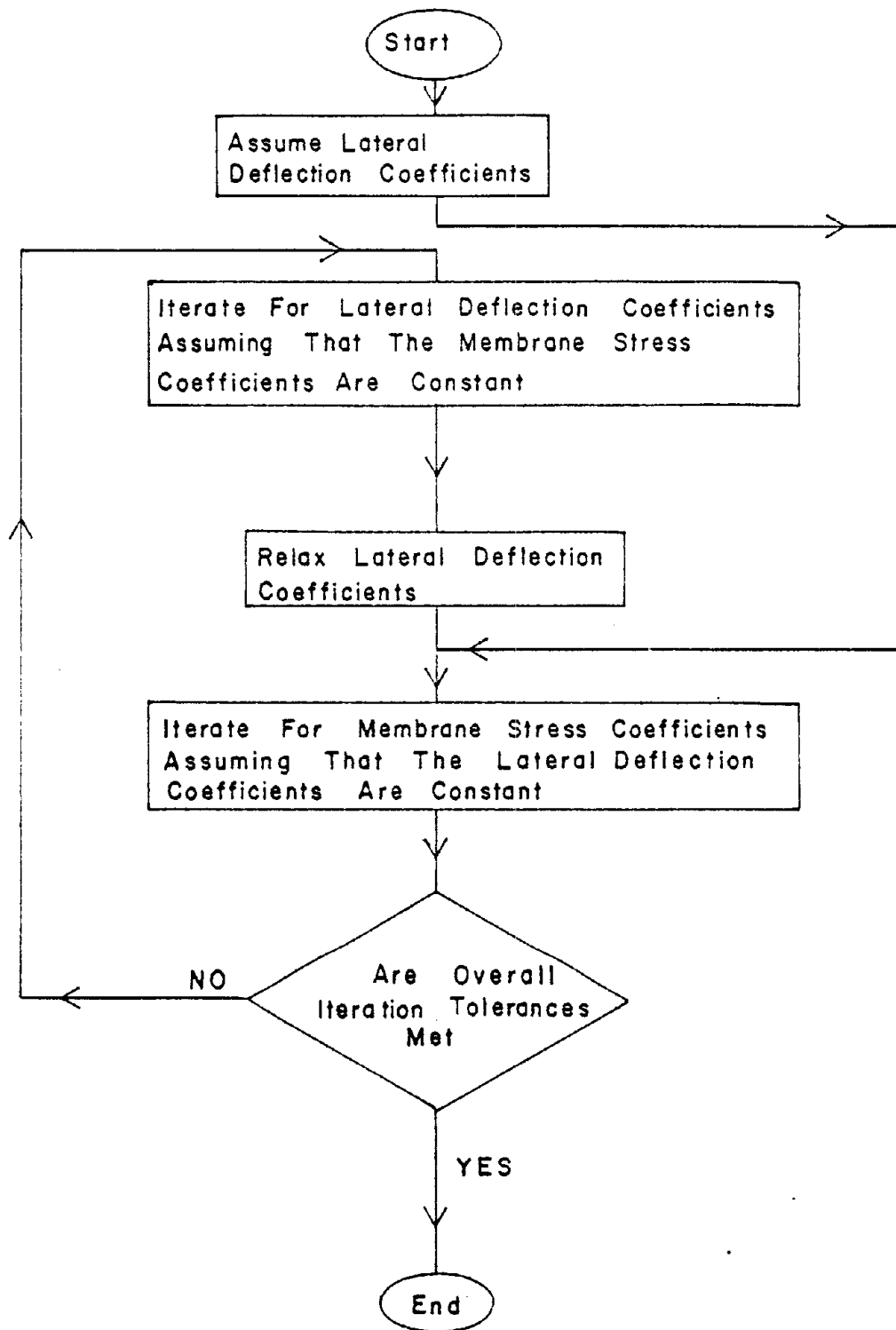


FIGURE 10. LOGIC FLOW CHART FOR NONLINEAR PLATE SOLUTION

subject to varying amounts of error depending upon the solution technique. Comparisons of central stresses and central deflections generated in the independent stress analyses reviewed reveals a reasonably good agreement (Moore 1979, Al-Tayyib 1980). Results presented by Kaiser (1936) were chosen to compare to results of the nonlinear analyses presented herein because Kaiser presented individual variations of bending and membrane stresses at the center of the plate instead of the variation of the combined stresses. The Kaiser (1936) results were presented for a square plate with a Poisson's ratio of 0.303.

Results for comparison to the Kaiser (1936) results were generated with the nonlinear plate analysis using four series terms to represent the lateral loading, the lateral deflection, and the membrane stress function. The numerical integrations were performed with the plate divided into 64 discrete zones. The convergence criteria for the lateral displacement coefficients was taken to be 0.01 in. More stringent criteria may be required to adequately represent the variations of stresses and deflections at different points on the plate or for different plate problems. It is strongly recommended that convergence studies be conducted for each type of problem considered. Reasonably good comparisons with central plate data presented by Kaiser are achieved with the above criteria.

Figure 11 presents the variations of central deflection with load as calculated by Kaiser (1936) using finite difference techniques and as calculated using the nonlinear plate analysis presented herein. It can be seen that the comparison is good. Good comparisons of lateral deflection results are to be expected because the displacement variable appears directly in the differential equations.

Figure 12 presents the variation of central stress with load as presented by Kaiser (1936) and as calculated using the nonlinear plate solution. Four load-stress curves are presented: the extreme fiber bending stress, the membrane stress, the total extreme fiber stress on the concave surface of the plate, and the stress present on the convex surface of the plate. The center of a symmetrically loaded square plate experiences no shear stresses, so that the stresses presented in Figure 12 are independent of orientation. Comparisons of the load-stress curves are good, but not as good as the central deflection comparisons. This is because stress is related through second order derivatives to the lateral displacement and membrane stress functions. Therefore, it is to be expected that calculated stresses should be less accurate than calculated deflections. This is true for both the Kaiser solution and the nonlinear plate solution presented herein.

Based upon favorable comparisons of calculated stresses and deflections with those presented by Kaiser (1936)

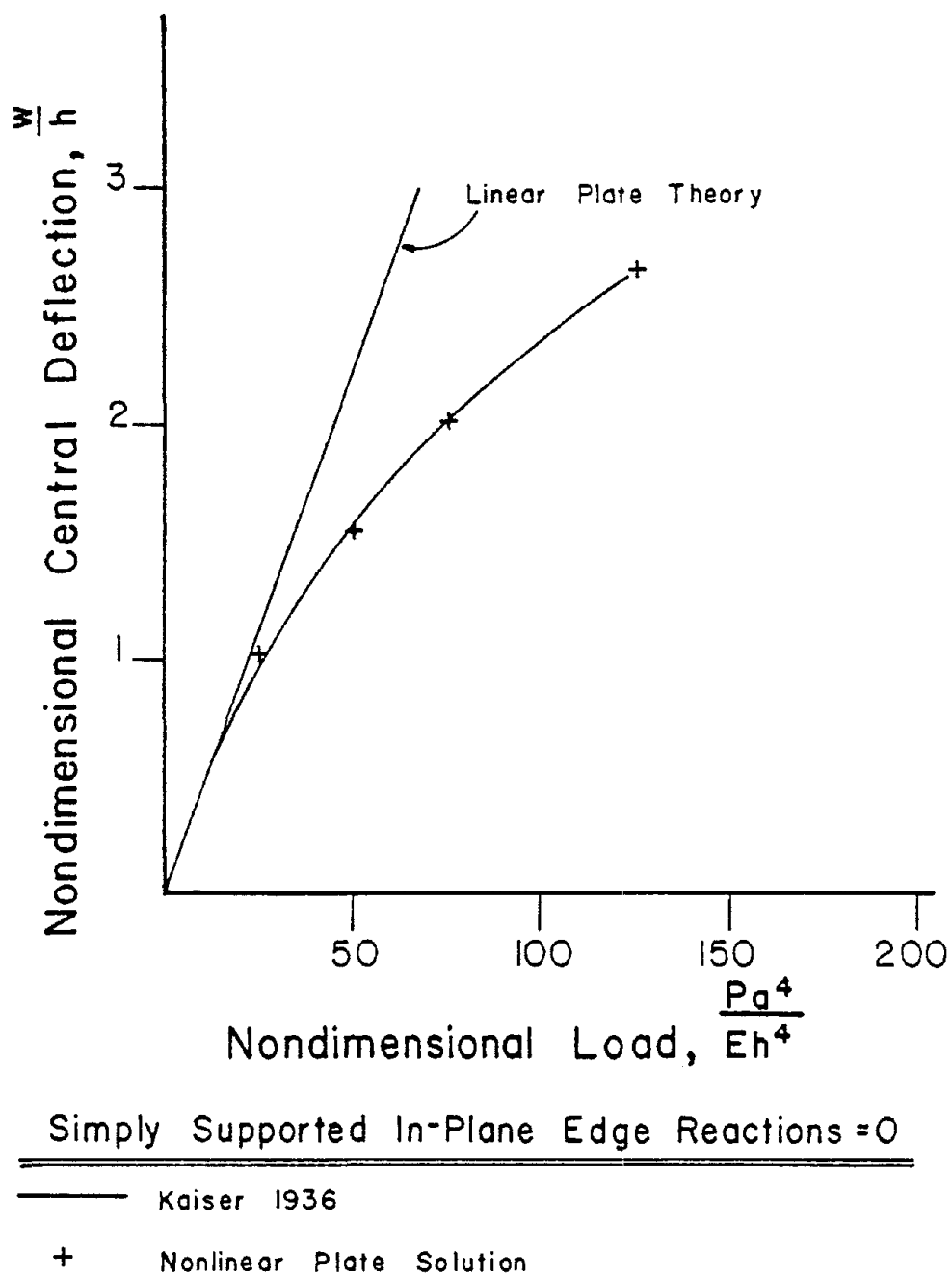
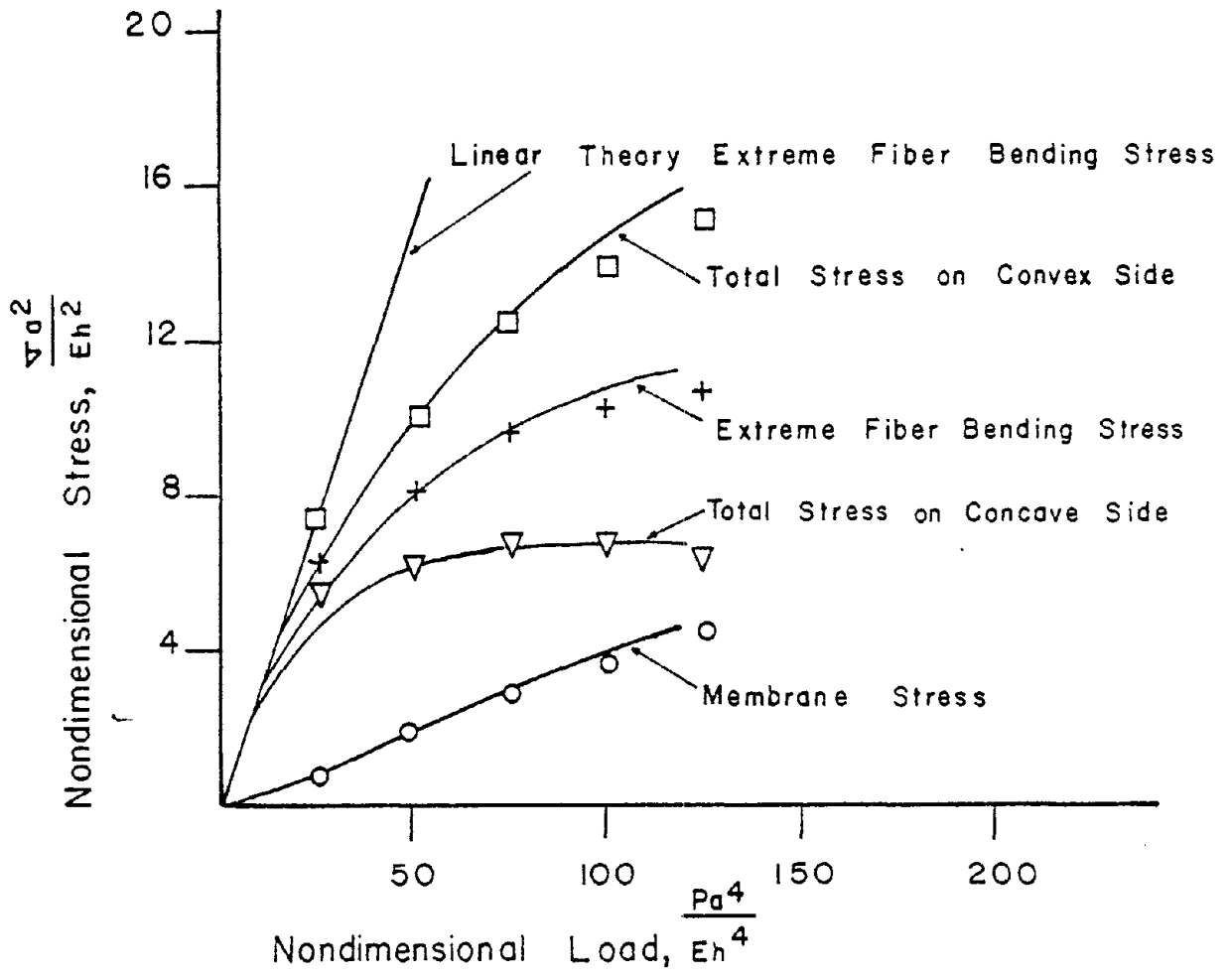


FIGURE 11. CENTRAL DEFLECTIONS OF SIMPLY SUPPORTED SQUARE PLATE WITH ZERO IN-PLANE REACTIONS



Simply Supported In-Plane Edge Reactions=0

— (Kaiser 1936)

$\circ, \nabla, +, \square$ Nonlinear Plate Solution

FIGURE 12. CENTRAL STRESSES OF SIMPLY SUPPORTED SQUARE PLATE WITH ZERO IN-PLANE REACTIONS

it is concluded that the nonlinear plate analysis models the case of a simply supported rectangular plate with no in-plane restraint at the boundary. If the program is used to calculate stresses for other plate problems, care should be taken to be sure that enough expansion terms and integration divisions are taken to adequately model the situation in question.

C. Comparison of Results of Nonlinear Plate Solution to Glass Test Results

In the previous section a nonlinear plate analysis was presented to model the response of a simply supported plate with in-plane movement of the edges allowed. In this section comparisons are made between computed stresses and deflections and those measured experimentally on glass plates of different aspect ratios. Several researchers have reported experimental results for glass plates mounted in different laboratory test rigs (Orr 1957, Bowles and Sugarman 1962, Ishizaki 1972, Hershey and Higgins 1973, Tsai and Stewart 1976). The edges of glass plates mounted in each of the different test rigs were supported on all sides with neoprene bearing surfaces supported by relatively rigid frames. With such a support system the glass plate edges experienced limited lateral displacements and relatively small amounts of rotational restraints. These support conditions were chosen by the various researchers to represent, in a practical sense, actual window installations.

The first full-scale glass plate strength tests found in the literature were presented by Orr (1957). The significance of the tests performed by Orr with respect to current glass strength charts is discussed in Chapter II. Orr tested twenty large glass plates to destruction with thicknesses ranging from 0.114 to 0.383 in., with areas ranging from 47 to 80 sq ft and with aspect ratios ranging from 1:1 to 1:1.67. Pertinent results presented by Orr consist of load deflection curves for the different glass plates tested.

Bowles and Sugarman (1962) presented a very extensive set of experimental results concerning tests to failure of 41 in. x 41 in. glass plates. The square glass plates ranged in thickness from 0.122 in. to 0.373 in. and were exposed to monotonically increasing uniform pressures resulting in failure in around 30 seconds. Complete load-deflection records were kept for each plate tested. Based upon an approximate analysis presented by Timoshenko (1959), Bowles and Sugarman developed Equation (4.26) which relates the central deflection of a square plate to the applied uniform lateral load. In addition, Bowles and Sugarman presented central plate stresses determined through use of strain gages for both the concave and convex surfaces of the different glass plates.

Ishizaki (1972) extended the work of Bowles and Sugarman (1962) to develop an empirical load-deflection rela-

tionship for rectangular glass plates. The empirical equation developed by Ishizaki is

$$\frac{p}{E} = \frac{\lambda}{C_1^3} \left(\frac{\delta}{a} \right)^3 + \frac{\lambda^3}{C_3(1-\mu^2)} \left(\frac{\delta}{a} \right) \quad (4.34)$$

where p is the uniform lateral load, E is the modulus of elasticity, λ is the ratio of the plate thickness to the length of the shorter side of the plate, a is half the length of the shorter side, μ is the Poisson's ratio of the glass plate, and C_1 and C_3 are constants which depend upon the plate aspect ratio. Values of the constants C_1 and C_3 suggested by Ishizaki (1972) for rectangular glass plates of different aspect ratios are presented in Figure 13. These values were determined based on results of tests conducted on large glass plates ranging in thickness from 4 to 5 mm, ranging in aspect ratio from 1:1 to 1:2.5, and ranging in area from 1 m² to 4 m².

Hershey and Higgins (1973) developed a statistical model to estimate the probability of breakage of glass plates exposed to sonic boom overpressures. In the final report submitted to the Federal Aviation Administration, data obtained from the Libbey-Owens-Ford Company was presented to quantify glass strength. In this glass test series 2513 large glass plates were tested to failure in 119 different sizes. The mean bursting pressure and associated central deflection for each of the 119 test series were presented.

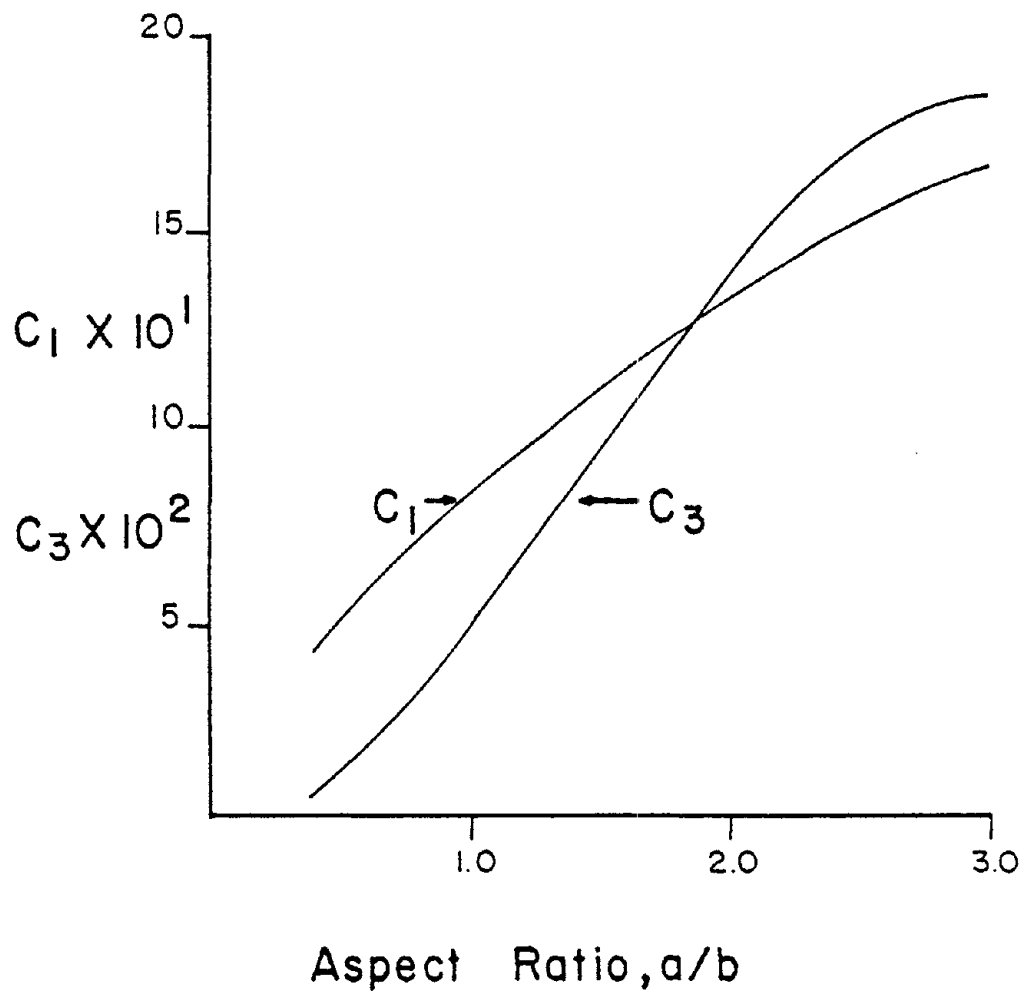
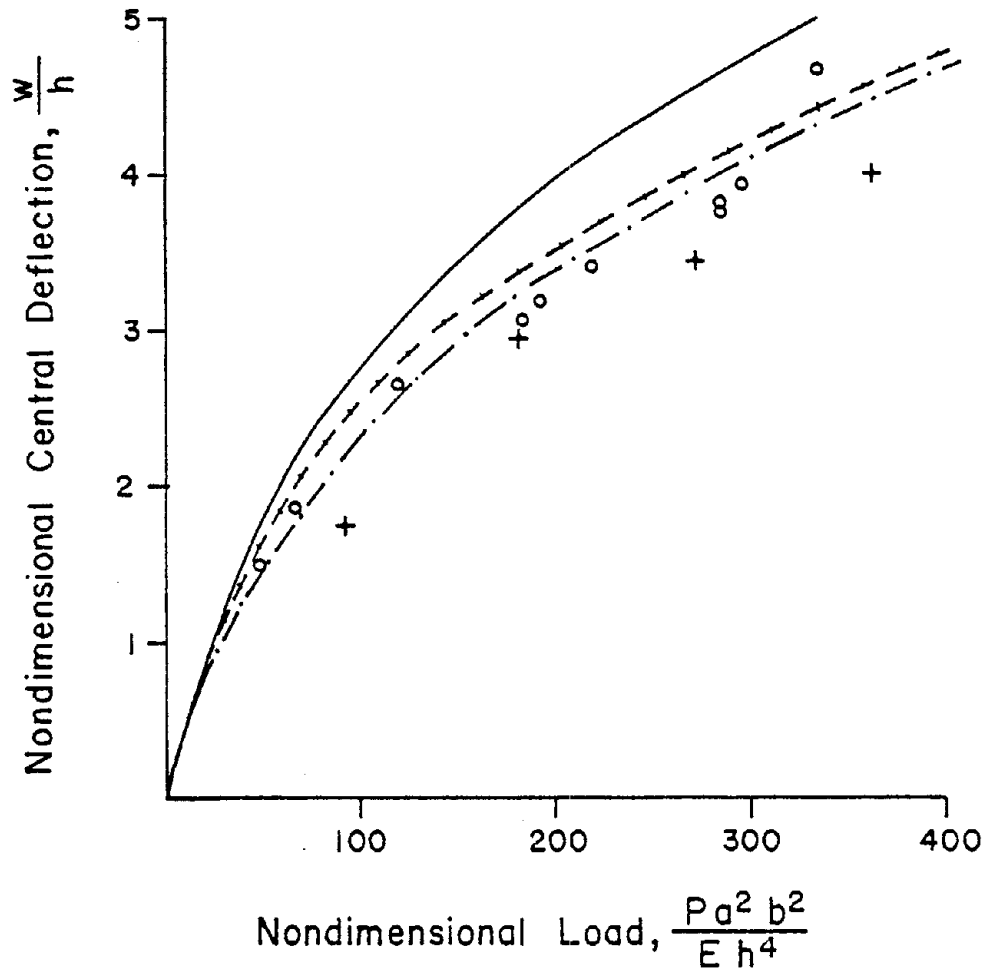


FIGURE 13. CONSTANTS USED IN ISHIZAKI'S EMPIRICAL LOAD DEFLECTION EQUATION

Tsai and Stewart (1976) presented analytical and experimental deflection and stress results for large glass plates. Experimental results were presented for glass plates with aspect ratios of 1:1, 1:2, and 1:4. Stresses reported by Tsai and Stewart were measured with bonded resistance strain gages on the convex plate surface.

Analytical results to compare with the theoretical glass plate data were computed with the nonlinear plate analysis assuming that the modulus of elasticity for glass is 10.0×10^6 psi and the Poisson's ratio for glass is 0.210. Four series terms were employed for the membrane stress function, the lateral deflection function, and the lateral loading function. A total of 64 numerical integration increments were used. Convergence of the solution was considered to be adequate when each of the lateral deflection coefficients changed less than 0.01 in. in an iterative cycle.

Figures 14-17 present comparison of the variations of central deflections with load from the different experimental sources with computed theoretical results for plate aspect ratios ranging from 1:1 to 1:1.67. The empirical load deflection equations are presented as continuous curves while direct observations are presented as discrete points. The experimental load-deflection results taken from the literature appear to compare reasonably well with results calculated using the nonlinear plate analysis.



- Bowles and Sugarman 1962
- Ishizaki 1972
- Hershey and Higgins 1973
- + Tsai and Stewart 1976
- · - · - Nonlinear Plate Solution

FIGURE 14. COMPARISONS OF ACTUAL AND CALCULATED GLASS PLATE CENTRAL DEFLECTIONS: ASPECT RATIO = 1:1

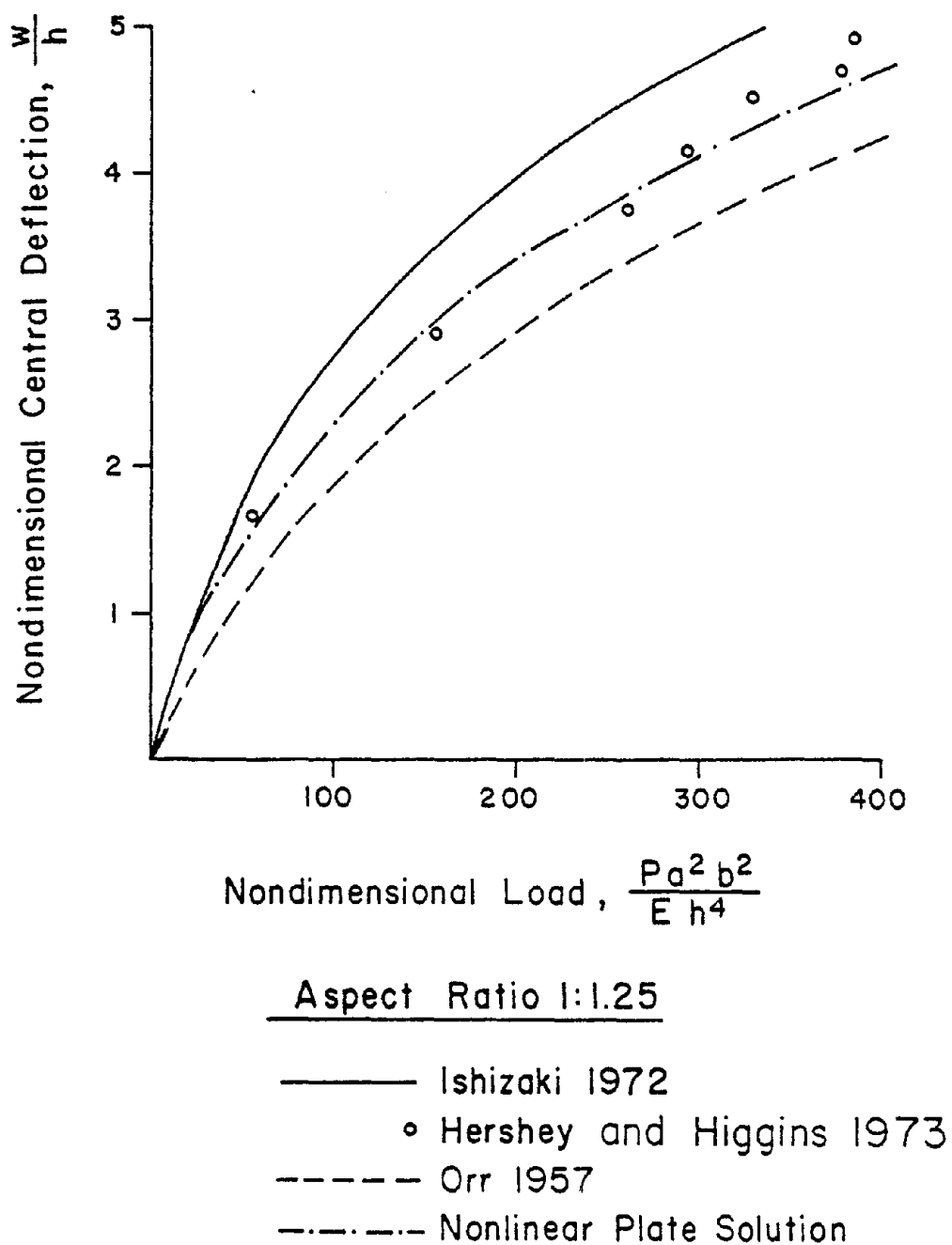
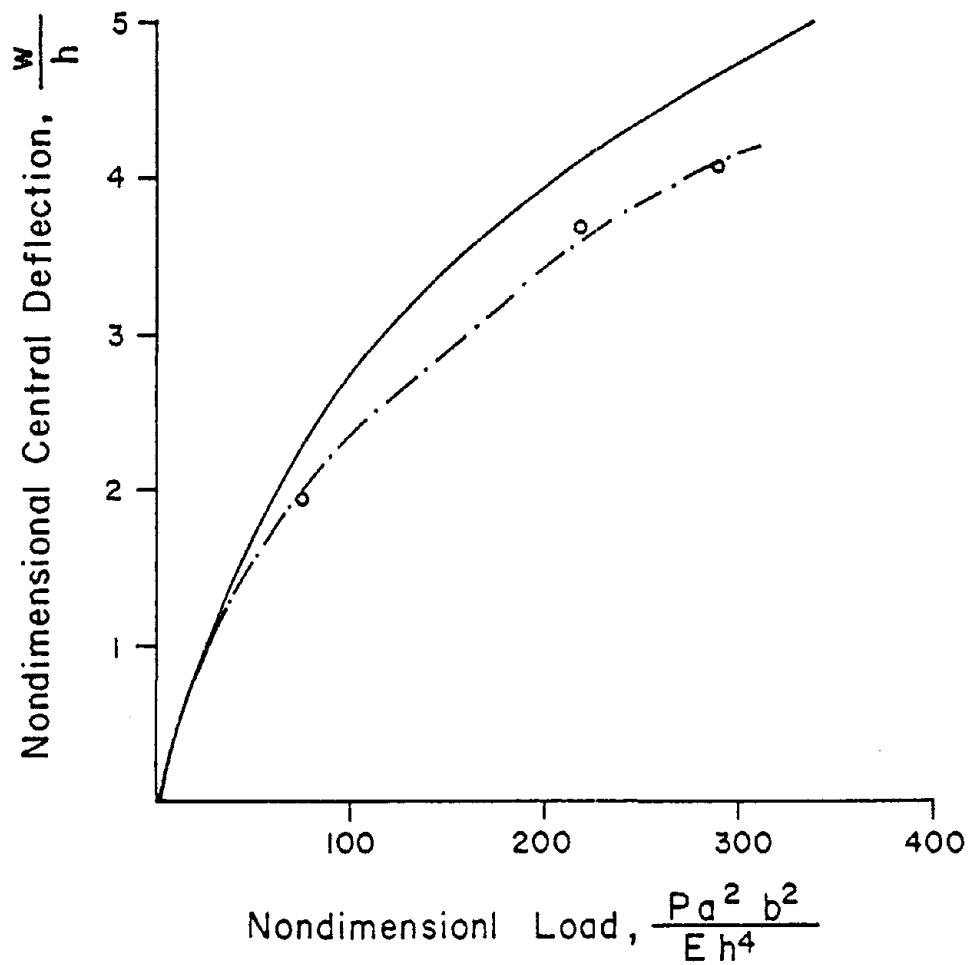


FIGURE 15. COMPARISONS OF ACTUAL AND CALCULATED GLASS PLATE CENTRAL DEFLECTIONS: ASPECT RATIO = 1:1.25



Aspect Ratio 1:1.33

————— Ishizaki 1972

○ Hershey and Higgins 1973

- · - · - Nonlinear Plate Solution

FIGURE 16. COMPARISONS OF ACTUAL AND CALCULATED GLASS PLATE CENTRAL DEFLECTIONS: ASPECT RATIO = 1:1.33

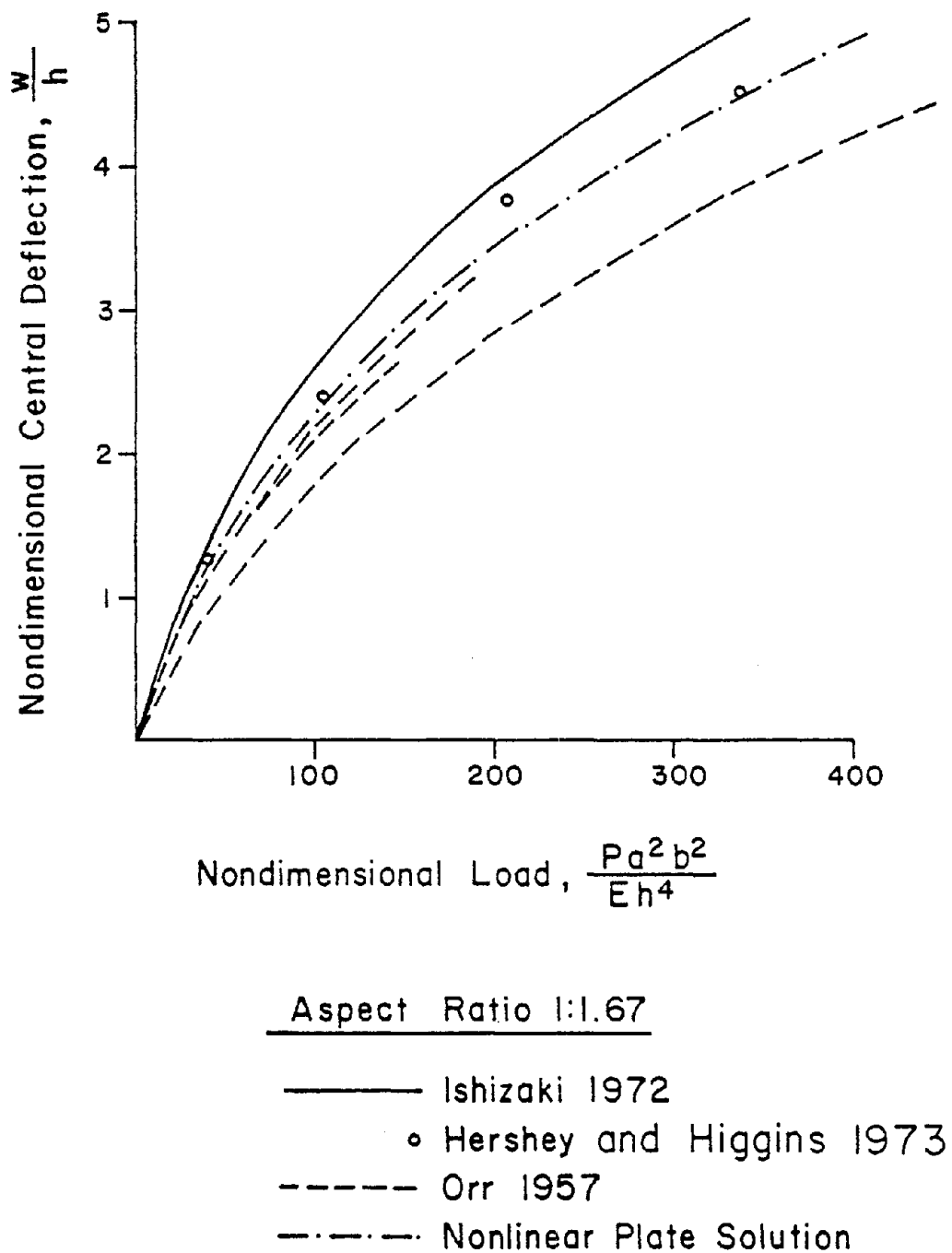


FIGURE 17. COMPARISONS OF ACTUAL AND CALCULATED GLASS PLATE CENTRAL DEFLECTIONS: ASPECT RATIO = 1:1.67

Figures 18-20 present comparisons of the variation of the maximum principal central tensile stresses with load for the convex plate surface with analogous calculated values for glass plates of different aspect ratios. The experimental stress data presented were all determined using bonded resistance strain gages. The calculated and measured data compare very well.

Based upon comparisons of both stress and deflection data taken during full-scale glass plate tests with computed data, it is concluded that the nonlinear plate analysis presented herein adequately represents the response of a large rectangular glass plate supported on four sides. Experimental and theoretical stresses agree exceptionally well. This is particularly pleasing since the failure prediction model presented in the next chapter incorporates the calculated stresses.

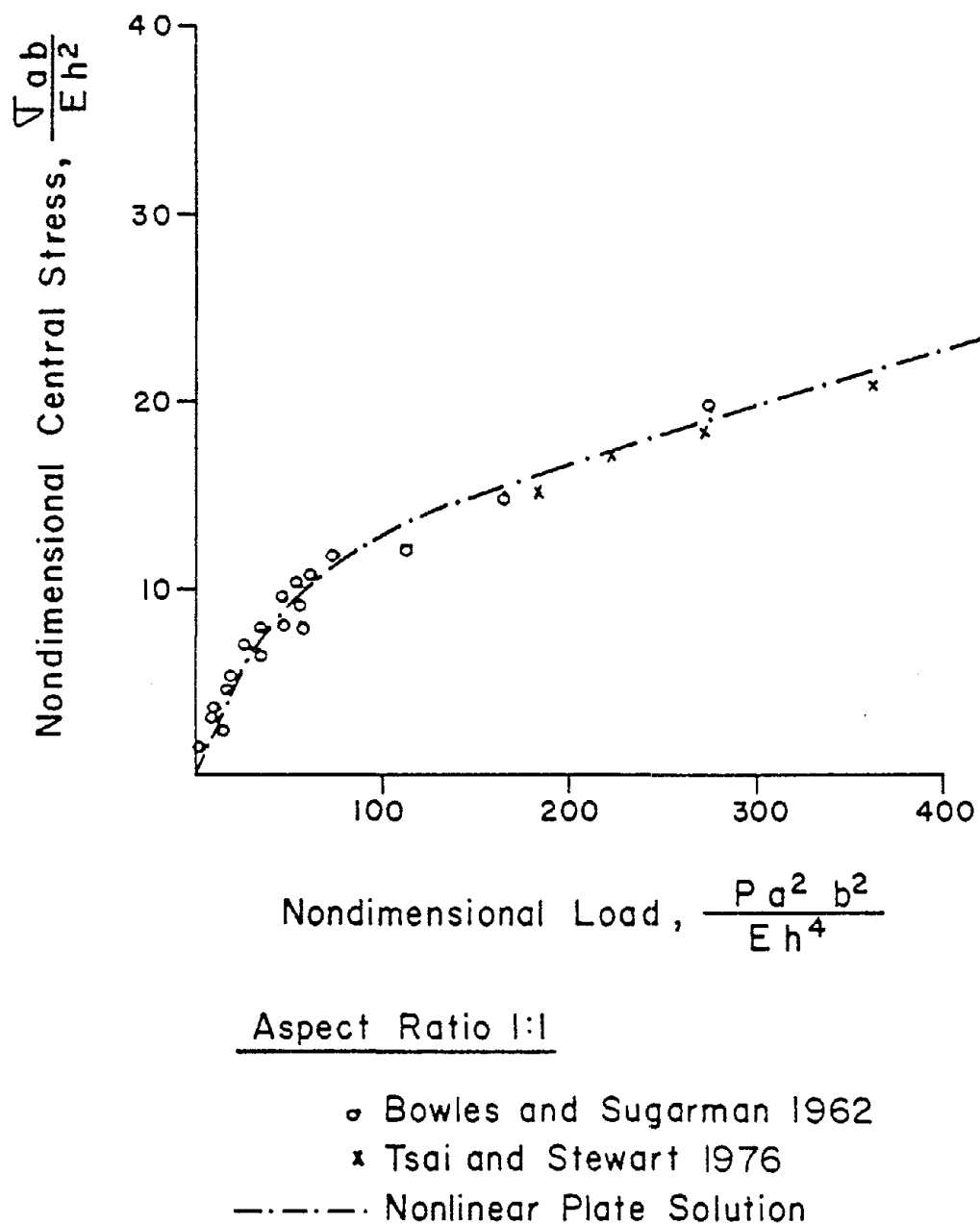
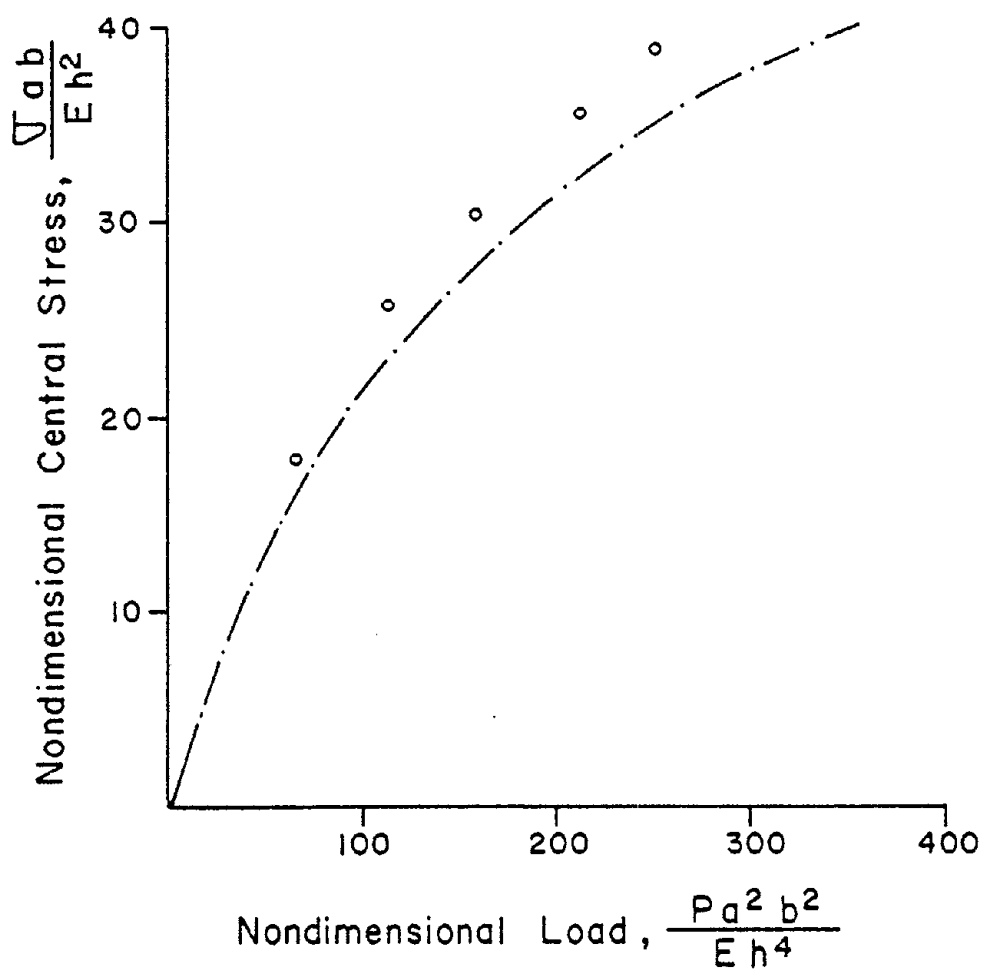


FIGURE 18. COMPARISONS OF ACTUAL AND CALCULATED GLASS PLATE CENTRAL STRESSES: ASPECT RATIO = 1:1



Aspect Ratio 1:2

○ Tsai and Stewart 1976

----- Nonlinear Plate Solution

FIGURE 19. COMPARISONS OF ACTUAL AND CALCULATED GLASS PLATE CENTRAL STRESSES: ASPECT RATIO = 1:2

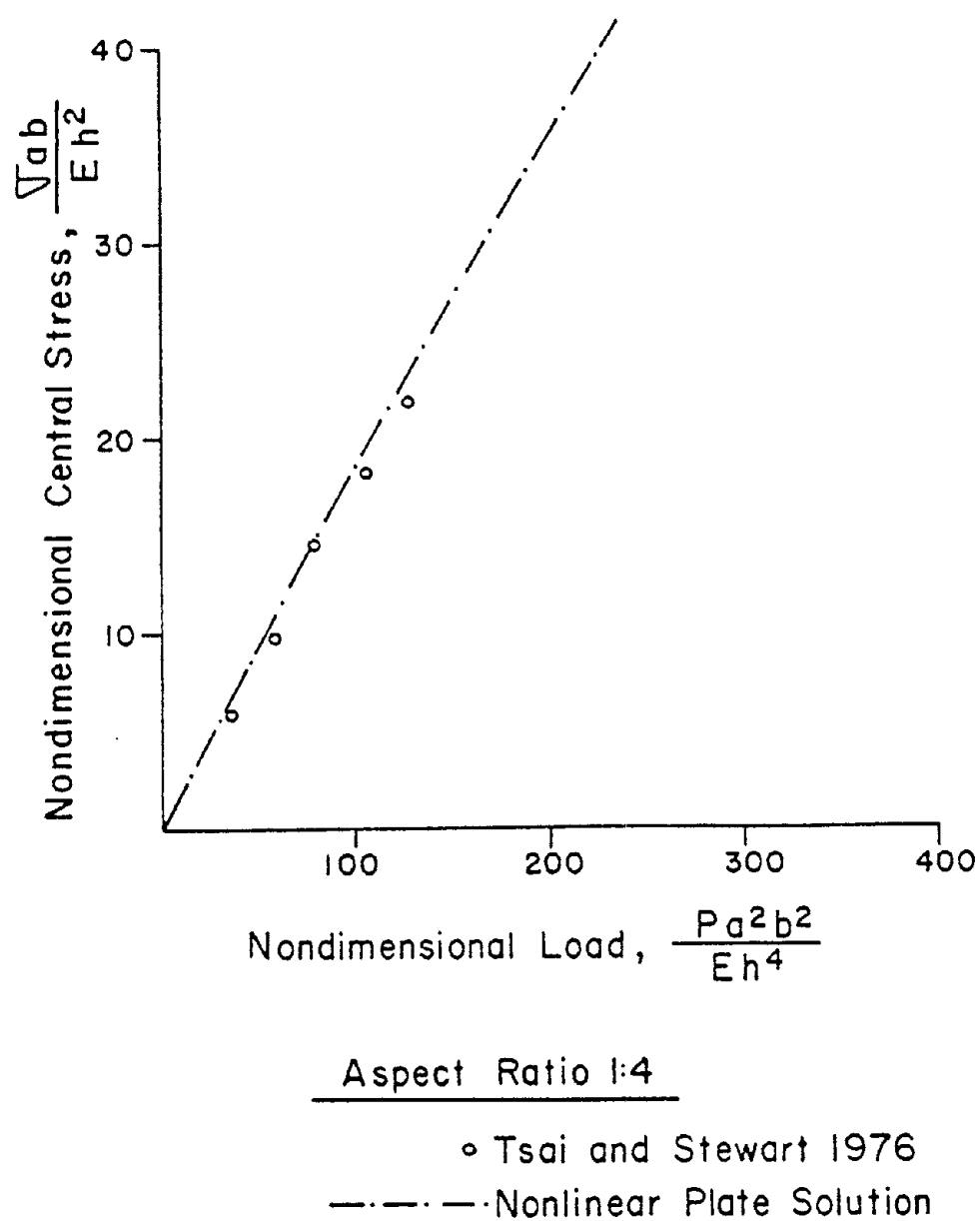


FIGURE 20. COMPARISONS OF ACTUAL AND CALCULATED GLASS PLATE CENTRAL STRESSES: ASPECT RATIO = 1:4

CHAPTER V

GLASS PLATE FAILURE PREDICTION MODEL

A failure prediction model for window glass is presented in this chapter. The failure prediction model relates the probability of failure of a glass plate under lateral load to the characteristics of glass plate surface flaws. The failure prediction model considers variations of glass strength with load duration, relative humidity, and temperature. The failure prediction model also recognizes the complex nature of the stresses developed in thin rectangular plates subjected to lateral loads. Variations of glass strength with different factors are addressed in Chapter III. An appropriate plate analysis is presented in Chapter IV. Remaining elements of the failure prediction model are discussed in this chapter.

A statistical theory advanced by Weibull(1939) is incorporated in the failure prediction model. Weibull presented a complete statistical theory for the strength of materials, such as glass, which exhibit failure characteristics that are difficult to explain using a failure theory which is based upon stress or strain at a point. The Weibull theory is reviewed in detail, and is adapted to model the strength of glass plates.

The surface flaw characteristics of glass plates utilized in the failure prediction model are fundamental, strength-related properties of glass plates. Two

parameters are used to model the surface flaw character⁷⁹istics. Numerical values of the surface flaw parameters cannot be measured directly, but have to be estimated from the results of carefully controlled experiments. Methodology to estimate the numerical values of the two surface flaw parameters is presented.

To demonstrate use of the failure prediction model, values of the surface flaw parameters are independently estimated for two different geometries of glass plates. The two plate geometries were of the same thickness and surface condition, but were of significantly different aspect ratio and surface area. To demonstrate the validity of the failure prediction model, it is then shown that the strength of one geometry of glass plate can be predicted using the surface flaw parameters estimated from strength data generated from the other geometry of glass plate, and vice versa. This exercise demonstrates that the calculated surface flaw parameters are independent of glass plate geometry and plate response.

A. Formulation of the Glass Plate Failure Prediction Model

A model which predicts the strength of glass plates cannot be based on a maximum stress-oriented failure theory because glass plate failure rarely initiates at the point of maximum stress. Rather, glass plate failure initiates at a point where flaw severity and surface

tensile stress combine to cause a critical local stress ⁸⁰ concentration on the plate surface. Because of the inherent variability associated with the surface flaw characteristics, the strength of glass must be treated in a statistical sense.

The probability that a glass plate fails as the result of a particular loading is the probability that there is at least one surface flaw capable of initiating failure, given the distribution of surface tensile stresses, the duration of loading, the temperature, and the relative humidity. The failure prediction model advanced in this section can be used to evaluate this probability. The failure prediction model employs the Brown (1974) stress corrosion theory (presented in Chapter III) to account for strength variations with load duration and ambient conditions, the nonlinear plate analysis (presented in Chapter IV) to determine the plate surface tensile stresses, and a statistical theory advanced by Weibull (1939) (discussed below) to model the characteristics of the surface flaws.

1. Equivalent Stresses

It was shown in Chapter III that the strength of glass varies significantly with load duration, temperature, and humidity. To account for these strength variations, actual stresses occurring in a glass plate are converted to equivalent stresses (denoted by $\bar{\sigma}$) at

reference conditions using Equation (3.7). In this manner ⁸¹ variations of glass strength are treated prior to the statistical analysis. Selection of the reference conditions is arbitrary.

2. Statistical Theory

If similar glass plates are exposed to linearly increasing lateral loads to failure, there will be a significant variation in loads at which failure occurs. A typical coefficient of variation for failure loads is about 22 percent (PPG 1979). A representative cumulative probability function for such a test is shown in Figure 21. According to Weibull (1939), the cumulative probability of failure function, P_f , can be represented as

$$P_f = 1 - \exp[-B] \quad (5.1)$$

where B is a risk function which relates the probability of failure to the stresses present in the glass plate, which are in turn a function of the lateral load on the plate. An appropriate risk function must be selected based upon the failure characteristics of glass plates.

Because the strength of glass plates is controlled by the distribution of flaws across the surface of the glass, the probability of failure of a glass plate logically should increase with the amount of surface area exposed to tensile stress. Further, it is clear that probability of glass plate failure should increase with

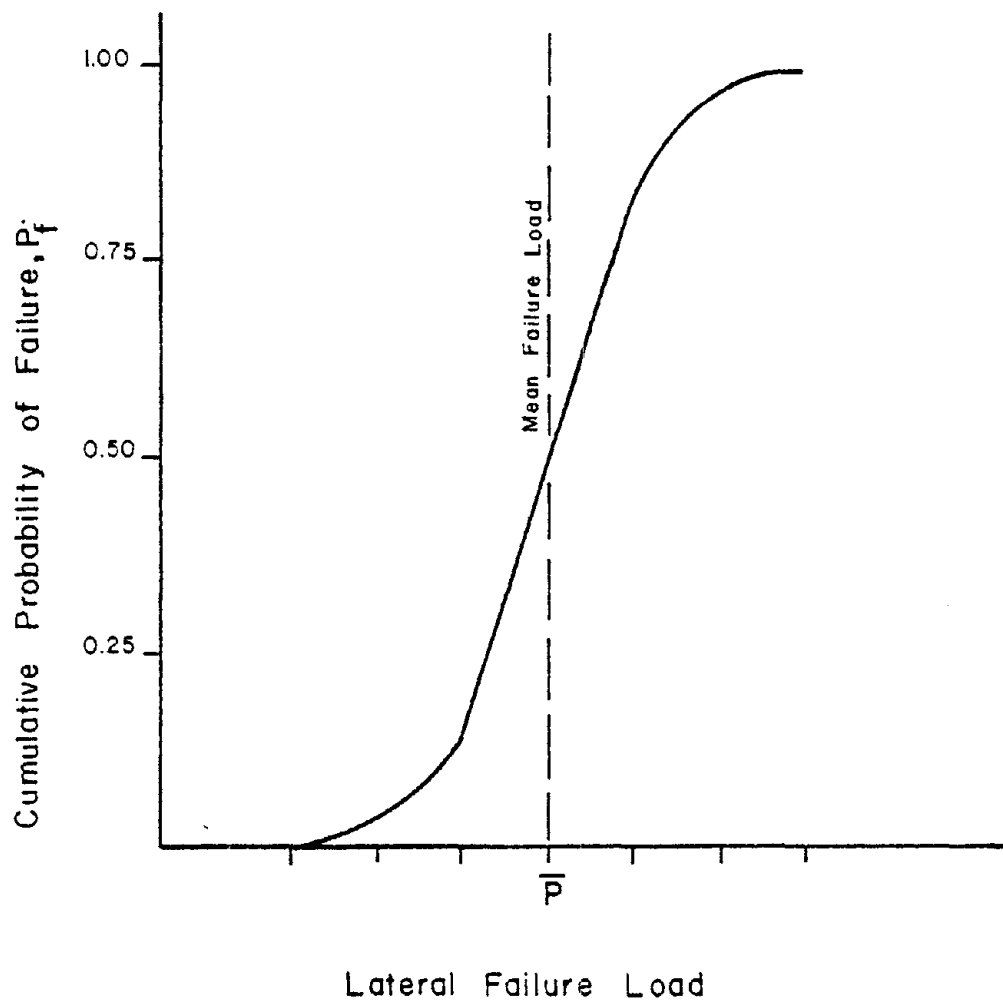


FIGURE 21. REPRESENTATIVE RELATIVE CUMULATIVE FREQUENCY FOR GLASS PLATE FAILURE LOAD

the magnitudes of the induced tensile stresses. For the⁸³ special case of a uniformly stressed (the same state of biaxial stress across the plate surface) glass plate surface with equal equivalent principal stresses, the following risk function suggested by Weibull(1939) is used

$$B = k (\tilde{\sigma}_{\max})^m A_0 \quad (5.2)$$

where m and k are the two surface flaw parameters for the reference conditions, A_0 is the total surface area of the glass plate exposed to the uniform tensile stress, and $\tilde{\sigma}_{\max}$ is the magnitude of the maximum equivalent principal tensile (MEPT) stress. As either the magnitude of the MEPT stress increases or the area of the plate increases, the risk function given in Equation (5.2) increases, resulting in an increase in the failure probability predicted with Equation (5.1).

The risk of failure experienced by a glass plate is related to the magnitude of the equivalent tensile stresses which act normal to the axes of the surface flaws. When a glass plate is exposed to a uniform state of biaxial stress with equal equivalent principal stresses, a flaw of any orientation produces the same risk of failure. This is true because the equivalent tensile stress which acts normal to the axis of a flaw is the same for any flaw orientation. If the state of stress is such that the maximum

and minimum equivalent principal stresses are not equal, the equivalent stress which acts normal to the axis of a flaw varies with flaw orientation. Hence, the risk function must take flaw orientation into account. The equivalent stress, $\tilde{\sigma}_\theta$, which acts on a plane rotated an angle θ from the plane of MEPT stress is given by the following biaxial stress transformation equation (Seely and Smith 1952)

$$\tilde{\sigma}_\theta = \tilde{\sigma}_{\max} \cos^2 \theta + \tilde{\sigma}_{\min} \sin^2 \theta \quad (5.3)$$

where $\tilde{\sigma}_{\max}$ and $\tilde{\sigma}_{\min}$ are the maximum and minimum equivalent principal stresses. To incorporate the variation of normal stress with flaw orientation, Weibull (1939) suggested a modified risk function similar to

$$B = \frac{2}{\pi} k A_0 \int_0^\alpha \left[\tilde{\sigma}_{\max} \cos^2 \theta + \tilde{\sigma}_{\min} \sin^2 \theta \right]^m d\theta \quad (5.4)$$

where the upper limit on the integration, α , is $\pi/2$ if both equivalent principal stresses are tensile stresses. If the minimum equivalent principal stress is compressive, α is calculated as follows

$$\alpha = \tan^{-1} \left[\left| \tilde{\sigma}_{\max} / \tilde{\sigma}_{\min} \right|^{1/2} \right] \quad (5.5)$$

Calculation of α using Equation (5.5) prevents compressive

equivalent stresses from influencing the risk function. When the maximum and minimum equivalent principal stresses are equal, Equation (5.4) reduces to Equation (5.2).

Equation (5.4) can be rewritten as follows

$$B = k A_o \left\{ \tilde{\sigma}_{\max} \left[\frac{2}{\pi} \int_0^{\alpha} (\cos^2 \theta + n \sin^2 \theta)^m d\theta \right]^{\frac{1}{m}} \right\}^m \quad (5.6)$$

where n is the ratio of the minimum to maximum equivalent principal stress. Equation (5.6) can then be rewritten as

$$B = k A_o (c \tilde{\sigma}_{\max})^m \quad (5.7)$$

where c is a correction factor for the biaxial state of stress given by

$$c = \left[\frac{2}{\pi} \int_0^{\alpha} (\cos^2 \theta + n \sin^2 \theta)^m d\theta \right]^{\frac{1}{m}} \quad (5.8)$$

The value of c is 1.0 for the case of equal equivalent principal stresses, and it decreases as n decreases. Values of the correction factor, c , for values of n ranging from 1.0 to -1.0, are presented in Table I for values of the surface flaw parameter, m , ranging from 4 to 7. These values for m are in the appropriate range

TABLE I.
 BIAXIAL STRESS CORRECTION FACTOR, c

Ratio of Minimum to Maximum Equivalent Principal Stress, n	Values of Biaxial Stress Correction Factor, c for Different Values of the Surface Flaw Parameter, m			
	<u>m=4</u>	<u>m=5</u>	<u>m=6</u>	<u>m=7</u>
1.00	1.00 ¹	1.00	1.00	1.00
0.80	0.91	0.91	0.91	0.92
0.60	0.84	0.85	0.86	0.86
0.40	0.78	0.80	0.82	0.83
0.20	0.75	0.78	0.80	0.81
0.00	0.72	0.76	0.78	0.80
-0.20	0.71	0.74	0.77	0.79
-0.40	0.69	0.73	0.76	0.78
-0.60	0.68	0.72	0.75	0.77
-0.80	0.67	0.71	0.74	0.77
-1.00	0.66	0.70	0.73	0.76

¹Values of the biaxial stress correction factor, c, calculated using Equation (5.8).

to model glass plate strength data presented later in 87
this chapter.

For the case of a rectangular plate subjected to a lateral load, the magnitudes of the equivalent principal stresses and their relationships to each other vary across the surface of the plate. Therefore, both the magnitude of the MEPT stress and the value of the correction factor vary with location on the plate surface. To account for these variations, Equation (5.7) is rewritten for the general case as

$$B = k \int_0^a \int_0^b \left[c(x,y) \tilde{\sigma}_{\max}(x,y) \right]^m dydx \quad (5.9)$$

where $c(x,y)$ and $\tilde{\sigma}_{\max}(x,y)$ are values of the correction factor and the MEPT stress as a function of location on the plate, and a and b are the rectangular dimensions of the plate.

3. Numerical Integration of Risk Function

Evaluation of the generalized risk functions (Equation 5.9) for a particular plate problem can be cumbersome. To simplify evaluation of the generalized risk function, a numerical integration procedure is introduced. Equation (5.9) is rewritten as

$$B = k \int_0^a \int_0^b \left[\hat{\sigma}(x,y) \right]^m dydx \quad (5.10)$$

where $\hat{\sigma}(x,y)$ is the maximum corrected equivalent principal tensile (MCEPT) stress given by

$$\hat{\sigma}(x,y) = c(x,y) \bar{\sigma}(x,y) \quad (5.11)$$

Equation (5.10) can be expressed as follows with plate surface area a as the variable

$$B = k \int_0^{A_0} \left[\hat{\sigma}(a) \right]^m da \quad (5.12)$$

where $\hat{\sigma}(a)$ is the threshold MCEPT stress to which the plate surface area, a , is exposed, and A_0 is the total plate surface area exposed to tensile stress.

Numerical integration of Equation (5.12) is accomplished using the following expression

$$B = k (5000)^m \sum_{i=1}^n A_i (\hat{\sigma}_i / 5000)^m \quad (5.13)$$

where $\hat{\sigma}_i$ are the midpoints of a set of n nonoverlapping, exhaustive MCEPT stress intervals ranging from zero to the maximum value of MCEPT stress. A_i is the amount of plate surface area exposed to MCEPT stresses in the range of the i^{th} MCEPT stress interval. These areas are deter-

mined using the nonlinear plate analysis presented in 89 Chapter IV. Evaluation of Equation (5.13) is accomplished in an equivalent area table (Ref. Table II). The constant 5000 is included in Equation (5.13) to keep the magnitudes of the entries in the equivalent area table manageable.

The first column of the equivalent area table defines the MCEPT stress intervals. Column two of the table contains the midpoints of the MCEPT stress intervals, $\hat{\sigma}_i$. The amount of plate area A_i exposed to MCEPT stresses in the i^{th} interval is presented in the third column. The fourth column contains values of the interval equivalent area, \tilde{A}_i , given by the following expression

$$\tilde{A}_i = A_i (\hat{\sigma}_i/5000)^m \quad (5.14)$$

The total equivalent area, S_m , of a plate for a given m parameter is found by summing the entries in the equivalent area column as follows

$$S_m = \sum_{i=1}^n \tilde{A}_i \quad (5.15)$$

The value of the generalized risk function is then found as follows

$$B = k (5000)^m S_m \quad (5.16)$$

TABLE II.
EXAMPLE EQUIVALENT AREA TABLE

MCEPT ¹ Stress Intervals (psi)	Midpoints of MCEPT Stress Intervals, $\hat{\sigma}_i$ (psi)	Plate Surface Areas Exposed to Interval MCEPT Stresses, A_i (in) ²	Equivalent Plate Surface Areas Exceed to Interval MCEPT Stresses, \tilde{A}_i (in) ²
0-1000	500	A_1	$\tilde{A}_1 = A_1 \left(\frac{500}{5000}\right)^m$
1000-2000	1500	A_2	$\tilde{A}_2 = A_2 \left(\frac{1500}{5000}\right)^m$
2000-3000	2500	A_3	$\tilde{A}_3 = A_3 \left(\frac{2500}{5000}\right)^m$
.	.	.	.
.	.	.	.
.	.	.	.
$-\hat{\sigma}_{\max}^2$	$\hat{\sigma}_n$	A_n	$\tilde{A}_n = A_n \left(\frac{\hat{\sigma}_n}{5000}\right)^m$
		$A_0 = \sum_{i=1}^n A_i$	$S_m = \sum_{i=1}^n \tilde{A}_i$

¹Maximum Corrected Equivalent Principal Tensile, MCEPT, Stress.

² $\hat{\sigma}_{\max}$ is a MCEPT stress which is larger than any MCEPT stress occurring in the plate.

Substitution of Equation (5.16) into Equation (5.1) re- 91
sults in the following expression for the cumulative
probability of glass plate failure.

$$P_f = 1 - \exp[-k 5000^m S_m] \quad (5.17)$$

4. Summary of Failure Prediction Model

The procedure to calculate the probability of failure
of a window glass plate subjected to a lateral loading is
as follows:

- (1) the variation of surface stresses across the
plate is determined, using the nonlinear plate
analysis presented in Chapter IV,
- (2) the actual surface stresses are converted to
MEPT stresses given the load duration, the
relative humidity, and the temperature using
Equation (3.7),
- (3) the MEPT stresses are then converted to MCEPT
stresses using the correction factor given in
Equation (5.8),
- (4) an equivalent area table is then constructed
and the value of the total equivalent plate
area, S_m , is calculated, and
- (5) finally, the probability of glass plate failure
is evaluated using Equation (5.17).

The failure prediction model thus formulated allows the probability of failure of glass plates exposed to lateral loads to be predicted as a function of the surface flaw parameters (m,k) .

B. Determination of the Glass Plate Surface Flaw Parameters

The glass plate surface flaw parameters (m,k) required in the failure prediction model are functions of the type of glass and the glass plate surface condition. Values for the surface flaw parameters cannot be measured directly. Rather, values for the surface flaw parameters must be estimated using data from glass plate failure tests.

The steps involved in estimating the surface flaw parameters using a set of glass plate strength data are:

- (1) the glass plate failure load data are converted to equivalent failure load data at reference conditions using methodology explained in Chapter III along with the nonlinear plate analysis presented in Chapter IV,
- (2) the mean and standard deviation of the equivalent failure load data are calculated and the data are grouped into frequency intervals,
- (3) the variation of the MCEPT stresses across the plate are determined for the equivalent failure

loads corresponding to the equivalent failure load intervals defined in Step (2) and the total equivalent plate areas, S_m , are calculated for a range of values of the surface flaw parameter, m , and

- (4) the best set of the surface flaw parameters to represent the equivalent failure load data is selected.

1. Glass Strength Data

Two different geometries of glass plates with similar surface conditions were tested to failure under time controlled conditions. The glass plates were 7/32 in. thick sheet glass that were removed from the 20-year-old Great Plains Life Building (GPL) in Lubbock, Texas during its renovation in 1975. Twenty rectangular glass plates 28.5 x 60.5 in., and 20 square glass plates 28.5 x 28.5 in., were tested to failure. Half of the glass plates were tested with their exterior surfaces in tension and half of the glass plates were tested with their interior surfaces in tension. The glass plates were mounted in an aluminum glazing system and exposed to monotonically increasing uniform lateral loads chosen to cause failure in about 60 seconds or less. Failure data collected included a complete load-deflection-time record, the location of each fracture initiation point, and photographs of the glass

plate fracture pattern. The raw data along with a description of the test apparatus is presented in Appendix D. 94

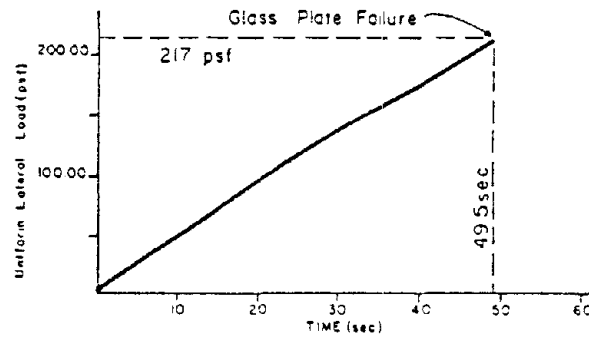
2. Equivalent Strength Conversion

The GPL failure load data, organized by glass plate geometry, were converted to equivalent failure load data using Equation (3.7) and the methodology presented in Chapter III. A 60-second duration constant reference load was chosen for the equivalent failure load conversion because of its relationship to current design information (Ref. Chapter II). The temperature and relative humidity were assumed to remain constant for the equivalent failure load conversions so that Equation (3.8) reduces to the following

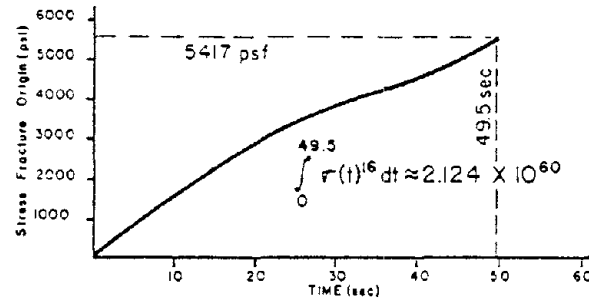
$$\bar{\sigma}_{60} = \left[\left(\int_0^{t_f} \sigma(t)^{16} dt \right) / 60 \right]^{\frac{1}{16}} \quad (5.18)$$

where $\bar{\sigma}_{60}$ is the equivalent 60 second duration failure stress at the failure initiation point. Mechanics of calculating the equivalent failure load are presented in an example calculation below.

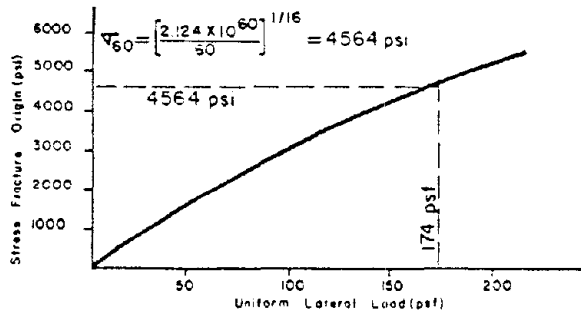
Figure 22(a) presents the variation of uniform lateral load with time to failure for a square GPL glass plate. The maximum load at failure was 217 psf after 49.5 sec of loading. Using the load-time variation, the location of the fracture origin point, and the nonlinear plate analysis, the variation of stress at the fracture origin point was found to be as shown in Figure 22(b). The



(a) Load-Time Variation



(b) Fracture Origin Stress-Time Variation



(c) Fracture Origin Stress-Load Variation

FIGURE 22. CALCULATION OF EQUIVALENT GLASS PLATE FAILURE LOADS

maximum principal tensile stress varied from 0 to 5417 psi. Using the stress-time relationship presented in Figure 22(b) and Equation (5.18), the MEPT stress at the fracture origin point was calculated to be 4564 psi. Figure 22(c) presents the variation of maximum principal tensile stress at the fracture origin point with load as determined with the nonlinear plate analysis. Using this load-stress relationship, the equivalent 60-second constant failure load was found to be 174 psf as indicated in Figure 22(c). A similar equivalent failure load conversion was made for each GPL glass plate tested. These equivalent failure load data are presented in Table III.

3. Equivalent Strength Statistics

Using the equivalent failure load data presented in Table III, the means and standard deviations were calculated to be 79 and 19 psf for the rectangular GPL glass plates and 168 and 37 psf for the square GPL glass plates. Tables IV and V present frequency groupings for the GPL equivalent failure load data. Included in these tables are interval frequencies, relative interval frequencies, and relative cumulative frequencies. Corresponding histograms for the equivalent failure loads for both the square and rectangular GPL glass plates are presented in Figure 23.

TABLE III.

EQUIVALENT FAILURE LOADS FOR
GPL GLASS PLATES

Equivalent Failure Loads for Rectangular GPL Glass Plates ¹	Equivalent Failure Loads for Square GPL Glass Plates
(psf)	(psf)
62	168
76	189
53	132
92	174
105	197
120	173
62	177
88	268
72	153
82	148
50	112
84	138
59	157
86	196
75	156
95	219
76	112
76	157
62	202
104	132
<hr/>	<hr/>
$\bar{x} = 79.0$	$\bar{x} = 168.0$
$s = 18.4$	$s = 37.5$

¹ Equivalent failure loads calculated using Equation (5.18) assuming a 60-second duration constant load.

TABLE IV.

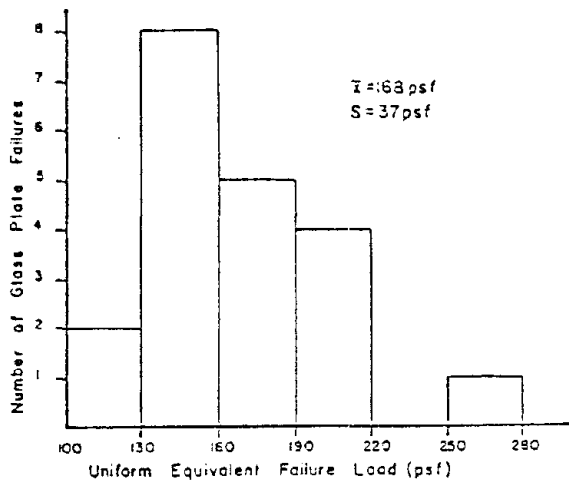
GROUPED FREQUENCY TABLE FOR
SQUARE GPL GLASS PLATE EQUIVALENT FAILURE LOADS

Equivalent Failure Load Interval (psf)	Interval Frequency, f_i	Relative Interval Frequency, p_i	Relative Cumulative Interval Frequency, P_i
100-130	2	0.10	0.10
130-160	8	0.40	0.50
160-190	5	0.25	0.75
190-220	4	0.20	0.95
220-250	0	0.00	0.95
250-280	1	0.05	1.00
	—	—	
	20	1.00	

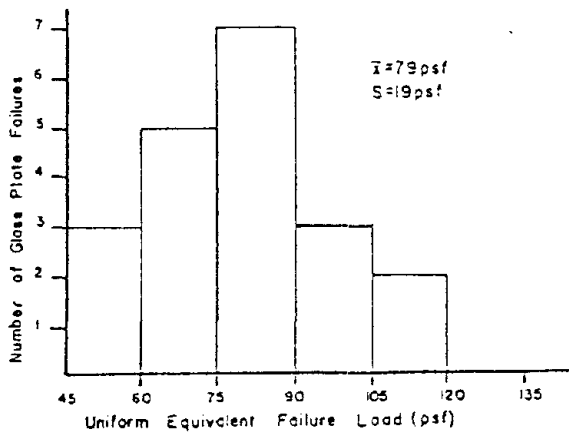
TABLE V.

GROUPED FREQUENCY TABLE FOR
RECTANGULAR GPL GLASS PLATE EQUIVALENT FAILURE LOADS

Equivalent Failure Load Interval (psf)	Interval Frequency, f_i	Relative Interval Frequency, p_i	Relative Cumulative Interval Frequency, P_i
45-60	3	0.15	0.15
60-75	5	0.25	0.40
75-90	7	0.35	0.75
90-105	3	0.15	0.90
105-120	2	0.10	1.00
	— 20	— 1.00	



(a) Square GPL Glass Plate Equivalent Failure Load Histogram



(b) Rectangular GPL Glass Plate Equivalent Failure Load Histogram

FIGURE 23. EQUIVALENT FAILURE LOAD HISTOGRAMS FOR GPL GLASS PLATES

4. Total Equivalent Plate Areas

Figures 24 and 25 present the variations of the MEPT stresses across a quarter of a square and rectangular GPL glass plate for their respective mean equivalent failure loads. Figures 26 and 27 present the variations of the MCEPT stresses for the GPL glass plates that were calculated assuming an m surface flaw parameter of 6. Tables VI and VII present the corresponding equivalent area tables for both situations. The total equivalent areas, S_g , thus calculated for the square and rectangular GPL glass plates are 62.8 and 102.8 in²., respectively.

Similar calculations were performed for both geometries of GPL glass plates assuming integer values of the m surface flaw parameter ranging from 4 to 7 and for each load interval defined in the equivalent failure load frequency tables (Tables IV and V). The resulting total equivalent areas are presented in Tables VIII and IX.

5. Determination of the Best k Surface Flaw Parameter

The cumulative probability of failure function given by Equation (5.17) is an exponential cumulative probability function of the following form

$$P_f = 1 - \exp[-ax] \quad (5.19)$$

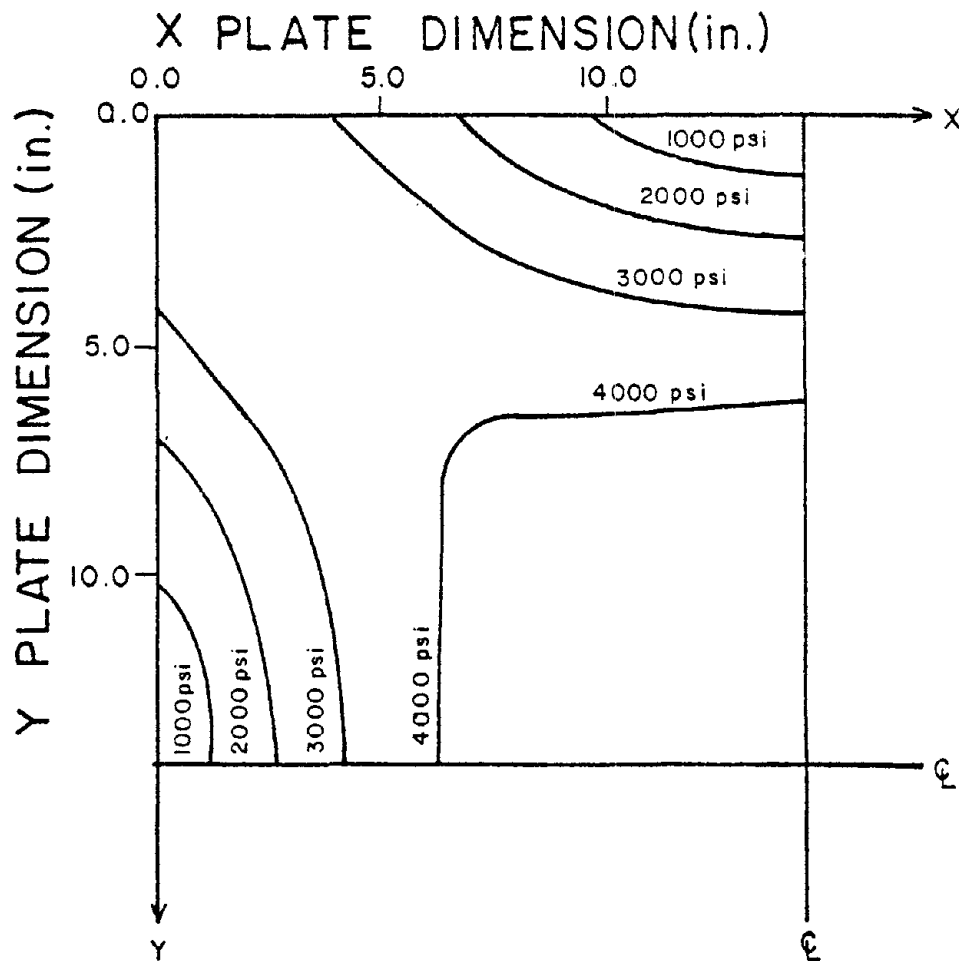


FIGURE 24. MEPT STRESS CONTOURS FOR SQUARE GPL GLASS PLATE FOR MEAN EQUIVALENT FAILURE LOAD

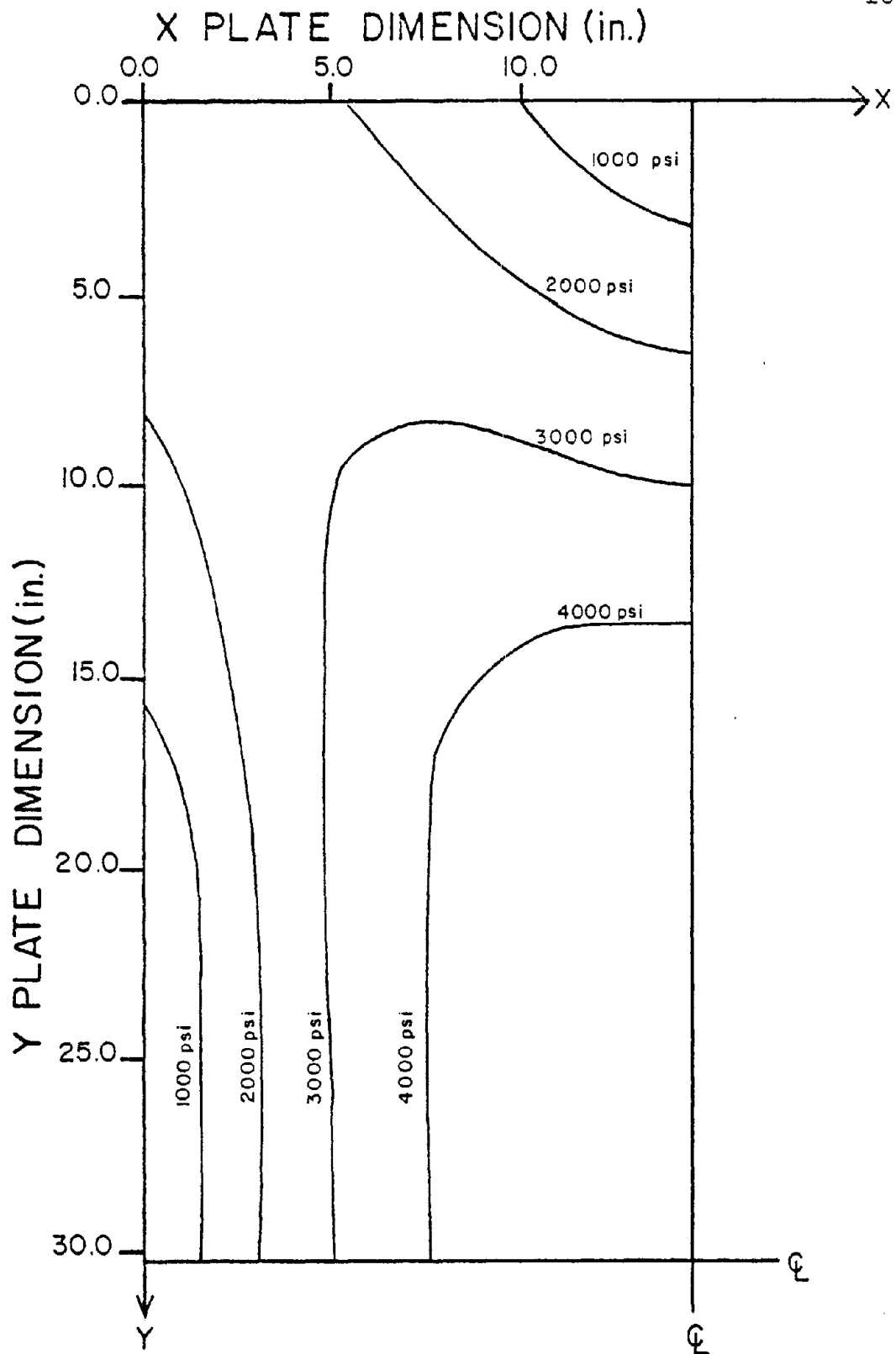


FIGURE 25. MEPT STRESS CONTOURS FOR RECTANGULAR GPL GLASS PLATE FOR MEAN EQUIVALENT FAILURE LOAD

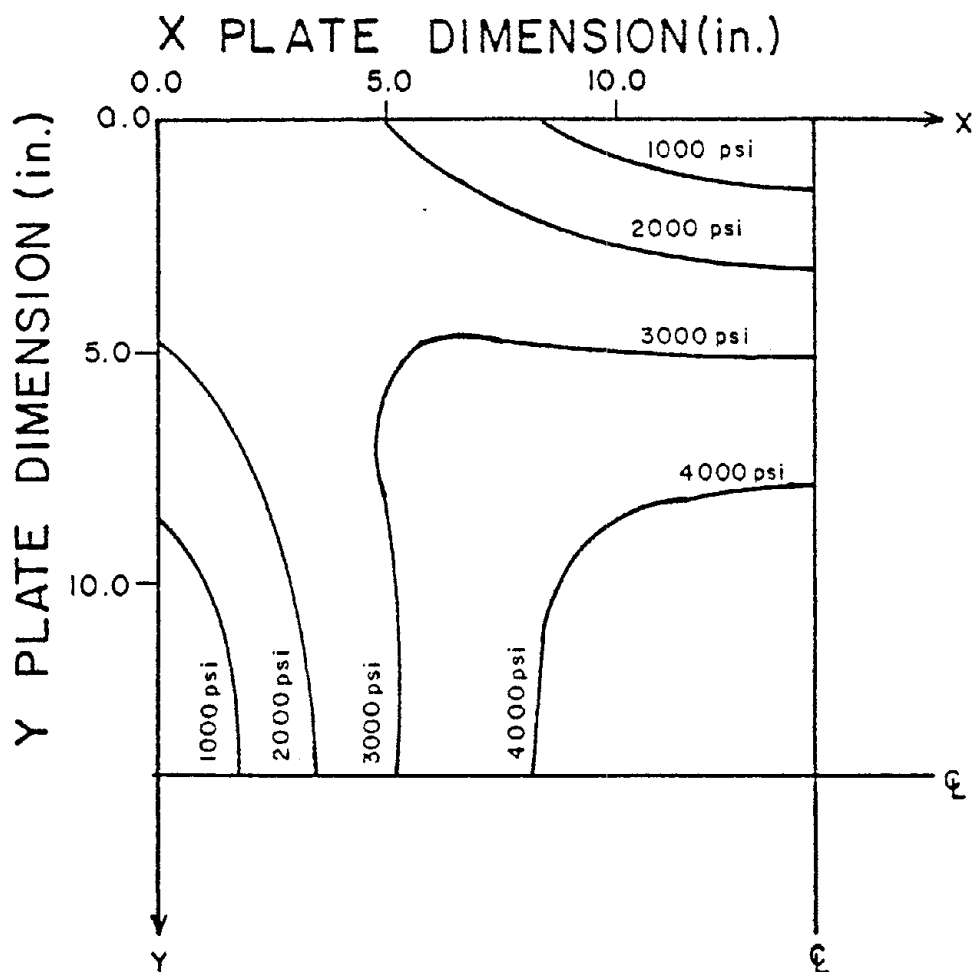


FIGURE 26. MCEPT STRESS CONTOURS FOR SQUARE
 GPL GLASS PLATE FOR MEAN EQUIVALENT
 FAILURE LOAD

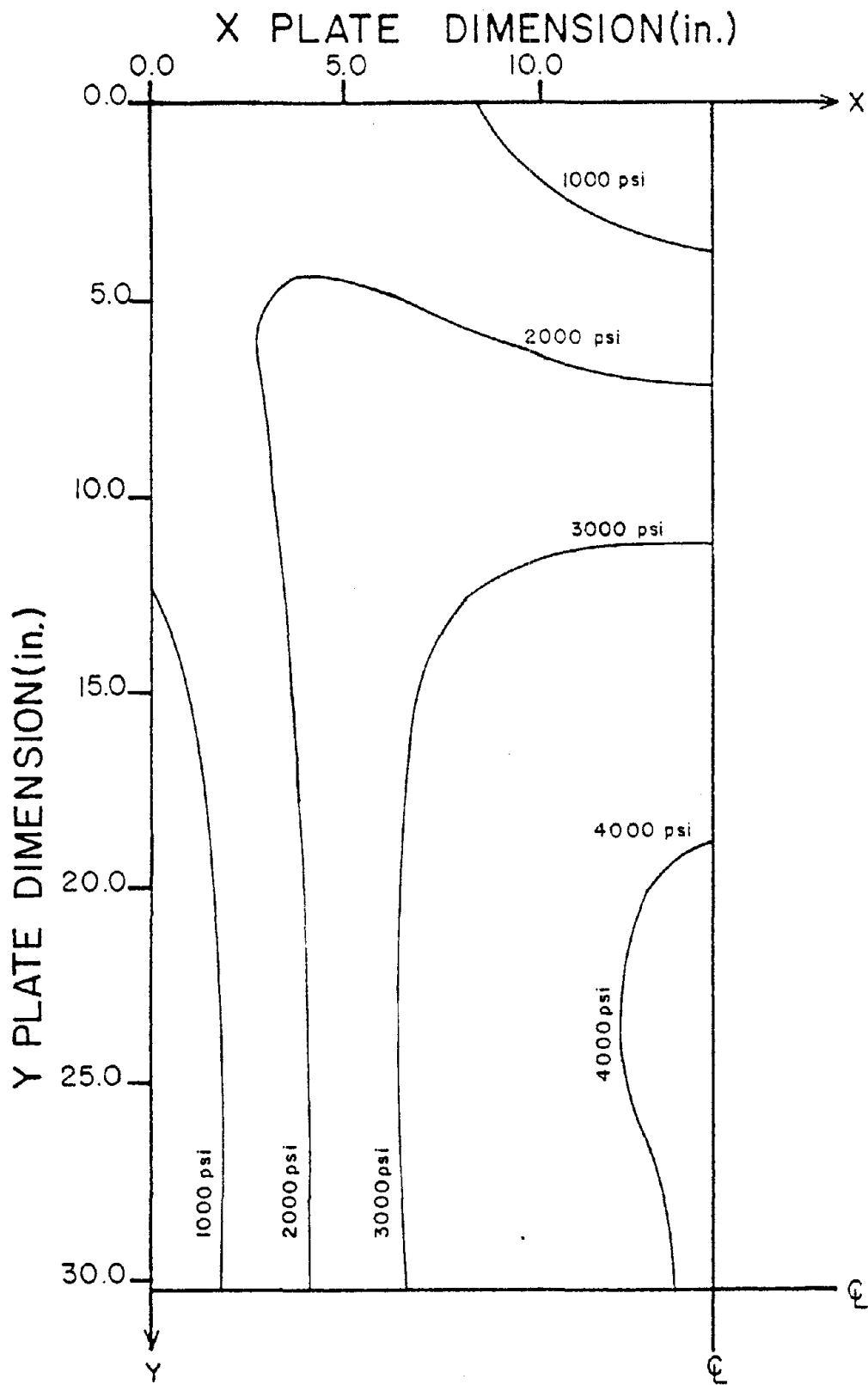


FIGURE 27. MCEPT STRESS CONTOURS FOR RECTANGULAR GPL GLASS PLATE FOR MEAN EQUIVALENT FAILURE LOAD

TABLE VI.

TOTAL EQUIVALENT AREA TABLE
FOR SQUARE GPL GLASS PLATES

MCEPT Stress Intervals ¹ (psi)	Midpoints of MCEPT Stress Interval, $\hat{\sigma}_i$ (psi)	Plate Surface Areas Exposed to Interval MCEPT Stresses, A_i (in) ²	Equivalent Plate Surface Areas Exposed to Interval MCEPT Stresses, \hat{A}_i (in) ²
0-500	250	16.3	-
500-1000	750	32.5	-
1000-1500	1250	65.0	0.02
1500-2000	1750	48.7	0.09
2000-2500	2250	130.0	1.08
2500-3000	2750	144.9	5.39
3000-3500	3250	73.1	5.51
3500-4000	3750	121.8	21.68
4000-4500	4250	130.0	49.03
		$A_o = 812.3 \text{ in}^2$	$S_s = 82.80 \text{ in}^2$

¹ Calculated for an equivalent failure load of 168 psf assuming an m surface flaw parameter of 6.

TABLE VII.

TOTAL EQUIVALENT AREA TABLE
FOR RECTANGULAR GPL GLASS PLATES

MCEPT Stress Intervals ¹ (psi)	Midpoints of MCEPT Stress Interval, $\hat{\sigma}_i$ (psi)	Plate Surface Areas Exposed to Interval MCEPT Stresses, A_i (in) ²	Equivalent Plate Surface Areas Exposed to Interval MCEPT Stresses, A_i (in) ²
0-500	250	69.0	=
500-1000	750	69.0	-
1000-1500	1250	224.2	.05
1500-2000	1750	327.6	.60
2000-2500	2250	275.9	2.29
2500-3000	2750	206.9	5.73
3000-3500	3250	206.9	15.60
3500-4000	3750	258.6	46.03
4000-4500	4250	86.2	32.51

$$A_o = 1724.3 \text{ in}^2 \quad S_e = 102.81 \text{ in}^2$$

¹Calculated for an equivalent failure load of 79 psf assuming a surface flaw parameter of 6.

TABLE VIII.

TOTAL EQUIVALENT AREAS, S_m , FOR
SQUARE GPL GLASS PLATES

Equivalent Failure Load (psf)	Calculated Total Equivalent Areas, S_m (in ²)			
	<u>m¹=4</u>	<u>m=5</u>	<u>m=6</u>	<u>m=7</u>
40	1.0	0.2	0.1	-
70	8.7	3.5	1.4	0.6
100	24.1	12.6	6.4	3.4
130	62.0	40.2	26.4	17.7
160	116.2	91.7	70.6	55.2
190	203.5	174.2	151.9	134.4
220	325.5	308.3	296.5	290.7
250	472.8	504.1	531.2	570.0
280	648.2	753.2	875.6	1005.9
310	876.6	1045.4	1310.9	1644.9
340	1156.6	1480.5	1900.6	2528.2
370	1438.7	1999.7	2886.0	3984.7

¹Assumed value of m surface flaw parameter.

TABLE IX.

TOTAL EQUIVALENT AREAS, S_m , FOR
RECTANGULAR GPL GLASS PLATES

Equivalent Failure Load (psf)	Calculated Total Equivalent Areas, S_m (in) ²			
	<u>m¹=4</u>	<u>m=5</u>	<u>m=6</u>	<u>m=7</u>
15	0.4	0.1	-	-
30	5.6	2.1	0.7	0.2
45	22.7	10.3	5.6	3.3
60	70.4	43.7	27.2	17.0
75	155.7	106.5	78.1	57.4
90	273.5	221.3	187.9	180.0
105	443.0	422.0	420.2	419.1
120	659.8	720.9	763.6	879.6
135	792.5	1118.3	1324.8	1625.7
150	1374.8	1680.6	2132.2	2806.6
165	1754.3	2392.4	3266.8	4449.7
180	2277.5	3080.5	4559.6	6897.5

¹Assumed value of m surface flaw parameter.

where α is a distribution parameter and x is the variate. The value of the α parameter is given by the following equation

$$\alpha = 1/\bar{x} \tag{5.20}$$

where \bar{x} is the mean value of the \bar{x} variate (Pfeiffer and Schum 1973).

In Equation (5.17), the total equivalent area, S_m , is the variate. Therefore, applying Equation (5.20), the best k surface flaw parameter to represent a given failure strength distribution for a particular m surface flaw parameter is calculated as follows

$$k = 1/(5000^m \bar{S}_m) \tag{5.21}$$

where \bar{S}_m is the mean total equivalent area which is calculated using the total equivalent area data presented in Tables VIII and IX along with the equivalent failure load frequency data presented in Tables IV and V. Calculation of the mean total equivalent area is performed in a mean total equivalent area table.

The first column of a mean total equivalent area table presents equivalent failure load intervals as defined in Tables IV and V. The second column contains corresponding total equivalent area intervals. The third column presents the frequency, f_i , of glass plate failure in each equiva-

lent failure load interval. The fourth column of the table contains the interval midpoint total equivalent areas, S_{mi} . The values of the interval midpoint total equivalent areas are found by averaging the total equivalent areas for the boundaries of each equivalent failure load interval. The values presented in the fifth column are calculated by multiplying the interval frequencies, f_i , by the interval midpoint total equivalent areas, S_{mi} . The mean total equivalent area for a given value of the m surface flaw parameter is then found by dividing the summation of column 5 by the summation of column 3.

Tabular calculations of the mean total equivalent areas for both geometries of the GPL equivalent failure load data for an m surface flaw parameter of 6 are presented in Tables X and XI. The resulting mean total equivalent areas are 128.9 in². and 167.0 in². for the square and rectangular GPL glass plates, respectively. Using Equation (5.21), the best corresponding values of the k surface flaw parameter are $4.97 \times 10^{-2.5}$ and $3.83 \times 10^{-2.5}$ for the square and rectangular GPL glass plates, respectively. Similar calculations were performed for both geometries of the GPL glass plates for each assumed value of the m surface parameter. Tables XII and XIII present values of the k surface flaw parameter thus calculated, along with pertinent theoretical equivalent failure load statistics.

TABLE X.

MEAN TOTAL EQUIVALENT AREA TABLE
FOR SQUARE GPL GLASS PLATES

Equivalent Failure Load Interval ¹ (psf)	Corresponding Total Equivalent Area Interval (in ²)	Midpoints of Total Equivalent Area Interval, $S_{\epsilon i}$ (in ²)	Interval Frequency f_i	$f_i S_{\epsilon i}$
100-130	6.4- 26.4	16.4	2	32.8
130-160	26.4- 70.6	48.5	8	388.0
160-190	70.6-151.9	111.3	5	556.5
190-220	151.9-296.5	224.2	4	896.8
220-250	296.5-531.2	413.9	0	0
250-280	531.2-875.6	703.4	1	703.4
			20	2577.50

$$\bar{S}_{\epsilon} = \frac{2577.50}{20} = 128.9 \text{ in}^2$$

¹Mean total equivalent area calculated assuming an m surface flaw parameter of 6.

TABLE XI.

MEAN TOTAL EQUIVALENT AREA TABLE
FOR RECTANGULAR GPL GLASS PLATES

Equivalent Failure Load Interval ¹ (psf)	Corresponding Total Equivalent Area Interval (in ²)	Midpoints of Total Equivalent Area Interval, $S_{\bar{s}_i}$ (in ²)	Interval Frequency f_i	$f_i S_{\bar{s}_i}$
45- 60	5.6- 27.2	16.4	3	49.2
60- 75	27.2- 78.1	52.6	5	263.0
75- 90	78.1-187.9	133.0	7	931.0
90-105	187.9-420.2	304.1	3	912.3
105-120	420.2-763.6	591.9	2	1183.8
			20	3339.3

$$\bar{S}_6 = \frac{3339.3}{20} = 167.0 \text{ in}^2$$

¹Mean total equivalent area calculated assuming that the m surface flaw parameter is 6.

TABLE XII.
 COMPARISON OF CALCULATED AND THEORETICAL
 SQUARE GPL GLASS PLATE FAILURE LOAD STATISTICS

Assumed m Surface Flaw Parameter	Calculated k Surface Flaw Parameter	Mean of ¹ Theoretical Equivalent Failure Load Data (psf)	Standard Deviation ¹ of Theoretical Equivalent Failure Load Data (psf)	Coefficient ¹ of Variation of Theoretical Equivalent Failure Load Data (percent)
4	9.94×10^{-18}	158.8	55.5	35.0
5	2.25×10^{-21}	163.3	47.4	29.0
6	4.97×10^{-25}	167.8	41.7	24.9
7	1.06×10^{-28}	171.9	37.8	22.0

¹Mean, standard deviation, and coefficient of variation of actual square GPL data are 168.0 psf, 37.5 psf, and 22.3 percent, respectively.

TABLE XIII.

COMPARISON OF CALCULATED AND THEORETICAL
RECTANGULAR GPL GLASS PLATE FAILURE LOAD STATISTICS

Assumed m Surface Flaw Parameter	Calculated k Surface Flaw Parameter	Mean of ¹ Theoretical Equivalent Failure Load Data (psf)	Standard Deviation ¹ of Theoretical Equivalent Failure Load Data (psf)	Coefficient ¹ of Variation of Theoretical Equivalent Failure Load Data (percent)
4	7.30×10^{-18}	76.2	25.4	33.3
5	1.72×10^{-21}	78.3	21.6	27.6
6	3.83×10^{-25}	80.3	19.6	23.7
7	7.89×10^{-29}	82.4	17.0	20.6

¹Mean, standard deviation, and coefficient of variation of actual rectangular GPL data are 79.0 psf, 18.4 psf, and 23.3 percent, respectively.

The best sets of surface flaw parameters to model the equivalent failure load distributions for both geometries of GPL glass plates were independently selected from the surface flaw parameter sets presented in Tables XII and XIII. Selections of the best sets of surface parameters were based upon comparisons of the theoretical means, standard deviations, relative density functions, and coefficients of variations with corresponding statistics of the actual equivalent failure data and manufacturer's data.

Comparisons of actual and theoretical data show that sets of surface flaw parameters with m equal to 6 gives the best representations of the mean of the square GPL equivalent failure load data (Ref. Table XII). Similar comparisons for the rectangular GPL data show that the sets of surface flaw parameters with m equal to 5 or 6 seem to estimate the mean of the rectangular GPL equivalent failure load data equally well (Ref. Table XII). Comparisons of actual and theoretical standard deviations of the equivalent failure load distribution suggest that the surface flaw parameters with m equal to 7 and 6 are the best choices to model the square and rectangular GPL equivalent failure load data, respectively. Comparisons of actual and theoretical relative cumulative equivalent failure load frequencies suggest that the sets of surface flaw parameters with m equal to 6 provide the best

representations for the GPL failure strength data 117

(Ref. Figures 28 and 29). Finally, manufacturer's literature published concerning glass similar to the GPL glass suggests that the coefficients of variations of glass plate failure load suggests that the coefficients of variations of glass plate failure load data should be 25 percent (PPG Industries 1964). The sets of surface flaw parameters with m equal to 6 give coefficients of variations closest to 25 percent.

Based upon the above comparisons, preferred surface flaw parameters chosen to represent the square GPL equivalent failure load data are m equal to 6 and k equal to $4.97 \times 10^{-2.5}$. The preferred surface flaw parameters to represent the rectangular GPL equivalent failure load data are equal to 6 and k equal to $3.83 \times 10^{-2.5}$. Statistical tests are presented in Appendix E to demonstrate that the statistics of theoretical equivalent failure load distributions determined using the preferred surface flaw parameters are not significantly different to the actual distributions.

According to the probability theory employed in development of the failure prediction model the preferred GPL surface flaw parameters should be the same. This is expected because both geometries of GPL glass had similar surface conditions. The preferred sets of GPL surface flaw parameters compare reasonably well, but there are

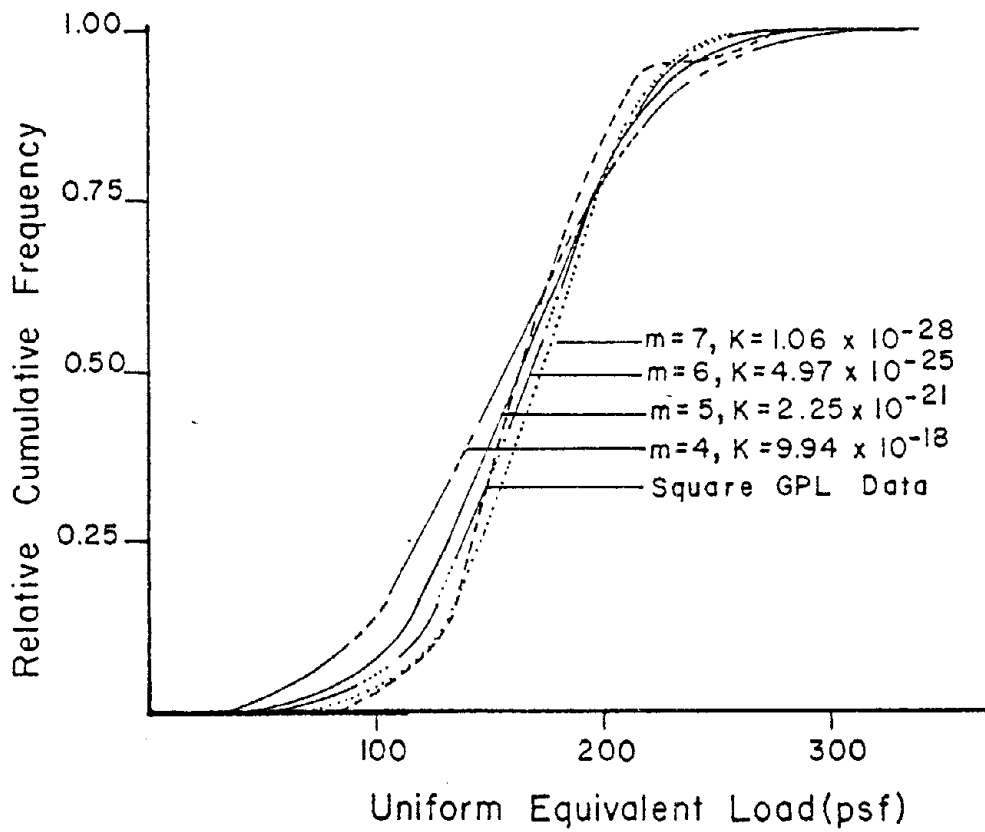


FIGURE 28. COMPARISONS OF ACTUAL AND THEORETICAL SQUARE GPL RELATIVE CUMULATIVE EQUIVALENT FAILURE LOAD FREQUENCIES

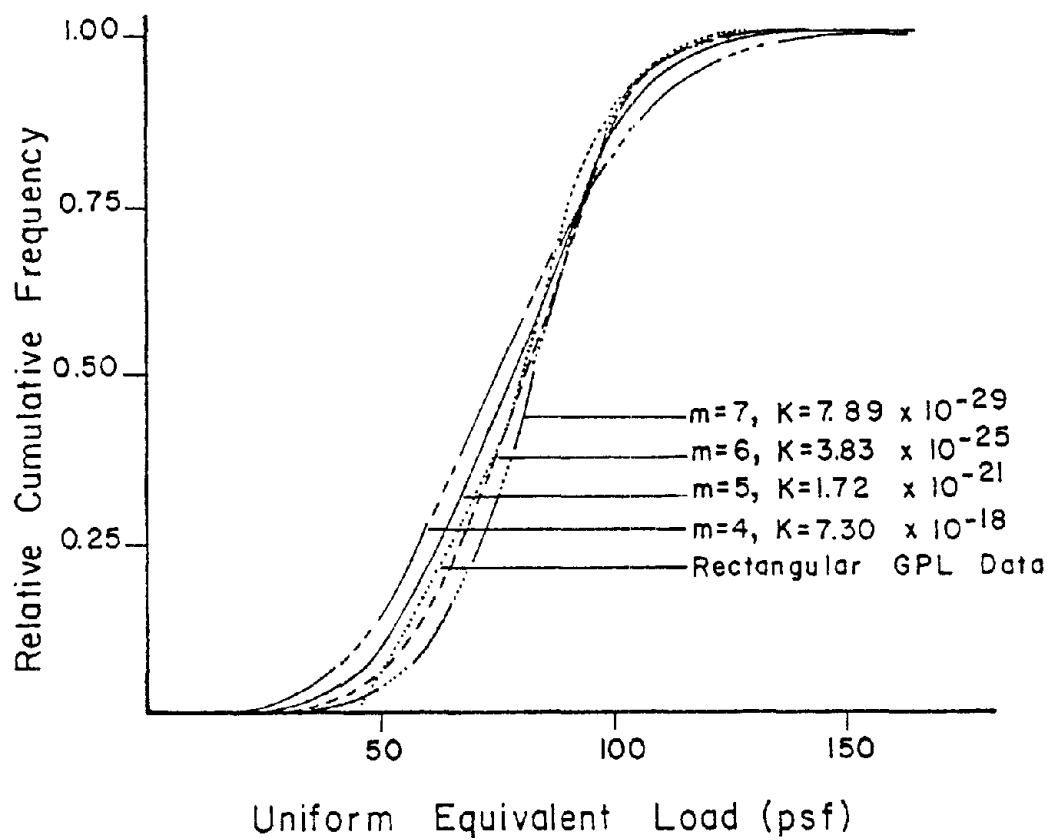


FIGURE 29. COMPARISONS OF ACTUAL AND THEORETICAL RECTANGULAR GPL RELATIVE CUMULATIVE EQUIVALENT FAILURE LOAD FREQUENCIES

distinct differences. It is shown in the next section 120
that the differences in the two different sets of GPL surface
flaw parameters are not statistically significant.

C. Validity of the Failure Prediction Model

The failure prediction model presented herein relates the strength of rectangular glass plates under lateral load to fundamental properties of the glass plate surface flaws. Variations of glass strength with load duration, temperature, and relative humidity are accounted for using a stress corrosion theory advanced by Brown (1974). Variations of glass plate strength due to plate behavior are accounted for using a statistical treatment of the surface flaw characteristics in conjunction with the nonlinear plate analysis presented in Chapter IV. Brown presented sufficient evidence to demonstrate the validity of the stress corrosion theory for glass. Validity of the nonlinear plate analysis was discussed in Chapter IV. Validity of the failure prediction model is, therefore, dependent upon demonstration that the strength of glass can be related to two surface flaw parameters which are independent of plate behavior.

1. Differences in GPL Plates

The glass plate surface flaw parameters (m, k) were independently determined for two different geometries of GPL glass plates of similar surface conditions in the

previous section. The GPL rectangular glass plates had¹²¹ a surface area of about 12 sq ft with an aspect ratio of 1:2.12. The GPL square glass plates had a surface area of about 6 sq ft. These differences in plate geometry produced significant differences in the stress fields induced in the plates.

The rectangular GPL plate response was dominated by bending action. The high tensile stress regions in the rectangular GPL plates were located in central plate areas as shown in Figure 24. In addition, the areas of high tensile stresses were characterized by a situation where the maximum equivalent principal stresses were significantly larger than the corresponding minimum equivalent principal stresses. This is substantiated by examination of the rectangular GPL fracture patterns (Ref. Appendix A) and by observing the changes in magnitudes of the maximum principal stresses when converted from MEPT to MCEPT stresses (Ref. Figures 24 and 25).

The square GPL plate response was characterized by a significant amount of membrane action. Unlike the rectangular plates, the region of high stress on the square glass plates extended from the center of the plate toward the corners of the plate (Ref. Fig. 26). Further, differences between the maximum and minimum equivalent principal stresses in the high stress regions were less pronounced than with the case of the rectangular plates. This is

substantiated by examination of the square GPL fracture patterns (Ref. Appendix A) and by comparing the MEPT and MCEPT stress fields for the square GPL plates presented in Figures 26 and 27.

Differences in the GPL plate geometries coupled with resulting differences in the attendant MEPT stress fields combine to suggest that the two geometries of GPL glass are significantly different from the standpoint of the failure prediction model.

2. Independence of the Glass Plate Surface Flaws

To demonstrate that the surface flaw parameters (m, k) are independent of plate response, a theoretical equivalent failure load distribution for the square GPL glass plates was calculated using the preferred GPL rectangular glass plate surface flaw parameters. Likewise, a theoretical equivalent failure load distribution for GPL rectangular glass plates was calculated using the preferred GPL square glass plate surface flaw parameters. Comparisons are then made between these theoretical and the actual equivalent failure load distributions.

Table XIV presents the theoretical and actual equivalent failure load distributions for GPL square glass plates. The mean and standard deviations of the theoretical equivalent failure load distribution for the square GPL glass plates were calculated to be 177.5 and 44.3 psf, respec-

TABLE XIV.

COMPARISON OF ACTUAL AND
CALCULATED SQUARE GPL THEORETICAL
EQUIVALENT FAILURE LOAD DATA

Equivalent Failure Load Interval (psf)	Corresponding Equivalent Area Interval (in ²)	Theoretical Interval Frequency ¹	Actual Interval Frequency
-130	- 26.4	2.92	2
130-160	21.4- 70.6	3.97	8
160-190	70.6-151.9	5.05	5
190-220	151.9-296.5	4.67	4
220-250	296.5-531.2	2.56	0
250-	531.2-	.83	1
		<hr style="width: 50%; margin: auto;"/> 20.00	<hr style="width: 50%; margin: auto;"/> 20

¹Theoretical interval frequencies calculated using the rectangular GPL surface flaw parameters ($m=6$, $k=3.83 \times 10^{-2.5}$).

tively (Ref. Appendix E). Table XV presents the theoretical and actual equivalent failure load distributions for the GPL rectangular glass plates. The mean and standard deviation of the theoretical equivalent failure load distribution for the GPL rectangular glass plates were calculated to be 76.2 and 18.2 psf, respectively (Ref. Appendix E).¹²⁴

The error involved in estimating the mean equivalent failure load for the GPL square glass plates using the preferred GPL rectangular glass plate surface flaw parameters is 6 percent. The error involved in estimating the mean equivalent failure load for the GPL rectangular glass plates using the preferred GPL square glass plate surface flaw parameters is 4 percent. Using a t test, the differences in the actual and theoretical means are not statistically significant. Further, no statistically significant differences between theoretical and actual variances (standard deviation squared) of the equivalent failure load distributions are detected using F tests. Finally, Chi-squared tests are used to show that there are no statistically significant differences between the actual and theoretical equivalent failure load distributions. These statistical comparisons are presented in Appendix E.

Based upon the statistical tests outlined above, it is concluded that the square GPL glass plate strength can be reasonably represented using the preferred rectangular

TABLE XV.

COMPARISON OF ACTUAL AND CALCULATED
RECTANGULAR GPL THEORETICAL
EQUIVALENT FAILURE LOAD DATA

Equivalent Failure Load Interval (psf)	Corresponding Equivalent Area Interval (in ²)	Theoretical Interval Frequency ¹	Actual Interval Frequency
- 60	- 27.2	3.80	3
60- 75	27.2- 78.1	5.28	5
75- 90	78.1-187.9	6.26	7
90-105	187.9-420.2	3.89	3
105-	420.2-	.77	2
		20.00	20

¹Theoretical interval frequencies calculated using the square GPL surface flaw parameters ($m=6$, $k=4.97 \times 10^{-2.5}$).

GPL glass plate surface parameters and vice versa. This demonstrates that the surface flaw parameters are indeed independent of glass plate area and plate response. It is thus shown that glass plate strength can be related to fundamental properties of the glass plate surface.

CONCLUSION

A. Summary of
Accomplishments

The strength of glass plates varies significantly with plate geometry, load duration, relative humidity, and temperature. As a result of the complexities attendant to defining glass strength, current window glass design procedures rely on empirical representations of glass plate strength. The empirically derived glass strength charts and tables in use today have served well for more than twenty years. During this time, window glass has evolved into a major structural component of the building envelope. Therefore, there is need for a new method to predict the strength of window glass for design purposes. An analytically derived failure prediction model for window glass is offered to answer this need.

Major tasks accomplished in development of the failure prediction model include:

- (1) a literature search was conducted to establish a plausible glass plate failure mechanism and to document variations of glass strength with load duration, relative humidity, and temperature,

- (2) a unique nonlinear plate solution was developed to model the response of thin rectangular glass plates subjected to uniform lateral loads, and
- (3) an available statistical theory of material strength was adapted to model the failure strength of glass plates.

The principal contribution of this research is the successful integration of the above tasks into a tractable process for predicting the strength of glass plates.

The failure prediction model relates the strength of glass plates to fundamental properties of glass plate surface flaws. The failure prediction model employs a stress corrosion theory advanced by Brown (1974) to represent the variation of glass strength with load duration, relative humidity, and temperature. In addition, the failure prediction model incorporates a geometrically nonlinear plate analysis and a statistical theory of material strength presented by Weibull (1939). All factors known to cause variability of glass plate strength are accounted for in the failure prediction model.

Brown (1974) presented sufficient evidence to verify the stress corrosion theory used in the failure prediction model. Validity of the nonlinear plate analysis was demonstrated by comparison of actual and theoretically derived glass plate stresses and deflections. Finally,

it was shown using glass plate failure data that the sur-¹²⁹face flaw parameters employed in the failure prediction model are independent of plate response. Therefore, a failure prediction model which relates the failure strength of glass to fundamental properties of the glass plate surface was presented and verified.

B. Directions of Future Research

The research reported herein is a segment of a much more extensive research project whose purpose it is to develop and present a new rational window glass design method (Minor and Beason 1976). The failure prediction model is a tool that is to be used to develop new window glass design relationships. To achieve this goal, two additional topics must be addressed:

- (1) research must be conducted to define the surface flaw characteristics of window glass found in practice, and
- (2) an investigation must be conducted to determine the degree to which deviations of actual window glass boundary conditions from the assumed set of idealized boundary conditions affect predicted glass strength results.

Once these additional areas have been addressed, a new window glass design procedure can be advanced.

LIST OF REFERENCES

- Anians, D. C., "Experimental Study of Edge Displacements of Laterally Loaded Window Glass Plates," Master Thesis, Texas Tech University, 1979.
- Al-Tayyib, A. J., "Geometrically Nonlinear Analysis of Rectangular Glass Panels by the Finite Element Method," Ph.D. Dissertation, Texas Tech University, 1980.
- Associate Committee on the National Building Code, "Commentary on the Design of Glass (draft for public comment)," Canadian Journal of Civil Engineering, Vol. 4, 1977, pp. 271-277.
- The BOCA Basic Building Code/1975, Sixth ed., Building Officials and Code Administrators International, Inc., Chicago, Illinois, 1975, p. 466.
- Baker, T. C., and F. W. Preston, "Fatigue of Glass Under Static Loads," Journal of Applied Physics, Vol. 17, Mar., 1945, pp. 170-178.
- Beason, W. L., and J. E. Minor, "Response of Window Glass to Wind Loads," Proceedings of The Third U.S. National Conference Wind Engineering Research, Division of Continuing Education, University of Florida, Gainesville, Florida, Feb. 26-Mar. 1, 1978, pp. 199-202.
- Black, L. V., "Effect of the Rate of Loading on the Breaking Strength of Glass," Bulletin of the American Ceramic Society, Vol. 15, No. 8, 1935, pp. 274-275.
- Bowles, R., and B. Sugarman, "The Strength and Deflection Characteristics of Large Rectangular Glass Panels Under Uniform Pressure," Glass Technology, Vol. 3, No. 5, 1962, pp. 156-170.
- Brown, W. G., "A Practicable Formulation for the Strength of Glass and Its Special Application to Large Plates," National Research Council of Canada, Publication No. NRC 14372, Ottawa, Nov., 1974.
- Charles, R. J., "Static Fatigue of Glass. I," Journal of Applied Physics, Vol. 29, No. 11, 1958, pp. 1549-1553.

- Charles, R. J., "Static Fatigue of Glass. II, Journal of Applied Physics, Vol. 29, No. 11, 1958, pp. 1554-1560.
- Charles, R. J., "Dynamic Fatigue of Glass," Journal of Applied Physics, Vol. 29, No. 12, 1958, pp. 1657-1662.
- Dalgliesh, W. A., "Assessment of Wind Loads for Glazing Design," Preprint of Paper Presented at IAHR Symposium, Karlsruhe, Germany, Sep. 3-6, 1979.
- Davenport, A. G., "Discussion of Peterka, J. A., and Cermak, J. E. (Wind Pressures on Buildings - Probability Densities)," Boundary Layer Wind Tunnel, University of Western Ontario, London, Ontario, Canada, 1976.
- Engineering News Record, "High Winds Smash 43 Sears Tower Windows," McGraw-Hill Publishing Co., New York, Feb. 28, 1974, p. 13.
- Engineering News Record, "\$6-Million Reglazing Starts on a 60-Story Tower Delayed 40 Months," McGraw-Hill Publishing Co., New York, Jun. 6, 1974, p. 14.
- Engineering News Record, "Hancock Windows Will Get 18-Hour Watch," McGraw-Hill Publishing Co., New York, Jul. 28, 1977, p. 15.
- Engineering News Record, "Hancock Loses 23rd New Window," McGraw-Hill Publishing Co., New York, Aug. 11, 1977, p. 3.
- Gilvarry, J. J., "Fracture of Brittle Solids. I. Distribution Function for Fragment Size in Single Fracture (Theoretical)," Journal of Applied Physics, Vol. 32, No. 3, 1961, pp. 391-399.
- Glathart, J. L., and F. W. Preston, "The Fatigue Modulus of Glass," Journal of Applied Physics, Vol. 17, Mar., 1946, pp. 189-195.
- Griffith, A. A., "The Phenomena of Rupture and Flow in Solids," Philosophical Transactions of the Royal Society of London, Vol. CCXXI-A587, Oct., 1920, pp. 163-179.

- Hershey, R. L., and T. H. Higgins, "Statistical Prediction Model for Glass Breakage from Nominal Sonic Boom Loads," Booz-Allen Applied Research, Inc., Report No. Faa-RD-73-79, Bethesda, Maryland, Jan., 1973.
- Ishizaki, H., "On the Large Deflections of Rectangular Glass Panes Under Uniform Pressure," Bulletin of the Disaster Prevention Research Institute, Kyoto University, Vol. 22, Part 1, No. 197, Dec., 1972.
- Ishizaki, H., S. Miyoshi, and T. Miura, "On the Design of Glass Pane Against Wind Loading," Proceedings of the Fourth International Conference on Wind Effects on Buildings and Structures, Cambridge University Press, Cambridge, Massachusetts, 1977, pp. 655-661.
- Johnson, J. W., and D. G. Holloway, "On the Shape and Size of the Fracture Zones on Glass Fracture Surfaces," Philosophical Magazine, Vol. 14, 1966, pp. 731-743.
- Jones, G. O., "The Interpretation of the Experimental Data on the Strength of Glass," Journal of the Society of Glass Technology, Vol. 33, 1949, pp. 120-137.
- Kaiser, R., "Rechnerische und experimentelle Ermittlung der Durchbiegungen und Spannungen von quadratischen Platten bei freier Auflagerung an den Randern, gleichmassig verteilter Last und grossen Ausbiegungen," Z.f.a.M.M., Bd. 16, Heft 2, Apr., 1936, pp. 73-98.
- Kennedy, J. B., and A. M. Neville, Basic Statistical Methods for Engineers and Scientists, Second ed., Harper and Row Publishers, New York, 1976.
- Kerper, M. J., and T. G. Scuderi, "Modulus of Rupture of Glass in Relation to Fracture Pattern," Ceramic Bulletin, Vol. 43, No. 9, 1964, pp. 622-625.
- Ketter, L., and S. P. Prawel, Modern Methods of Engineering Computation, McGraw-Hill Book Company, New York, 1969.
- Levengood, W. C., and W. E. Fowler, "Morphology of Fractures in Polished Glass Surfaces," Journal of the American Ceramic Society, Vol. 40, No. 1, 1957, pp. 31-34.

- Levy, S., "Bending of Rectangular Plates with Large Deflections," NACA Tech. Note no. 846, 1942.
- Libbey Owens Ford Company, "Strength of Glass Under Wind Loads," File: #1 - Strength of Glass, ATS-109, Toledo, Ohio, Jan. 21, 1980.
- Mehta, K. C., J. R. McDonald, J. E. Minor, and A. J. Sanger, "Response of Structural Systems to the Lubbock Storm," TTU SRR 03, Texas Tech University, Oct., 1971.
- Minor, J. E., "Window Glass in Windstorms," Civil Engineering Report series CE 74-01, Texas Tech University, May, 1974.
- Minor, J. E., and W. L. Beason, "Development of a Unified Approach to the Design of Window Glass Subjected to Dynamic Forces," National Science Foundation Award No. PFR77-24063, 1976.
- Moore, D., "Design Curves for Non-Linear Analysis of Simply-Supported, Uniformly-Loaded Rectangular Plates," Preprint of paper presented at AIAA/ASME/ASCE/AHS 20th Structure, Structural Dynamics and Materials Conference, St. Louis, Missouri, Apr. 4-6, 1979.
- Mould, R. E., and R. D. Southwick, "Strength and Static Fatigue of Abraded Glass Under Controlled Ambient Conditions: I, General Concepts and Apparatus," Journal of the American Ceramic Society, Vol. 42, No. 11, 1959, pp. 542-547.
- Mould, R. E., and R. D. Southwick, "Strength and Static Fatigue of Abraded Glass Under Controlled Ambient Conditions: II, Effect of Various Abrasions and the Universal Fatigue Curve," Journal of the American Ceramic Society, Vol. 42, No. 12, 1959, pp. 582-592.
- Orr, L., "Engineering Properties of Glass," Publication 478, Building Research Institute, National Academy of Sciences, National Research Council, Washington, D.C., 1957, pp. 51-61.
- Orr, L., "Practical Analysis of Fractures in Glass Windows," Materials Research and Standards, MTRSA, Vol. 12, No. 1, 1972, pp. 21-23, 47.

- Oughton, D., "Analysis of Glass Fractures," The Glass Industry, Feb., 1945, pp. 72-74, 90.
- Peterka, J. A., and J. E. Cermak, "Wind Pressures on Buildings - Probability Densities," Journal of Structural Division, Proceedings of ASCE, Vol. 101, No. ST6, June, 1975, pp. 1255-1267.
- Pfeiffer, P. E., and David A. Schum, Introduction to Applied Probability, Academic Press, New York, 1973.
- PPG Industries, "Glass Product Recommendations: Structural," Technical Service Report 101, Pittsburgh Plate Glass Company, Pittsburgh, Pennsylvania, 1964.
- PPG Industries, "Glass Product Recommendations: Wind Load Performance," Technical Service Report 101A, PPG Industries, Pittsburgh, Pennsylvania, 1975.
- PPG Industries, "PPG Glass Thickness Recommendations to Meet Architects' Specified 1-Minute Wind Load," Technical Services/Flat Glass Division, PPG Industries, Pittsburgh, Pennsylvania, Apr. 23, 1979.
- Preston, F. W., "A Study of the Rupture of Glass," Journal of Applied Physics, Vol. 13, Oct., 1942, pp. 623-624.
- Rader, "On the Dynamics of Crack Growth in Glass," Experimental Mechanics, Apr., 1967, pp. 160-167.
- Saffir, H. S., "Effects of High Wind on Glazing and Curtainwalls, and Rational Design Methods for Glazing Curtainwalls," Proceedings of the Second U.S.A.-Japan Research Seminar on Wind Effects on Structures, University of Tokyo Press, 1976, pp. 227-235.
- Schoening, F. R. L., "On the Strength of Glass in Water Vapor," Journal of Applied Physics, Vol. 31, No. 10, 1960, pp. 1779-1784.
- Seely, F. B., and J. O. Smith, Advanced Mechanics of Materials, Second ed., John Wiley and Sons, Inc., New York, 1952.

- Shand, E. B., "Experimental Study of Fracture of Glass: I, The Fracture Process," Journal of the American Ceramic Society, Vol. 37, No. 2, 1954, pp. 52-60.
- Shand, E. B., "Experimental Study of Fracture of Glass: II, Experimental Data," Journal of the American Ceramic Society, Vol. 37, No. 12, 1954, pp. 559-572.
- Shand, E. B., Glass Engineering Handbook, McGraw-Hill Book Company, Inc., New York, 1958.
- Shand, E. B., "Breaking Stress of Glass Determined from Dimensions of Fracture Mirrors," Journal of the American Ceramic Society, Vol. 42, No. 10, 1959, pp. 474-477.
- Shand, E. B., "Fracture Velocity and Fracture Energy of Glass in the Fatigue Range," Journal of the American Ceramic Society, Vol. 44, No. 1, 1961, pp. 21-26.
- Shand, E. B., "Correlation of Strength of Glass With Fracture Flaws of Measured Size," Journal of the American Ceramic Society, Vol. 44, No. 9, 1961, pp. 451-455.
- Shand, E. B., "Strength of Glass-The Griffith Method Revised," Journal of the American Ceramic Society, Vol. 48, No. 1, 1965, pp. 43-49.
- Shand, E. B., "New Information on Glass Fracture," Proceedings of American Scientific Glass Blowers Society Symposium, 1969, pp. 117-128.
- Smekal, Adolf, "Festigkeitseigenschaften spöder Körper," Ergeb. d. exakt. Naturwiss. Vol. 15, 1936, p. 106.
- Standard Building Code, 1979 ed., Southern Building Code Congress International, Inc., Birmingham, Alabama, 1979, p. 27-7.
- Stanworth, J. E., Physical Properties of Glass, Clarendon Press, Oxford, 1950.

- Stockdale, G. F., F. V. Tooley, and C. W. Ying, "Changes in the Tensile Strength of Glass Caused by Water Immersion Treatment," Journal of the American Ceramic Society, Vol. 34, No. 4, 1951, pp. 116-121.
- Szilard, R., Theory and Analysis of Plates: Classical and Numerical Methods, Prentice-Hall, Inc., Englewood Cliffs, New Jersey, 1974.
- Thom, H. C. S., "Frequency of Maximum Wind Speeds," Proceedings Sep. No. 539, ASCE, Vol. 80, Nov., 1954.
- Thom, H. C. S., "Distributions of Extreme Winds in the United States," Journal of the Structural Division, Proceedings of ASCE, Vol. 86, No. ST4, Apr., 1960, pp. 11-24.
- Thom, H. C. S., "New Distributions of Extreme Winds in the United States," Journal of the Structural Division, Proceedings of ASCE, Vol. 94, No. ST7, Jul., 1968.
- Thompson, N. J., and E. W. Cousins, "Explosion Tests on Glass Windows; Effect on Glass Breakage of Varying the Rate of Pressure Application," Journal of the American Ceramic Society, Vol. 32, No. 10, 1949, pp. 313-315.
- Timoshenko, S., and S. Woinowsky-Krieger, Theory of Plates and Shells, McGraw-Hill Book Company, New York, 1959.
- Tsai, C. R., and R. A. Stewart, "Stress Analysis of Large Deflection of Glass Plates by the Finite-Element Method," Journal of the American Ceramic Society, Vol. 59, No. 9-10, 1976, pp. 445-448.
- Uniform Building Code, 1973 ed., International Conference of Building Officials, Whittier, California, 1973, p. 616.
- Vonnegut, B., and J. G. Glathart, "Effect of Water on Strength of Glass," Journal of Applied Physics, Vol. 17, No. 12, 1946, pp. 1082-1085.

- Weibull, W. , "A Statistical Theory of the Strength of Materials," Ingeniörsvetenskapsakademiens, Handlingar NR151, Stockholm, 1939.
- Weyl, W. A. , "The Mechanical Strength of Glass: Part I," The Glass Industry, Vol. 27, No. 1, 1946, pp. 17-21, 32, 34, 36, 38, 48-50.
- Weyl, W. A. , "The Mechanical Strength of Glass: Part II," The Glass Industry, Vol. 27, No. 2, 1946, pp. 74-76, 96, 98, 100-101.
- Weyl, W. A. , "The Mechanical Strength of Glass: Part III," The Glass Industry, Vol. 27, No. 3, 1946, pp. 126-129, 130, 152, 154-156.
- Wiederhorn, S. M. , "Influence of Water Vapor on Crack Propagation in Soda-Lime Glass," Journal of the American Ceramic Society, Vol. 50, No. 8, 1967, pp. 407-414.

APPENDICES

- A. Analysis of Glass Plate Fracture Patterns
- B. Algebraic Manipulations of Nonlinear Plate Equations
- C. Computer Program to Perform Nonlinear Plate Analysis
- D. Glass Plate Tests
- E. Statistical Calculations

Appendix A
Analysis of Glass Plate Fracture Patterns

APPENDIX A

ANALYSIS OF GLASS PLATE FRACTURE PATTERNS

Much can be learned regarding the nature of the loading and the stress distribution present in a glass plate at the time of failure by examining the glass plate fracture pattern. Information that can be taken from a glass plate fracture pattern analysis depends upon the extent to which the fracture pattern can be reconstructed without introducing secondary fractures which obscure the nature of the original fracture pattern. In most instances of window glass failure in buildings exposed to wind loadings, it is not possible to reconstruct the total glass plate fracture pattern because of the catastrophic nature of the failure. In glass testing reported herein, a tape grid was applied to the compression surface of each glass plate prior to testing and the applied pressure was vented immediately after the plate failed so that the fracture pattern was preserved. The following discussion presents the fundamental concepts involved in a thorough analysis of a glass plate fracture pattern.

When a glass plate fails as the result of an applied pressure, the fracture usually originates at a single point on the glass plate surface. An estimate of the magnitude of the maximum nominal tensile stress present in the glass plate at the instant of fracture initiation

can be made by examining the characteristics of the fracture surface at the fracture origination point. The orientation of the initial crack direction at the point of fracture origination tends to be normal to the direction of the maximum principal tensile stress, particularly if the maximum principal stress is much larger than the minimum principal stress. All other cracks in the glass plate emanate from this original crack.

If the fracture initiation point is located away from the plate edge the initial crack will proceed in opposite directions away from the critical flaw. Then, depending upon the magnitude and state of stress present in the glass plate, the initial cracks may branch. These newly formed branch cracks will propagate and may subdivide in a similar manner until a free edge is encountered or the energy involved in crack propagation is dissipated. The fracture origination point can be located by tracing the branching cracks back to their common source as shown in Figure A.1.

Examination of the newly formed crack surface reveals the presence of markings which have been termed "rib-marks" and "hackle-marks" by Preston (1926). Typical rib-marks which might appear on the fracture surface of the glass plate which was failed with a uniform lateral pressure are shown in Figure A.2. Cracks propagate through rib-marks from the concave side. The direction of crack pro-

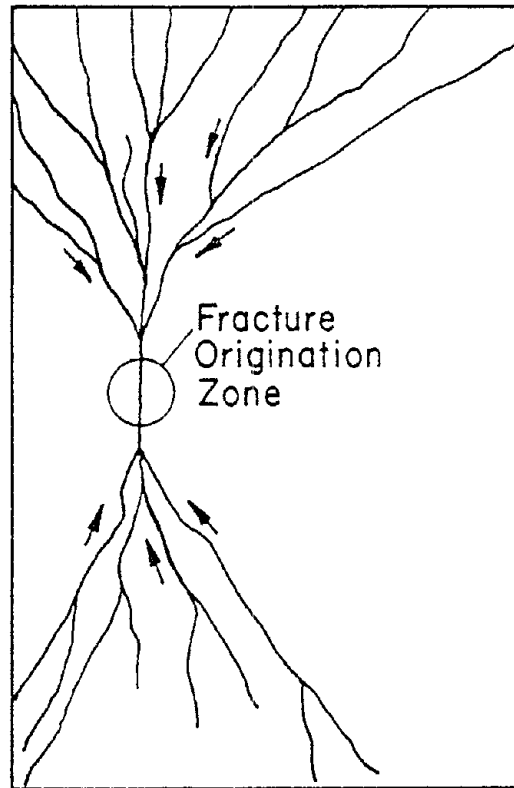


FIGURE A.1. LOCATION OF FRACTURE ORIGIN

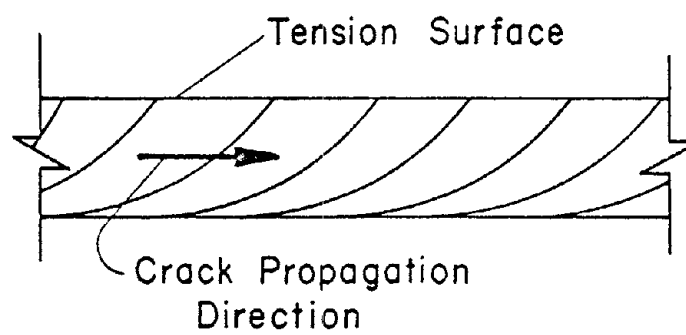
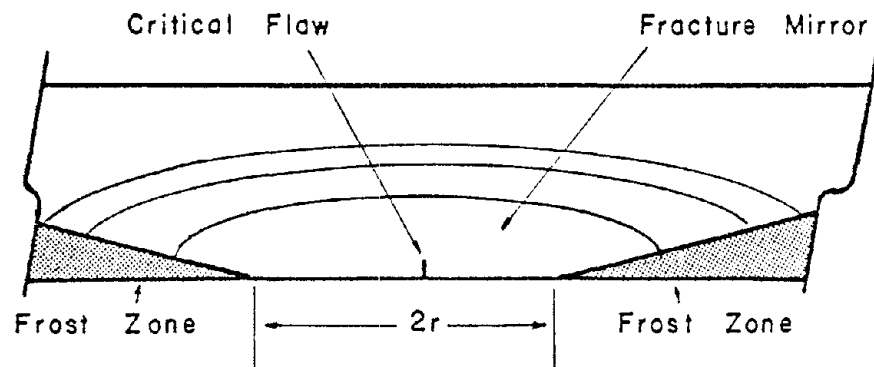


FIGURE A.2. SCHEMATIC OF GLASS PLATE FRACTURE SURFACE

pagation is indicated for the fracture surface shown in Figure A.2. The rib-marks will tend to be tangent to the surface of the glass plate which was in compression and the rib-marks will tend to intersect the tension surface of the glass plate as shown in Figure A.2 (Preston 1926, Oughton 1945, Orr 1972). Confirmation of crack propagation directions lends credence to the preliminary location of the fracture origination point made by examining the overall fracture pattern.

The precise location of the fracture initiation point can be identified by location of the fracture mirror on the fracture surface (Preston 1926, Oughton 1945, Shand 1959, Orr 1972, Johnson and Holloway 1966, Kerper and Scuderi 1964). The fracture mirror appears on the fracture surface as a highly polished, semicircular shaped area. The fracture mirror is centered about the fracture inducing flaw and is bounded by regions of frost as shown in Figure A.3. The fracture mirror radius is defined as half of the distance between the initiation of the frost zones on either side of the critical flaw as indicated in Figure A.3. The magnitude of the maximum nominal principal tensile stress present at the critical flaw prior to failure is inversely proportional to the fracture mirror radius (Shand 1961). Orr (1972) suggested the following empirical relationship between the maximum nominal tensile stress, σ_p , and the fracture mirror radius, r , for window glass



$$\sigma_p (\text{psi}) = \frac{1950}{\sqrt{r(\text{in.})}}$$

FIGURE A.3. SCHEMATIC OF FRACTURE MIRROR

$$\sigma_p = \frac{1950}{\sqrt{r}} \quad (\text{A.1})$$

where the fracture mirror radius is given in in. and the stress is given in psi.

The mechanism which produces the fracture mirror is extremely complex. The crack propagates away from the critical flaw with an initial velocity which is proportional to the magnitude of the maximum nominal principal tensile stress. The initial crack propagation velocity is low with respect to the limiting crack velocity. The rate of crack propagation increases until a condition of instability is reached at which point the crack propagation velocity jumps rapidly to its limiting value of 1500 m/s (Shand 1961). The highly polished portion of the fracture mirror forms during the early stages of crack propagation when the crack velocity is low. The frost region forms when the crack propagation velocity enters the unstable region (Shand 1959). The higher the nominal tensile stress is at the onset of fracture, the higher the initial crack propagation velocity and the smaller the distance required to reach the unstable regime; hence, the smaller the fracture mirror radius. Conversely, the lower the nominal tensile stress present at the fracture initiations the larger the fracture mirror radius.

Many generalizations can be made regarding the appearance of the total fracture pattern. If the state of biaxial stress in the plate at the point of fracture origination is such that the maximum principal stress is much larger than the minimum principal stress, the cracks will tend to propagate so that at each point they will tend to be normal to the direction of the maximum principal stress in a well-defined pattern. This situation occurred in the rectangular plates tested, as shown in Figure A.4. If the state of biaxial stress is such that the maximum and minimum principal stresses are very nearly the same at the point of fracture initiation, then the primary crack direction will still tend to be normal to the maximum principal stresses. However, in this later situation there will be a large number of secondary cracks at other orientations. This situation occurred in square plates tested as shown in Figure A.5.

For a given glass plate geometry and loading situation the number of cracks and the size of the resulting pieces of glass are related to the magnitude of strain energy stored in the annealed glass specimens or the relative load intensity at failure. The more individual pieces that are generated when a plate fractures, the higher the stress levels that were in the plate (Gilvary 1961). Therefore, the more cracks that are produced in a specimen, the higher the stress levels that were in the plate.

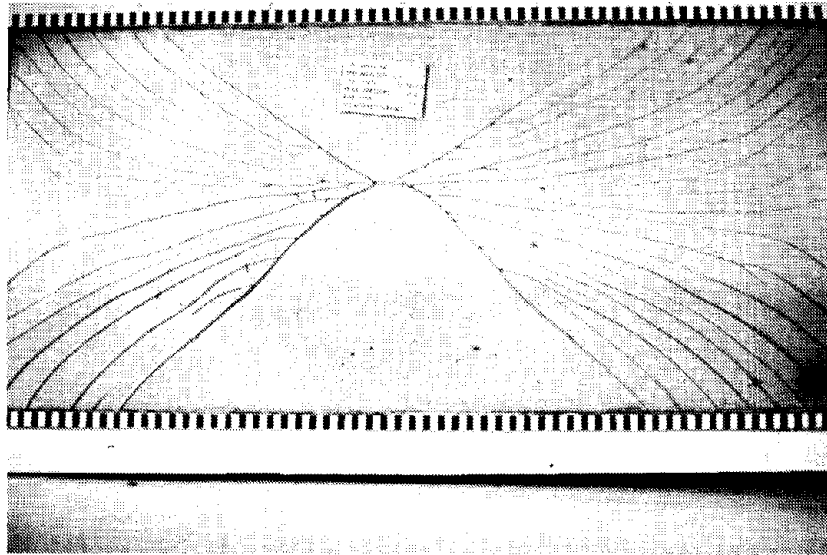


FIGURE A.4 TYPICAL RECTANGULAR GPL GLASS PLATE
FRACTURE PATTERN: $\sigma_{\max} \gg \sigma_{\min}$

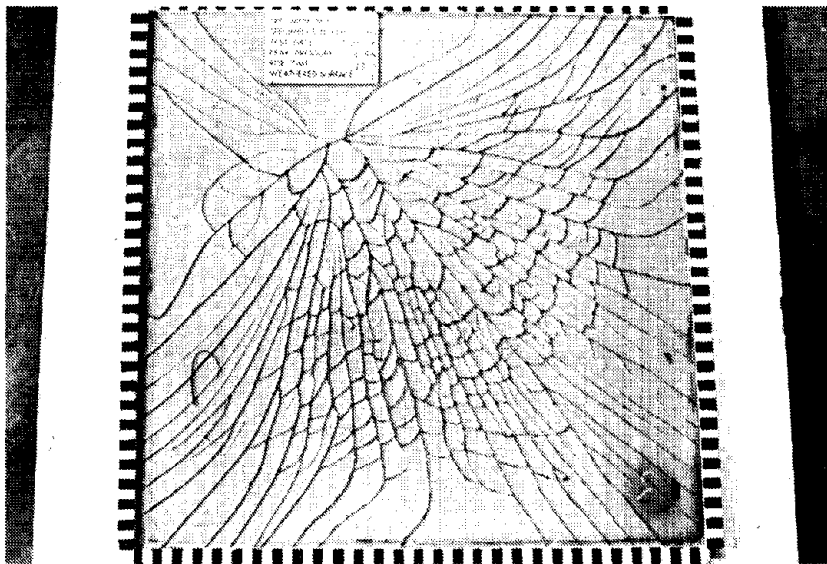


FIGURE A.5 TYPICAL SQUARE GPL GLASS PLATE
FRACTURE PATTERN: $\sigma_{\max} \approx \sigma_{\min}$

With the information presented in this appendix it is possible to examine a failed glass plate and determine the fracture origination point and estimate the maximum nominal stress present at the fracture origin. It is also possible to make generalizations regarding the bi-axial state of stress present in the plate at the time of failure. Finally, for similar glass plates, it is possible to rank the failed plates according to the relative load intensities present at failure.

Appendix B

Algebraic Manipulations of
Nonlinear Plate Equations

APPENDIX B

ALGEBRAIC MANIPULATIONS OF NONLINEAR PLATE EQUATIONS

The fundamental differential equations employed in the nonlinear plate solution are presented in Chapter IV. In addition, selections of infinite series to represent the variables in the nonlinear equations are presented. The series expansions are chosen to represent important plate boundary conditions. Details of the algebraic substitutions of the series expansions into the nonlinear plate equations are presented in this appendix. Information presented should aid in interpreting the computer program presented in Appendix C.

Equation (4.27) is written for a rectangular plate as follows

$$\frac{D}{h} \int_0^a \int_0^b \left(\frac{\partial^4 w}{\partial x^4} + 2 \frac{\partial^4 w}{\partial x^2 \partial y^2} + \frac{\partial^4 w}{\partial y^4} \right) \delta w \, dy dx = \quad (B.1)$$

$$\int_0^a \int_0^b \left(\frac{\partial^2 F}{\partial y^2} \frac{\partial^2 w}{\partial x^2} + \frac{\partial^2 F}{\partial x^2} \frac{\partial^2 w}{\partial y^2} - 2 \frac{\partial^2 F}{\partial x \partial y} \frac{\partial^2 w}{\partial x \partial y} + \frac{Pz}{h} \right) \delta w \, dy dx$$

There will be one independent equation generated from Equation (B.1) for each expansion function used to represent the lateral deflections. The general form of the equation for the mn^{th} series expansion term is

$$w_{mn} = \int_0^a \int_0^b (B1 + C1) \, dydx \Big/ \int_0^a \int_0^b A1 \, dydx \quad (B.2)$$

where A1, B1, and C1 are notations used in the computer program (Ref. Appendix C). The values of A1, B1, and C1 are

$$A1 = \frac{D}{h} (\alpha_m^4 + 2\alpha_m^2\beta_n^2 + \beta_n^4) \sin^2\alpha_m x \sin^2\beta_n y \quad (B.3)$$

$$\begin{aligned}
 B1 = & \left[\left(\begin{array}{cc} K & L \\ \Sigma & \Sigma \end{array} \right)_{k=1,3\dots \quad \ell=1,3\dots} -w_{k\ell} \alpha_k^2 \sin\alpha_k x \sin\beta_\ell y \right) : \\
 & \cdot \left(\begin{array}{cc} I & J \\ \Sigma & \Sigma \end{array} \right)_{i=2,4\dots \quad j=2,4\dots} -F_{ij} \beta_j^2 (-\cos\beta_j y + \cos\alpha_i x \cos\beta_j y) \Big) + \\
 & + \left(\begin{array}{cc} K & L \\ \Sigma & \Sigma \end{array} \right)_{k=1,3\dots \quad \ell=1,3\dots} -w_{k\ell} \beta_\ell^2 \sin\alpha_k x \sin\beta_\ell y \Big) \cdot \\
 & \cdot \left(\begin{array}{cc} I & J \\ \Sigma & \Sigma \end{array} \right)_{i=2,4\dots \quad j=2,4\dots} -F_{ij} \alpha_i^2 (-\cos\alpha_i x + \cos\alpha_i x \cos\beta_j y) \Big) - \\
 & - 2 \left(\begin{array}{cc} K & L \\ \Sigma & \Sigma \end{array} \right)_{k=1,3\dots \quad \ell=1,3\dots} w_{k\ell} \alpha_k \beta_\ell \cos\alpha_k x \cos\beta_\ell y \Big) \cdot \\
 & \cdot \left(\begin{array}{cc} I & J \\ \Sigma & \Sigma \end{array} \right)_{i=2,4\dots \quad j=2,4\dots} F_{ij} \alpha_i \beta_j \sin\alpha_i x \sin\beta_j y \Big) \Big] \cdot \\
 & \cdot \sin^2\alpha_m x \sin^2\beta_n y \quad (B.4)
 \end{aligned}$$

$$C1 = \frac{16P_0}{h\pi^2 mn} (\sin^2 \alpha_m x \sin^2 \beta_n y) \quad (B.5) \quad 152$$

where

$$\alpha_m = m\pi/a \quad (B.6)$$

$$\beta_n = n\pi/b \quad (B.7)$$

All of the other terms are defined in Chapter IV.

Equation (B.2) is used to generate simultaneous equations in terms of the lateral deflection coefficients. A Gauss-Seidel iterative technique (Ketter and Prawel 1969) is then used to estimate the lateral deflection coefficients.

Equation (4.27) is written for a rectangular plate as follows

$$\frac{1}{E} \int_0^a \int_0^b \left(\frac{\partial^4 \phi}{\partial x^4} + 2 \frac{\partial^4 \phi}{\partial x^2 \partial y^2} + \frac{\partial^4 \phi}{\partial y^4} \right) \delta F \, dy dx =$$

$$+ \int_0^a \int_0^b \left[\left(\frac{\partial^2 w}{\partial x \partial y} \right)^2 - \frac{\partial^2 w}{\partial x^2} \frac{\partial^2 w}{\partial y^2} \right] \delta F \, dy dx \quad (B.8)$$

One independent equation will be generated from Equation (B.8) for each series expansion term used to represent the membrane stress function. The general form of the equation for the mn^{th} series expansion term is:

$$F_{mn} = \int_0^a \int_0^b -(E1 + F1) \, dy dx \Bigg/ \int_0^a \int_0^b D1 \, dy dx \quad (B.9)$$

where D1, E1, and F1 are notations used in the computer program (Ref. Appendix C). Values of D1, E1, and F1 are as follows

$$D1 = \left[\frac{1}{E} (\alpha_m^4 + 2\alpha_m^2 \beta_n^2 + \beta_n^4) \cos \alpha_m x \cos \beta_n y - \frac{1}{E} (\alpha_m^4 \cos \alpha_m x + \beta_n^4 \cos \beta_n y) \right] (1 - \cos \alpha_m x) (1 - \cos \beta_n y) \quad (B.10)$$

$$E1 = \left[\left(\sum_{k=1,3,\dots}^K \sum_{\ell=1,3,\dots}^L -w_{k\ell} \alpha_k^2 \sin \alpha_k x \sin \beta_\ell y \right) \cdot \left(\sum_{k=1,3,\dots}^K \sum_{\ell=1,3,\dots}^L -w_{k\ell} \beta_\ell^2 \sin \alpha_k x \sin \beta_\ell y \right) - \left(\sum_{k=1,3,\dots}^K \sum_{\ell=1,3,\dots}^L \alpha_k \beta_\ell \cos \alpha_k x \cos \beta_\ell y \right)^2 \right] \cdot (1 - \cos \alpha_m x) (1 - \cos \beta_n y) \quad (B.11)$$

$$F1 = \sum_{\substack{i=2,4,\dots \\ i \neq m}}^I \sum_{\substack{j=2,4,\dots \\ j \neq n}}^J \frac{F_{ij}}{E} \left[(\alpha_i^4 + 2\alpha_i^2 \beta_j^2 + \beta_j^4) \cdot (\cos \alpha_i x \cos \beta_j y) - (\alpha_i^4 \cos \alpha_i x + \beta_j^4 \cos \beta_j y) \right] \cdot (1 - \cos \alpha_m x) (1 - \cos \beta_n y) \quad (B.12)$$

where all of the terms are defined in Chapter IV.

Equation (B.9) is used to generate simultaneous equations in terms of the membrane stress function coefficients. The lateral deflection coefficients are assumed to be constant. Simultaneous solution of the set of equations is then achieved using Gauss-Seidel iteration.

Appendix C

Computer Program to Perform
Nonlinear Plate Analysis

APPENDIX C

COMPUTER PROGRAM TO PERFORM NONLINEAR PLATE ANALYSIS

A listing of the computer program used to perform the geometrically nonlinear plate analysis described in Chapter IV is presented in Figure C.1. This computer program was written using ANSI FORTRAN. A sample computer output is presented in Figure C.2.

Pertinent plate theory is discussed in Chapter IV and specific equations relating to the program logic are presented in Appendix B. Validity of the computer program is demonstrated in Chapter IV by comparing results generated by the analysis with independent analytical results.

Input/output instructions for the computer program are presented in comment statements in the computer listing. In addition to input which describes the plate geometry, loading, and output characteristics, the user must input parameters which are unique to this method of solution. These solution parameters include the number of series expansion terms used to represent the different functions, the number of integration divisions, the iteration tolerances, and assumed values of lateral deflection coefficients. It was determined by the writer that a reasonably accurate and economical solution is obtained for most problems using four series expansion terms (NUM=3), 36 integration divisions across the total plate

Pages 157-166 have been removed.

Due to legibility problems, the following Figures have been omitted:

Fig. C.1 Computer Program for Nonlinear Plate Analysis

Fig. C.2 Sample Output from Nonlinear Plate Analysis Computer Program*

*For further information regarding these figures, please contact:

Dr. William L. Beason
Institute for Disaster Research
Texas Tech University
Lubbock, TX 79409

(INT=3), and an iteration tolerance on the lateral deflection coefficients of 0.01 in. If the number of series expansion terms is increased, the quality of the assumed lateral deflection coefficients must be increased, the number of integration divisions must be increased, and the iteration tolerance should be decreased. Even with these changes, the solution tends to be unstable. Therefore, it is not recommended to use more than four series terms.

Appendix D
Glass Plate Tests

APPENDIX D

GLASS PLATE TESTS

A homogeneous sample of 7/32 in. sheet glass was taken from the Great Plains Life (GPL) building located in Lubbock, Texas during renovation in 1975. The GPL glass was exposed to approximately 20 years of weathering as well as the peripheral effects of one tornado (Menta et al. 1971). Rectangular GPL glass plates were tested in their original dimensions, 28.5 x 60.5 in., and square GPL glass plates, 28.5 x 28.5 in., were prepared and tested. These specimens were tested to failure with controlled uniform lateral loads. A description of the test facility and test procedures along with the raw glass strength data are presented in this section.

D.1 Glass Test Facility

A facility was designed to test the GPL glass plates with a controlled uniform lateral load. The test facility consists of three major components: a glass plate test chamber, a loading system, and a data acquisition system. The glass test facility was constructed and located in the Civil Engineering Testing Laboratory located on the campus of Texas Tech University. A schematic of the plate test facility is presented in Figure D.1.

The glass plate test chamber consists of a steel reinforced plywood panel with a 1/8 in. steel plate laminated

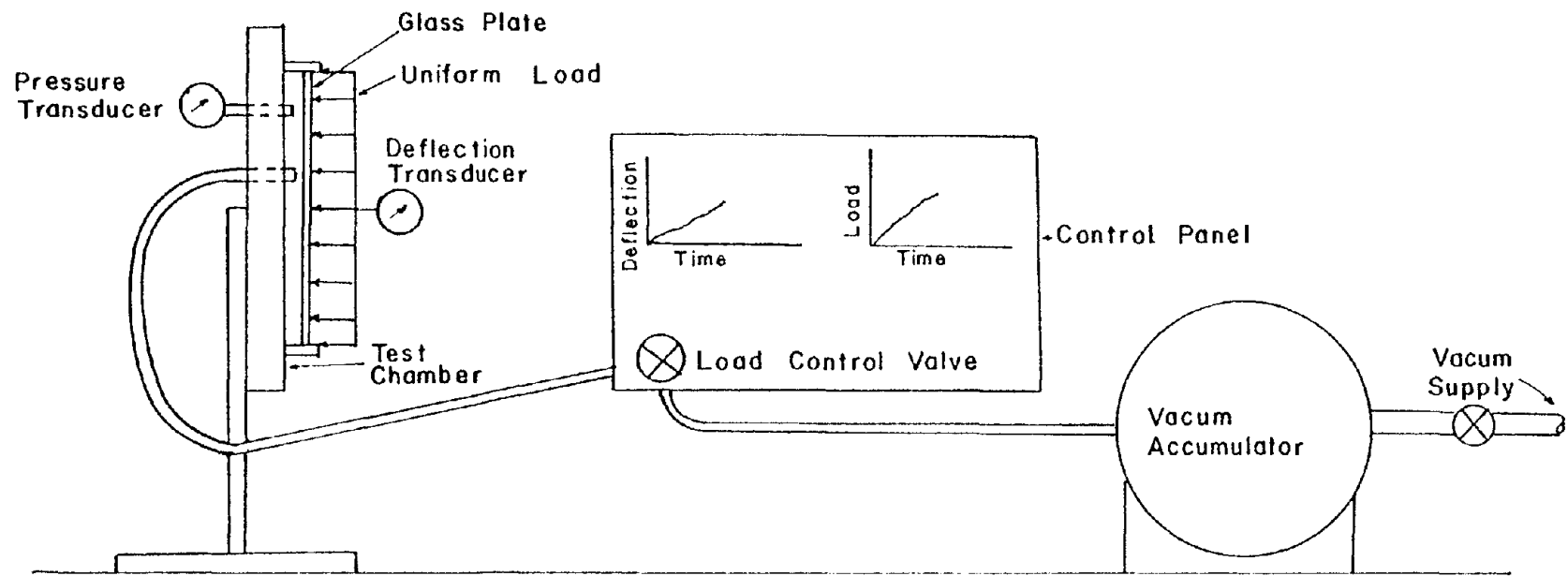


FIGURE D.1. SCHEMATIC OF GLASS PLATE TEST FACILITY

to the front side. This plywood/steel panel served as the backside of an airtight test chamber. An evacuation manifold was mounted to the backside of the plywood/steel panel. Four sections of aluminum window framing were mounted to the front side of the plywood/steel panel such that the pieces of the aluminum window framing served as the sides of the glass plate test chamber. All of the joints and seams in the glass plate test chamber were sealed with silicon sealant. When a glass plate is glazed into the aluminum glazing system using neoprene gaskets, it becomes the final side of the glass plate test chamber. Figure D.2 presents a view of the test chamber used for square glass plates.

A uniform lateral load is induced on a glass plate by reducing the internal pressure of the glass plate test chamber. The loading apparatus consists of a vacuum accumulation tank, a delivery manifold and appropriate hoses and valving. Once a test is begun the pressure reduction inside the vacuum test chamber is continuously monitored and appropriate corrections in the evacuation rate are performed manually to achieve the desired loading rate.

The instrumentation system consists of linear potentiometric pressure and displacement transducers. The pressure transducer is used to monitor the pressure differential between the inside of the glass plate test

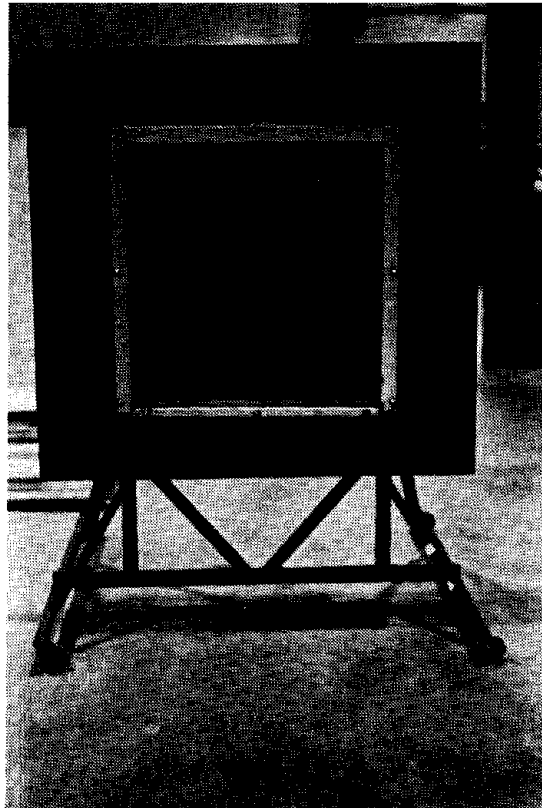


FIGURE D.2 SQUARE GPL GLASS
PLATE TEST CHAMBER

chamber and the atmospheric pressure. The displacement transducer is attached to the center of the glass plate. Outputs from the pressure and displacement transducers are monitored using a Mark IV Brush Recorder and a Hewlett Packard x-y plotter.

D.2 Glass Test Results

The strength of glass is a function of the glass plate surface condition. When glass plates are manufactured, there are significant differences in the strength characteristics of the two different sides due to the manufacturing exposure. Further, it was anticipated that the condition of the glass surfaces exposed to the internal building environment might be different than the condition of the glass surfaces exposed to the external building environment. There are a total of four different test conditions: two different glass plate surfaces and two different glass plate geometries. It was shown by Minor (1974) that a minimum of ten replications of a particular combination of test conditions should be performed to estimate the mean glass plate strength with acceptable confidence. Four different test conditions with ten replications each yields a total of 40 glass plate tests that were performed using the GPL glass.

The glass plates were exposed to monotonically increasing uniform lateral loads selected to cause failure in about 60 seconds or less. An attempt was made to

induce a linearly increasing uniform load. Variations of the loading rate posed no problem because the Brown (1974) stress corrosion theory allows load duration corrections to be made to the resulting data.

The raw glass strength data are presented in Tables D.I, D.II, D.III, and D.IV. Data presented in these tables are the time to failure, the coordinates of the fracture origination point, and the fracture mirror radius.

TABLE D.1

FAILURE DATA FOR SQUARE GPL
GLASS-EXTERIOR SURFACE IN TENSION

Failure Load (psf)	Time to Failure (sec)	Rectangular Coordinates of Failure ¹		Fracture Mirror Radius (in.)
		x (in.)	y (in.)	
225	64	8.5	14.1	.06
217	50	9.8	18.8	.10
216	40	8.8	10.3	.15
330	62	17.4	18.0	.07
189	37	12.1	15.6	.18
170	35	17.1	16.8	.14
233	50	17.1	23.3	.18
269	60	13.0	23.4	.09
200	27	12.6	17.8	.19
167	22	5.0	16.3	1.32 ²

¹Referenced to plate corner

²Poorly defined fracture mirror

TABLE D.II

FAILURE DATA FOR SQUARE GPL
GLASS-INTERIOR SURFACE IN TENSION

Failure Pressure	Time to Failure	Rectangular Coordinates of Failure Initiation ¹		Fracture Mirror Radius
		<u>x</u> (in.)	<u>y</u> (in.)	
202	40	11.6	21.8	.33 ²
161	34	16.4	9.6	.22
233	47	4.0	11.0	.35 ²
207	42	15.8	9.3	.14
189	38	16.0	7.5	.17
138	27	7.5	11.8	.86
196	38	12.0	17.0	.15
187	35	24.9	13.5	.72
144	26	13.3	14.5	.52
238	44	22.8	11.0	.35 ²

¹Referenced to plate corner

²Poorly defined fracture mirror

TABLE D.III

FAILURE DATA FOR RECTANGULAR GPL
GLASS-EXTERIOR SURFACE IN TENSION

Failure Pressure	Time to Failure	Rectangular Coordinates of Failure Initiation ¹		Fracture Mirror Radius
		x (in.)	y (in.)	
<u>(psf)</u>	<u>(sec)</u>	<u>(in.)</u>	<u>(in.)</u>	<u>(in.)</u>
95	34	33.0	12.5	.11
111	42	13.5	11.5	.19
144	57	44.5	13.5	.08
197	42	25.5	9.0	.14
96	50	24.0	11.0	.11
107	31	28.5	15.5	.11
105	43	38.5	8.5	.13
109	49	50.8	8.3	.20
95	30	35.3	22.5	.22
128	23	26.0	12.5	.06

¹Referenced to plate corner

TABLE D.IV

FAILURE DATA FOR RECTANGULAR GPL
GLASS-INTERIOR SURFACE IN TENSION

Failure Pressure	Time to Failure	Rectangular Coordinates of Failure Initiation ¹		Fracture Mirror Radius		
		(psf)	(sec)		(in.)	(in.)
78	28			31.0	22.0	.49
66	25			39.5	11.8	.35 ²
130	51			44.5	13.5	.09
76	36			32.5	8.0	.28
81	43			39.5	20.0	.28 ²
65	21			38.0	12.5	.45
76	18			19.5	15.0	.25
88	45			30.0	9.5	.17
96	29			32.0	12.8	.12
75	35			28.5	12.0	.22

¹Referenced to plate corner

²Poorly defined fracture mirror

Appendix E
Statistical Calculations

APPENDIX E
STATISTICAL CALCULATIONS

This appendix contains statistical calculations which support conclusions and data presented in Chapter V. Calculations presented can be divided into three categories:

- (1) calculation of surface flaw parameters,
- (2) calculation of theoretical equivalent failure load statistics given a set of surface flaw parameters, and
- (3) comparisons of actual and theoretical equivalent failure load statistics.

Methodology for selection of glass plate surface flaw parameters to represent glass plate failure load data is presented in Chapter V. Calculation of theoretical equivalent load statistics is accomplished in tabular form using standard statistical techniques. Comparisons of actual and theoretical equivalent failure load statistics are accomplished using the t test to compare means, the F test to compare variances, and the Chi-squared test to compare frequency distributions. Fundamentals of the statistical methods employed to accomplish these tasks are reviewed as presented by Kennedy and Neville (1976) and specific calculations referenced in Chapter V are presented in this Appendix.

E.1 Fundamentals of
Statistical Methods

Calculations of the mean and standard deviations for the theoretical equivalent failure load distributions are accomplished in tabular form using standard statistical methods. The first column in a statistical calculation table (Ref. Table IX) defines a set of n non-overlapping, exhaustive, equivalent failure load intervals. The minimum equivalent failure load presented in the table is chosen so that its probability of occurrence is effectively zero. The maximum equivalent failure load presented in the table is chosen so that its probability of occurrence is effectively one. The second column contains the median values, x_i , of each equivalent failure load interval. Column three contains the theoretical probability of interval occurrence, p_i . These probabilities are calculated using Equation (5.17) and the total equivalent area data presented in Tables VIII and IX. The summation of column three should be effectively equal to one. Column four contains values obtained by multiplying the median intervals, x_i , by the corresponding interval probabilities, p_i . The mean, μ , theoretical equivalent failure load is then calculated as follows

$$\mu = \sum_{i=1}^n x_i p_i$$

Column five of the table contains a value calculated by multiplying the interval probability, p_i , by the square of the difference of median interval value and the mean equivalent failure load, $(x_i - \mu)^2$. The theoretical standard deviation, σ , of the equivalent failure load distribution is then calculated as follows

$$\sigma = \sqrt{\sum_{i=1}^n p_i (x_i - \mu)^2} \quad (\text{E.2})$$

The t test is used to compare actual and theoretical mean equivalent failure loads. It is assumed that there is no significant difference between the actual and theoretical mean equivalent failure loads. Then the probability of the difference between the actual and theoretical mean equivalent failure loads being as large as observed is calculated. If this probability is sufficiently small, it is concluded that the actual and theoretical means are significantly different. To evaluate this probability, the t statistic is calculated as follows:

$$t = \frac{|\mu - \bar{x}|}{s/\sqrt{n}} \quad (\text{E.3})$$

where μ is the theoretical mean equivalent failure load, \bar{x} is the actual mean equivalent failure load, s is the actual

standard deviation of the equivalent failure load data, and n is the number of glass plates tested. Values of the t statistic associated with different levels of significance are commonly available in tabular form given the number of degrees of freedom associated with the t statistic. The number of degrees of freedom associated with the t statistic is the sample size minus one.

An F test is used to compare actual and theoretical variances (standard deviations squared). It is assumed that the difference between the actual and theoretical variances is not significant. Then the probability of the differences of the variances being as large as observed is calculated. If this probability is small, it is concluded that the variances are significantly different. To evaluate this probability, the F statistic is calculated as follows

$$F = \frac{S_1^2}{S_2^2} \quad (\text{E.4})$$

where S_1^2 is the largest variance and S_2^2 is the smallest variance. Values of the F statistic associated with different levels of significance are available as a function of the number of degrees of freedom associated with the actual equivalent failure load distribution ($n-1$) and the number of degrees of freedom associated with the theoretical variance (∞).

A Chi-squared test is used to compare actual and calculated frequency distributions. Again, it is assumed that the actual and theoretical frequency distributions are not significantly different and the probability of the differences being as large as observed is evaluated. If that probability is small, it is concluded that the frequency distributions are significantly different. To evaluate this probability, the theoretical and actual equivalent failure load frequency distributions are divided into k classes with common boundaries. The Chi-squared statistic, χ^2 , is then calculated as follows

$$\chi^2 = \sum_{i=1}^k \frac{(E_i - O_i)^2}{E_i} \quad (\text{E.5})$$

where O_i is the observed frequency of the i^{th} class and E_i is the theoretical frequency of the i^{th} class. Probabilities of occurrence of different values of χ^2 statistic are available in tables as a function of the number of degrees of freedom (d.o.f.) associated with the test. The d.o.f. associated with the Chi-squared statistic is found as follows

$$\text{d.o.f.} = k - 1 - m \quad (\text{E.6})$$

where m is the number of independent distribution parameters used to calculate the theoretical frequencies, if these are determined using the observed statistics.

Finally, due to assumptions involved in the Chi-squared tests, each theoretical class must have a frequency of at least five.

E.2 Calculations

Tables E.I - E.VIII present mean total equivalent area tables for both geometries of GPL glass plates assuming integer values of the m surface flaw parameter ranging from 4 to 7. In addition, calculation of the best k surface flaw for each situation using Equation (5.21) is presented at the bottom of each table.

Calculations of the means and standard deviations of the theoretical equivalent failure load distributions defined by the different sets of surface flaw parameters are presented in Tables E.IX - E.XIII. Selections of the preferred sets of surface flaw parameters to represent both geometries of GPL glass are made in Chapter V based upon comparisons of the theoretical equivalent failure load statistics with the actual equivalent failure load statistics.

Statistical tests are conducted to compare the actual GPL equivalent failure load statistics to the corresponding theoretical equivalent failure load statistics using the preferred sets of surface flaw parameters. These tests are conducted for both geometries of GPL glass. Table E. XIX presents results for the t tests, Table E.XX

TABLE E.1
 MEAN TOTAL EQUIVALENT AREA TABLE
 FOR SQUARE GPL GLASS PLATES: $m=4$

Equivalent Failure Load Interval (psf)	Corresponding Total Equivalent Area Interval (in. ²)	Midpoint of Total Equivalent Area Interval, $S_{u,i}$ (in. ²)	Internal Frequency f_i	$f_i S_{u,i}$
100-130	24.1- 62.0	43.1	2	86.2
130-160	62.0-116.2	89.1	8	712.8
160-190	116.2-203.5	159.9	5	799.5
190-220	203.5-325.5	264.5	4	1058.0
220-250	325.5-472.8	399.2	0	0
250-280	472.8-648.2	560.5	1	560.5
			<hr style="width: 100%; border: 0.5px solid black;"/> 20	<hr style="width: 100%; border: 0.5px solid black;"/> 3217.0

$$\bar{S}_u = \frac{3217.0}{20} = 160.9 \text{ in.}^2$$

$$k = \frac{1}{(5000)^4 160.9} = 9.94 \times 10^{-16}$$

TABLE E.II

MEAN TOTAL EQUIVALENT AREA TABLE
FOR SQUARE GPL GLASS PLATES: m=5

Equivalent Failure Load Interval (psf)	Corresponding Total Equivalent Area Interval (in. ²)	Midpoint of Total Equivalent Area Interval, S_{5i} (in. ²)	Interval Frequency f_i	$f_i S_{5i}$
100-130	12.6- 40.2	26.4	2	52.8
130-160	40.2- 91.7	66.0	8	528.0
160-190	91.7-174.2	133.0	5	665.0
190-220	174.2-308.3	241.3	4	965.2
220-250	308.3-504.1	406.2	0	0
250-280	504.1-753.2	628.7	1	628.7
			20	2839.7

$$\bar{S}_5 = \frac{2839.7}{20} = 142.0 \text{ in.}^2$$

$$k = \frac{1}{(5000)^5 142.0} = 2.25 \times 10^{-21}$$

TABLE E.III

MEAN TOTAL EQUIVALENT AREA TABLE
FOR SQUARE GPL GLASS PLATES: m=6

Equivalent Failure Load Interval (psf)	Corresponding Total Equivalent Area Interval (in. ²)	Midpoint of Total Equivalent Area Interval, S_{6i} (in. ²)	Interval Frequency f_i	$f_i S_{6i}$
100-130	6.4- 26.4	16.4	2	32.8
130-160	26.4- 70.6	48.5	8	388.0
160-190	70.6-151.9	111.3	5	556.5
190-220	151.9-296.5	224.2	4	896.8
220-250	296.5-531.2	413.9	0	0
250-280	531.2-875.6	703.4	1	703.4
			<u>20</u>	<u>2577.5</u>

$$\bar{S}_6 = \frac{2577.5}{20} = 128.9 \text{ in.}^2$$

$$k = \frac{1}{(5000)^6 128.9} = 4.97 \times 10^{-25}$$

TABLE E.IV

MEAN TOTAL EQUIVALENT AREA TABLE
FOR SQUARE GPL GLASS PLATES: m=7

Equivalent Failure Load Interval (psf)	Corresponding Total Equivalent Area Interval (in. ²)	Midpoint of Total Equivalent Area Interval, S_{7i} (in. ²)	Interval Frequency f_i	$f_i S_{7i}$
100-130	3.4- 17.7	10.6	2	21.2
130-160	17.7- 55.2	36.5	8	292.0
160-190	55.2- 134.4	94.8	5	474.0
190-220	134.4- 290.7	212.6	4	850.4
220-250	290.7- 570.0	430.4	0	0
250-280	570.0-1005.9	788.0	1	788.0
			<u>20</u>	<u>2425.6</u>

$$\bar{S}_7 = \frac{2425.6}{20} = 121.3 \text{ in.}^2$$

$$k = \frac{1}{(5000)^7 121.3} = 1.06 \times 10^{-28}$$

TABLE E.V

MEAN TOTAL EQUIVALENT AREA TABLE
FOR RECTANGULAR GPL GLASS PLATES: m=4

Equivalent Failure Load Interval (psf)	Corresponding Total Equivalent Area Interval (in. ²)	Midpoint of Total Equivalent Area Interval, S_{4i}	Interval Frequency f_i	$f_i S_{4i}$
45-60	22.7- 70.4	46.6	3	139.8
60-75	70.4-155.7	113.1	5	565.5
75-90	155.7-273.5	214.6	7	1502.2
90-105	273.5-443.0	358.3	3	1074.9
105-120	443.0-659.8	551.4	2	1102.8
			<u>20</u>	<u>4385.2</u>

$$\bar{S}_4 = \frac{4385.2}{20} = 219.3 \text{ in.}^2$$

$$k = \frac{1}{(5000)^4 219.3} = 7.30 \times 10^{-18}$$

TABLE E.VI

MEAN TOTAL EQUIVALENT AREA TABLE
FOR RECTANGULAR GPL GLASS PLATES: m=5

Equivalent Failure Load Interval (psf)	Corresponding Total Equivalent Area Interval (in. ²)	Midpoint of Total Equivalent Area Interval, S_{s_i}	Interval Frequency f_i	$f_i S_{s_i}$
45-60	10.3- 43.7	27.0	3	81.0
60-75	43.7-106.5	75.1	5	375.5
75-90	106.5-221.3	163.9	7	1147.3
90-105	221.3-422.0	321.7	3	965.1
105-120	422.0-720.9	571.5	2	1143.0
			20	3711.9

$$\bar{S}_s = \frac{3711.9}{20} = 185.6 \text{ in.}^2$$

$$k = \frac{1}{(5000)^5 185.6} = 1.72 \times 10^{-21}$$

TABLE E.VII

MEAN TOTAL EQUIVALENT AREA TABLE
FOR RECTANGULAR GPL GLASS PLATES: m=6

Equivalent Failure Load Interval (psf)	Corresponding Total Equivalent Area Interval (in. ²)	Midpoint of Total Equivalent Area Interval, S_{6i}	Interval Frequency f_i	$f_i S_{6i}$
45-60	5.6- 27.2	16.4	3	49.2
60-75	27.2- 78.1	52.7	5	263.5
75-90	78.1-187.9	133.0	7	931.0
90-105	187.9-420.2	304.1	3	912.3
105-120	420.2-763.6	591.9	2	1183.8
			<u>20</u>	<u>3339.8</u>

$$\bar{S}_6 = \frac{3339.8}{20} = 167.0 \text{ in.}^2$$

$$k = \frac{1}{(5000)^6 167.0} = 3.83 \times 10^{-25}$$

TABLE E.VIII

MEAN TOTAL EQUIVALENT AREA TABLE
FOR RECTANGULAR CPL GLASS PLATES: m=7

Equivalent Failure Load Interval (psf)	Corresponding Total Equivalent Area Interval (in. ²)	Midpoint of Total Equivalent Area Interval, S_{7i}	Interval Frequency f_i	$f_i S_{7i}$
45-60	3.3- 17.0	10.2	3	30.6
60-75	17.0- 57.4	37.2	5	186.0
75-90	57.4-180.0	118.7	7	830.9
90-105	180.0-419.1	299.6	3	898.8
105-120	419.1-879.6	649.4	2	1298.8
			<u>20</u>	<u>3245.1</u>

$$\bar{S}_7 = \frac{3245.1}{20} = 162.3 \text{ in.}^2$$

$$k = \frac{1}{(5000)^7 162.3} = 7.89 \times 10^{-29}$$

TABLE E.IX

CALCULATION OF THEORETICAL SQUARE GPL GLASS
 PLATE EQUIVALENT FAILURE LOAD STATISTICS: $m=4$, $k=9.94 \times 10^{-10}$

Equivalent Failure Load Interval (psf)	Midpoint of Equivalent Failure Load Interval, x_i (psf)	Theoretical Interval Probability p_i	$x_i p_i$	$(x_i - \mu)^2 p_i$
10- 40	25	0.006	0.15	107.33
40- 70	55	0.047	2.59	505.91
70-100	85	0.086	7.31	467.76
100-130	115	0.181	20.82	346.45
130-160	145	0.195	28.28	36.87
160-190	175	0.203	35.53	53.60
190-220	205	0.150	30.75	320.86
220-250	235	0.079	18.57	459.31
250-280	265	0.035	9.28	395.12
280-310	295	0.014	4.13	259.90
310-340	325	0.003	.98	82.92
340-370	355	0.001	.36	38.51
			<u>158.75</u>	<u>3074.54</u>

$$\mu = 158.75 \text{ psf}$$

$$\sigma = \sqrt{3074.54} = 55.45 \text{ psf}$$

TABLE E.X

CALCULATION OF THEORETICAL SQUARE GPL GLASS
 PLATE EQUIVALENT FAILURE LOAD STATISTICS: $m=5$, $k=2.25 \times 10^{-21}$

Equivalent Failure Load Interval (psf)	Midpoint of Equivalent Failure Load Interval, x_i (psf)	Theoretical Interval Probability p_i	$x_i p_i$	$(x_i - \mu)^2 p_i$
10- 40	25	.002	0.05	38.24
40- 70	55	.022	1.21	257.89
70-100	85	.061	5.19	373.70
100-130	115	.162	18.63	377.46
130-160	145	.229	33.21	76.44
160-190	175	.231	40.43	31.78
190-220	205	.179	36.70	311.71
220-250	235	.085	19.98	437.34
250-280	265	.024	6.36	248.38
280-310	295	.004	1.18	69.41
310-340	325	.001	0.33	26.16
			<u>163.27</u>	<u>2248.51</u>

$$\mu = 163.27 \text{ psf}$$

$$\sigma = \sqrt{2248.51} = 47.42 \text{ psf}$$

TABLE E.XI

CALCULATION OF THEORETICAL SQUARE GPL GLASS
 PLATE EQUIVALENT FAILURE LOAD STATISTICS: $m=6$, $k=4.97 \times 10^{-2.5}$

Equivalent Failure Load Interval (psf)	Midpoint of Equivalent Failure Load Interval, x_i (psf)	Theoretical Interval Probability p_i	$x_i p_i$	$(x_i - \mu)^2 p_i$
40- 70	55	0.011	0.61	139.86
70-100	85	0.038	3.23	260.27
100-130	115	0.136	15.64	378.57
130-160	145	0.237	34.37	122.77
160-190	175	0.270	47.25	14.15
190-220	205	0.208	42.64	288.46
220-250	235	0.084	19.74	379.74
250-280	265	0.015	3.98	141.83
280-310	295	0.001	0.30	16.19
			167.76	1741.84

$$\mu = 167.76 \text{ psf}$$

$$\sigma = \sqrt{1741.84} = 41.74 \text{ psf}$$

TABLE E.XII

CALCULATION OF THEORETICAL SQUARE GPL GLASS
 PLATE EQUIVALENT FAILURE LOAD STATISTICS: $m=7$, $k=1.06 \times 10^{-2}$

Equivalent Failure Load Interval (psf)	Midpoint of Equivalent Failure Load Interval, x_i (psf)	Theoretical Interval Probability p_i	$x_i p_i$	$(x_i - \mu)^2 p_i$
40- 70	55	0.005	0.28	68.29
70-100	85	0.023	1.96	173.57
100-130	115	0.108	12.42	349.28
130-160	145	0.230	33.35	166.06
160-190	175	0.304	53.20	2.98
190-220	205	0.239	49.00	262.33
220-250	235	0.082	19.27	326.80
250-280	265	0.009	2.39	78.06
			<u>171.87</u>	<u>1427.37</u>

$$\mu = 171.87 \text{ psf}$$

$$\sigma = \sqrt{1427.37} = 37.78 \text{ psf}$$

TABLE E.XIII

CALCULATION OF THEORETICAL RECTANGULAR GPL GLASS
 PLATE EQUIVALENT FAILURE LOAD STATISTICS: $m=4$, $k=7.30 \times 10^{-10}$

Equivalent Failure Load Interval (psf)	Midpoint of Equivalent Failure Load Interval, x_i (psf)	Theoretical Interval Probability p_i	$x_i p_i$	$(x_i - \mu)^2 p_i$
0- 15	7.5	0.002	0.02	9.43
15- 30	22.5	0.023	0.52	66.20
30- 45	37.5	0.073	2.74	109.05
45- 60	52.5	0.177	9.29	99.00
60- 75	67.5	0.233	15.73	17.43
75- 90	82.5	0.205	16.91	8.27
90-105	97.5	0.154	15.02	70.20
105-120	112.5	0.084	9.45	110.99
120-135	127.5	0.037	4.72	97.56
135-150	142.5	0.010	1.43	44.02
150-165	157.5	0.002	.32	13.24
			<u>76.15</u>	<u>645.39</u>

$$\mu = 76.15$$

$$\sigma = \sqrt{645.39} = 25.40$$

TABLE E.XIV

CALCULATION OF THEORETICAL RECTANGULAR GPL GLASS
 PLATE EQUIVALENT FAILURE LOAD STATISTICS: $m=5$, $k= 1.72 \times 10^{-2}$

Equivalent Failure Load Interval (psf)	Midpoint of Equivalent Failure Load Interval, x_i (psf)	Theoretical Interval Probability p_i	$x_i p_i$	$(x_i - \mu)^2 p_i$
15- 30	22.5	0.011	0.25	34.20
30- 45	37.5	0.043	1.61	71.44
45- 60	52.5	0.156	8.19	103.52
60- 75	67.5	0.227	15.32	26.28
75- 90	82.5	0.260	21.45	4.67
90-105	97.5	0.200	19.50	74.04
105-120	112.5	0.082	9.23	96.13
120-135	127.5	0.019	2.42	46.07
135-150	142.5	0.002	0.29	8.25
			<u>78.26</u>	<u>464.60</u>

$$\mu = 78.26 \text{ psf}$$

$$\sigma = \sqrt{464.60} = 21.55 \text{ psf}$$

TABLE E.XV

CALCULATION OF THEORETICAL RECTANGULAR GPL GLASS
 PLATE EQUIVALENT FAILURE LOAD STATISTICS: $m=6$, $k= 3.83 \times 10^{-2.5}$

Equivalent Failure Load Interval (psf)	Midpoint of Equivalent Failure Load Interval, x_i (psf)	Theoretical Interval Probability p_i	$x_i p_i$	$(x_i - \mu)^2 p_i$
15- 30	22.5	0.004	0.09	13.38
30- 45	37.5	0.029	1.09	53.20
45- 60	52.5	0.117	6.14	90.62
60- 75	67.5	0.223	15.05	36.71
75- 90	82.5	0.303	25.00	1.43
90-105	97.5	0.243	23.69	71.64
105-120	112.5	0.071	7.99	73.48
120-135	127.5	0.010	1.28	22.25
			<u>80.33</u>	<u>362.71</u>

$$\mu = 80.33 \text{ psf}$$

$$\sigma = \sqrt{362.71} = 19.04 \text{ psf}$$

TABLE E.XVI

CALCULATION OF THEORETICAL RECTANGULAR GPL GLASS
 PLATE EQUIVALENT FAILURE LOAD STATISTICS: $m=7$, $k=7.89 \times 10^{-27}$

Equivalent Failure Load Interval (psf)	Midpoint of Equivalent Failure Load Interval, x_i (psf)	Theoretical Interval Probability p_i	$x_i p_i$	$(x_i - \mu)^2 p_i$
15- 30	22.5	0.001	0.02	3.58
30- 45	37.5	0.019	0.71	38.25
45- 60	52.5	0.080	4.20	71.38
60- 75	67.5	0.198	13.37	43.78
75- 90	82.5	0.372	30.69	0.01
90-105	97.5	0.254	24.77	58.14
105-120	112.5	0.072	8.10	65.36
120-135	127.5	0.004	0.51	8.15
			<u>82.37</u>	<u>288.65</u>

$$\mu = 82.37 \text{ psf}$$

$$\sigma = \sqrt{288.65} = 16.99 \text{ psf}$$

TABLE E. XVII
 COMPARISONS OF ACTUAL AND THEORETICAL MEAN
 EQUIVALENT FAILURE LOADS-PREFERRED SURFACE FLAW PARAMETERS

GPL Glass Plate Geometry	Surface Flaw Parameters		Theoretical Mean	Actual Mean	Calculated t Statistic ¹	Critical t Statistic ²	Conclusion
	<u>m</u>	<u>k</u>	(psf)	(psf)			
Square	6	4.97×10^{-25}	167.8	168.0	0.02	2.093	No significant difference in actual and theo- retical means
Rectangular	6	3.83×10^{-25}	80.3	79.0	0.32	2.093	No significant difference in actual and theo- retical means

¹ Calculated using Equation (E.3).

² Found in t table assuming a 5 percent level of significance and 19 d.o.f.

TABLE E. XVIII

COMPARISONS OF VARIANCES OF ACTUAL AND THEORETICAL
EQUIVALENT FAILURE LOADS-PREFERRED SURFACE FLAW PARAMETERS

GPL Glass Plate Geometry	Surface Flaw Parameters		Theoretical Variance	Actual Variance	Calculated F Statistic ¹	Critical F Statistic ²	Conclusion
	m	k	(psf) ²	(psf) ²			
Square	6	$4.97 \times 10^{-2.5}$	1739	1406	1.24	1.88	No significant dif- ference in actual and theoretical variances
Rectangular	6	$3.83 \times 10^{-2.5}$	363	339	1.07	1.88	No significant dif- ference in actual and theoretical variances

¹ Calculated using Equation (E.4).² Found in F table assuming a 5 percent level of significance infinite d.o.f. for the theoretical variances and 19 d.o.f. for the actual variances.

TABLE E.XIX

COMPARISONS OF ACTUAL AND THEORETICAL SQUARE
GPL GLASS PLATE EQUIVALENT FAILURE LOADS

Equivalent Failure Load Interval (psf)	Corresponding Total Equivalent Area Interval (in. ²)	Actual Interval Frequency O_i	Theoretical Interval Frequency E_i	$\frac{(O_i - E_i)^2}{E_i}$
.137.5	- 38	4	5	0.20
137.5-166	38- 90	6	5	0.20
167.5-211	90-185	6	5	0.20
211-	185-	4	5	0.20
		<u>20</u>	<u>20</u>	<u>0.80</u>

$$\chi^2 \text{ critical} = 3.841^2$$

Therefore it is concluded that the difference in the actual and theoretical distributions is not significant.

¹Calculated assuming $m=6$ and $k=3.83 \times 10^{-25}$.

²Found in χ^2 table assuming a 5 percent level of significance and 1 d.o.f.

TABLE E.XX

COMPARISONS OF ACTUAL AND THEORETICAL RECTANGULAR
 GPL GLASS PLATE EQUIVALENT FAILURE LOAD
 DISTRIBUTIONS - PREFERRED SURFACE FLAW PARAMETERS

Equivalent Failure Load Interval (psf)	Corresponding Total Equivalent Area Interval (in. ²)	Actual Interval Frequency O_i	Theoretical Interval Frequency E_i	$\frac{(O_i - E_i)^2}{E_i}$
-67.5	- 48.0	6	5	0.20
67.5-81.5	48.0-120.0	5	5	0.00
81.5-95.5	120.0-250.0	6	5	0.20
95.5-	250.0-	3	5	0.80
		<u>20</u>	<u>20</u>	<u>1.20</u>

$$\chi^2 \text{ critical} = 3.841^2$$

Therefore it is concluded that the difference in the actual and theoretical distributions is not significant.

¹Calculated assuming that $m=6$ and $k=4.97 \times 10^{-25}$.

²Found in χ^2 table assuming a 5 percent level of significance and 1 d.o.f.

presents results of the F tests, and Tables E.XXI and E.XXII present results of the Chi-squared tests.

To demonstrate that the surface flaw parameters are independent of plate response, the preferred rectangular GPL surface flaw parameters are used to calculate a theoretical equivalent failure load distribution for the square GPL glass plates and vice versa. These calculations are presented in Tables E.XXIII and E.XXIV. Finally, statistical tests are presented to compare these theoretical equivalent failure load statistics to the corresponding actual statistics. Table E.XXV presents results of t tests, Table E.XXVI presents results of F tests, and Tables E.XXVII and E.XXVIII present results of Chi-squared tests.

TABLE E.XXI

CALCULATION OF THEORETICAL SQUARE GPL GLASS
 PLATE EQUIVALENT FAILURE LOAD STATISTICS: $m=6$, $k=3.83 \times 10^{-25}$

Equivalent Failure Load Interval (psf)	Midpoint of Equivalent Failure Load Interval, x_i (psf)	Theoretical Interval Probability p_i	$x_i p_i$	$(x-\mu)^2 p_i$
40- 70	55	0.008	0.44	120.01
70-100	85	0.030	2.55	256.58
100-130	115	0.108	12.42	421.61
130-160	145	0.199	28.86	209.94
160-190	175	0.252	44.10	1.55
190-220	205	0.234	47.97	177.22
220-250	235	0.127	29.85	420.19
250-280	265	0.037	9.81	283.41
280-310	275	0.005	1.48	69.05
			<u>177.48</u>	<u>1959.56</u>

$$\mu = 177.48 \text{ psf}$$

$$\sigma = \sqrt{1959.56} = 44.26 \text{ psf}$$

TABLE E.XXII

CALCULATION OF THEORETICAL RECTANGULAR GPL
 GLASS PLATE EQUIVALENT FAILURE LOAD STATISTICS: $m=6$, $k=4.97 \times 10^{-2.5}$

Equivalent Failure Load Interval (psf)	Midpoint of Equivalent Failure Load Interval, x_i (psf)	Theoretical Interval Probability p_i	$x_i p_i$	$(x-\mu)^2 p_i$
15- 30	22.5	0.006	0.14	17.32
30- 45	37.5	0.036	1.35	53.97
45- 60	52.5	0.148	7.77	83.27
60- 75	67.5	0.265	17.89	20.15
75- 90	82.5	0.312	25.74	12.30
90-105	97.5	0.195	19.01	88.30
105-120	112.5	0.035	3.94	46.07
120-135	127.5	0.003	0.38	7.89
			<u>76.22</u>	<u>329.27</u>

$$\mu = 76.22 \text{ psf}$$

$$\sigma = \sqrt{329.27} = 18.15 \text{ psf}$$

TABLE E.XXIII

COMPARISONS OF ACTUAL AND THEORETICAL MEAN EQUIVALENT
FAILURE LOADS-ALTERNATE SURFACE FLAW PARAMETERS

GPL Glass Plate Geometry	Surface Flaw Parameters		Theoretical Mean	Actual Mean	Calculated t Statistic ¹	Critical t Statistic ²	Conclusion
	<u>m</u>	<u>k</u>	(psf)	(psf)			
Square	6	$3.83 \times 10^{-2.5}$	177.5	168.0	1.13	2.093	No significant difference in actual and theo- retical means
Rectangular	6	$4.97 \times 10^{-2.5}$	76.2	79.0	0.68	2.093	No significant difference in actual and theo- retical means

¹ Calculated using Equation (E.3).

² Found in t table assuming a 5 percent level of significance and 19 d.o.f.

TABLE E. XXIV

COMPARISONS OF VARIANCES OF ACTUAL AND THEORETICAL
EQUIVALENT FAILURE LOADS-ALTERNATE SURFACE FLAW PARAMETERS

GPL Glass Plate Geometry	Surface Flaw Parameters		Theoretical Variance	Actual Variance	Calculated F Statistic ¹	Critical F Statistic ²	Conclusion
	m	k	(psf) ²	(psf) ²			
Square	6	3.83×10^{-25}	1960	1406	1.39	1.88	No significant difference in actual and theoretical variances
Rectangular	6	4.97×10^{-25}	329	339	1.03	1.59	No significant difference in actual and theoretical variances

¹Calculated using Equation (E.4).

²Found in F table assuming a 5 percent level of significance, infinite d.o.f. for the theoretical variances and 19 d.o.f. for the actual variances.

TABLE E.XXV

COMPARISONS OF ACTUAL AND THEORETICAL SQUARE
GPL GLASS PLATE EQUIVALENT
FAILURE LOAD DISTRIBUTION - ALTERNATE SURFACE FLAW
PARAMETERS

Equivalent Failure Load Interval (psf)	Corresponding Total Equivalent Area Interval (in. ²)	Actual Interval Frequency O_i	Theoretical Interval Frequency E_i	$\frac{(O_i - E_i)^2}{E}$
-143.5	- 48.0	5	5	0.00
143.5-176	48.0-118.0	8	5	1.80
176-209	118.0-245.0	5	5	0.00
209-	245.0-	2	5	1.80
		<hr/> 20	<hr/> 20	<hr/> 3.60

$$\chi^2 \text{ critical} = 7.815^4$$

Therefore it is concluded that the difference in the actual and theoretical distributions is not significant.

¹Calculated assuming that $m=6$ and $k=3.83 \times 10^{-2.5}$.

²Found in χ^2 table assuming a 5 percent level of significance and 3 d.o.f.

TABLE E, XXVI

COMPARISONS OF ACTUAL AND THEORETICAL
RECTANGULAR GPL GLASS PLATE EQUIVALENT
FAILURE LOAD DISTRIBUTIONS - ALTERNATE SURFACE
FLAW PARAMETERS

Equivalent Failure Load Interval (psf)	Corresponding Total Equivalent Area Interval (in. ²)	Actual Interval Frequency O_i	Theoretical Interval Frequency E_i	$\frac{(O_i - E_i)^2}{E}$
-67.5	- 38.0	6	5	0.20
67.5-77.0	38.0- 95.0	5	5	0.00
77.0-90.0	95.0-182.0	4	5	0.20
90.0-	182.0-	5	5	0.00
		20	20	0.40

$$\chi^2_{\text{critical}} = 7.815^2$$

Therefore it is concluded that the difference in the actual and theoretical distributions are not significant.

¹Calculated assuming that $m=6$ and $k=4.97 \times 10^{-2.5}$.

²Found in χ^2 table assuming a 5 percent level of significance and 3 d.o.f.

